AD NUMBER
ADC010072
CLASSIFICATION CHANGES
TO: unclassified
FROM: confidential
LIMITATION CHANGES
TO: Approved for public release, distribution unlimited
FROM: Distribution authorized to U.S. Gov't. agencies and their contractors; Administrative/Operational Use; JUL 1976. Other requests shall be referred to Office of Naval Research, 800 North Quincy Street, Arlington, VA 22217-5660.
AUTHORITY
31 Dec 1982, per document marking; ONR ltr, 31 Jan 2006

CONFIDENTIAL

Copy 80

(12) (2)

CHURCH ANCHOR EXPLOSIVE SOURCE (SUS) PROPAGATION MEASUREMENTS FROM R/P FLIP (U)

G. B. Morris

University of California, San Diego
Marine Physical Laboratory of the
Scripps Institution of Oceanography
San Diego, California 92152

1 July 1976

SIO REFERENCE 76-10

Sponsored by
Office of Naval Research
N00014-75-C-6049
NR 260-103

Classified by: NAVSEAAIR INST C5511.5
Subject to: General Declassification
Schedule of Executive Order: 11652
Automatically Downgraded at: 2 Year Intervals
Declassified on: 31 December 1982

NATIONAL SECURITY
INFORMATION
Unauthorized Disclosure Subject to
Criminal Sanctions

CONFIDENTIAL

CONFIDENTIAL

UNCLASSIFIED

SECURITY CLASSIFICATION OF THIS PAGE (When Data Entered)

REPORT DOCUMENTATION PAGE	READ INSTRUCTIONS BEFORE COMPLETING FORM
1. REPORT NUMBER: SIO Reference 76-10	2. GOVT ACCESSION NO. / 3. RECIPIENT'S CATALOG NUMBER
4. TITLE (and Subtitle): CHURCH ANCHOR EXPLOSIVE SOURCE (SUS) PROPAGATION MEASUREMENTS FROM R/P FLIP (U)	5. TYPE OF REPORT & PERIOD COVERED: Summary Sept. and - Sep 73
	6. PERFORMING ORG. REPORT NUMBER: MPL-C-42/76, SIO-Ref-76-10
7. AUTHOR(s): G.B. Morris	8. CONTRACT OR GRANT NUMBER(s): ONR N00014-75-C-6049 new
9. PERFORMING ORGANIZATION NAME AND ADDRESS: University of California, San Diego, Marine Physical Laboratory of the Scripps Institution of Oceanography, San Diego, California 92152	10. PROGRAM ELEMENT, PROJECT, TASK AREA & WORK UNIT NUMBERS
11. CONTROLLING OFFICE NAME AND ADDRESS: Office of Naval Research, Department of the Navy, Arlington, Virginia 22217	12. REPORT DATE: 1 July 1976
	13. NUMBER OF PAGES: 65
14. MONITORING AGENCY NAME & ADDRESS(if different from Controlling Office)	15. SECURITY CLASS. (of this report): CONFIDENTIAL
	15a. DECLASSIFICATION/DOWNGRADING SCHEDULE: 31 December 1982

16. DISTRIBUTION STATEMENT (of this Report)

National Security Information
Unauthorized Disclosure Subject to Criminal Sanctions.

17. DISTRIBUTION STATEMENT (of the abstract entered in Block 20, if different from Report)

18. SUPPLEMENTARY NOTES

19. KEY WORDS (Continue on reverse side if necessary and identify by block number)

propagation, range dependence, frequency, sound channel, attenuation, surface image interference

20. ABSTRACT (Continue on reverse side if necessary and identify by block number)

(U) As part of the CHURCH ANCHOR Exercise conducted in the central Northeastern Pacific Ocean during August and September 1975, the received signals from underwater explosive sources (SUS) detonated at a nominal depth of 18 meters were analyzed for signal propagation measurements. The signals received at four hydrophones were detected, digitally sampled and processed on-line by a digital minicomputer system aboard the Research Platform FLIP. The four hydrophone

(over)

DD FORM 1 JAN 73 1473 EDITION OF 1 NOV 65 IS OBSOLETE S/N 0102-014-6601

UNCLASSIFIED

SECURITY CLASSIFICATION OF THIS PAGE (When Data Entered)

CONFIDENTIAL

This page is unclassified

DDC

MAY 24

217

DEPARTMENT OF THE NAVY
OFFICE OF NAVAL RESEARCH
875 NORTH RANDOLPH STREET
SUITE 1425
ARLINGTON VA 22203-1995

IN REPLY REFER TO:

5510/1
Ser 321OA/011/06
31 Jan 06

MEMORANDUM FOR DISTRIBUTION LIST

Subj: DECLASSIFICATION OF LONG RANGE ACOUSTIC PROPAGATION PROJECT (LRAPP) DOCUMENTS

Ref: (a) SECNAVINST 5510.36

Encl: (1) List of DECLASSIFIED LRAPP Documents

1. In accordance with reference (a), a declassification review has been conducted on a number of classified LRAPP documents.

2. The LRAPP documents listed in enclosure (1) have been downgraded to UNCLASSIFIED and have been approved for public release. These documents should be remarked as follows:

   Classification changed to UNCLASSIFIED by authority of the Chief of Naval Operations (N772) letter N772A/6U875630, 20 January 2006.

   DISTRIBUTION STATEMENT A: Approved for Public Release; Distribution is unlimited.

3. Questions may be directed to the undersigned on (703) 696-4619, DSN 426-4619.

B F JR

BRIAN LINK
By direction

Subj: DECLASSIFICATION OF LONG RANGE ACOUSTIC PROPAGATION PROJECT (LRAPP) DOCUMENTS

DISTRIBUTION LIST:

NAVOCEANO (Code N121LC – Jaime Ratliff)
NRL Washington (Code 5596.3 – Mary Templeman)
PEO LMW Det San Diego (PMS 181)
DTIC-OCQ (Larry Downing)
ARL, U of Texas
Blue Sea Corporation (Dr.Roy Gaul)
ONR 32B (CAPT Paul Stewart)
ONR 321OA (Dr. Ellen Livingston)
APL, U of Washington
APL, Johns Hopkins University
ARL, Penn State University
MPL of Scripps Institution of Oceanography
WHOI
NAVSEA
NAVAIR
NUWC
SAIC

Declassified LRAPP Documents

Report Number	Personal Author	Title	Publication Source (Originator)	Pub. Date	Current Availability	Class.
ARLTR7952	Focke, K. C., et al.	CHURCH STROKE 2 CRUISE 5 PAR/ACODAC ENVIRONMENTAL ACOUSTIC MEASUREMENTS AND ANALYSIS (U)	University of Texas, Applied Research Laboratories	791029	ADC025102; NS; AU; ND	C
Unavailable	Van Wyckhouse, R. J.	SYNBAPS. VOLUME I. DATA BASE SOURCES AND DATA PREPARATION	Naval Ocean R&D Activity	791201	ADC025193	C
NORDATN63	Brunson, B. A., et al.	ENVIRONMENTAL EFFECTS ON LOW FREQUENCY TRANSMISSION LOSS IN THE GULF OF MEXICO (U)	Naval Ocean R&D Activity	800901	ADC029543; ND	C
NORDATN80C	Gereben, I. B.	ACOUSTIC SIGNAL CHARACTERISTICS MEASURED WITH THE LAMBDA III DURING CHURCH STROKE III (U)	Naval Ocean R&D Activity	800915	ADC023527; NS; AU; ND	C
NOSCTR664	Gordon, D. F.	ARRAY SIMULATION AT THE BEARING STAKE SITES	Naval Ocean Systems Center	810401	ADC025992; NS; AU; ND	C
NOSCTR703	Gordon, D. F.	NORMAL MODE ANALYSIS OF PROPAGATION LOSS AT THE BEARING STAKE SITES (U)	Naval Ocean Systems Center	810801	ADC026872; NS; AU; ND	C
NOSCTR680	Neubert, J. A.	COHERENCE VARIABILITY OF ARRAYS DURING BEARING STAKE (U)	Naval Ocean Systems Center	810801	ADC028075; NS; ND	C
HSECO735	Luehrmann, W. H.	SQUARE DEAL R/V SEISMIC EXPLORER FIELD OPERATIONS REPORT (U)	Seismic Engineering Co.	731121	AD0530744; NS; ND	C; U
MPL-C-42/76	Morris, G. B.	CHURCH ANCHOR EXPLOSIVE SOURCE (SUS) PROPAGATION MEASUREMENTS FROM R/P FLIP (U)	Marine Physical Laboratory	760701	ADC010072; AU; ND	C; U
ARLTR7637	Mitchell, S. K., et al.	SQUARE DEAL EXPLOSIVE SOURCE (SUS) PROPAGATION MEASUREMENTS. (U)	University of Texas, Applied Research Laboratories	760719	ADC014196; NS; AU; ND	C; U
NORDAR23	Fenner, D. F.	SOUND SPEED STRUCTURE OF THE NORTHEAST ATLANTIC OCEAN IN SUMMER 1973 DURING THE	Naval Ocean R&D Activity	800301	ADC029546; NS; ND	C; U
NOOTR230	Bucca, P. J.	SOUND VELOCITY CONDITIONS DURING THE CHURCH ANCHOR EXERCISE (U)	Naval Oceanographic Office	751201	NS; AU; ND	C;U
ONR SP 2-69; MC PLAN-01	Unavailable	PARKA II EXPERIMENT UTILIZING SEA SPIDER, ONR SCIENTIFIC PLAN 2-69 (U)	Maury Center for Ocean Science	690626	ADB020846; ND	U
Unavailable	Unavailable	PARKA I EXPERIMENT	Maury Center for Ocean Science	691101	AD0506209	U
USRD CR 3105	Unavailable	SEA SPIDER TRANSPONDER TRANSDUCER	Naval Research Laboratory	700505	ND	U
MC PLAN 05; ONR Scientific Plan 1-71	Unavailable	ATLANTIC TEST BED MEASUREMENT PROGRAM (U)	Maury Center for Ocean Science	701020	ND	U
ACR-170 VOL.1	Hurdle, B. G.	PROJECT NEAT- A COLLABORATIVE LONG RANGE PROPAGATION EXPERIMENT IN THE NORTHEAST ATLANTIC, PART I (U)	Naval Research Laboratory	701118	ND	U
MC-003-VOL-2	Unavailable	THE PARKA I EXPERIMENT. APPENDICES- PACIFIC ACOUSTIC RESEARCH KANEOHE-ALASKA (U)	Maury Center for Ocean Science	710101	ND	U

20. Abstract (Continued)

depths 775 meters, 2492 meters, 4250 meters, and 5180 meters, correspond to depths near the sound channel axis, a depth roughly midway between the axis and the critical depth, near the critical depth, and 142 meters above the bottom, respectively. Analyses were made at selected frequencies in the band from 10 Hz to 400 Hz. Signal propagation characteristics and signal-to-noise ratios were examined as a function of source-to-receiver range, receiver depth, and frequency. Bathymetric or changing water mass effects on the sound propagation were also noted.

UNIVERSITY OF CALIFORNIA, SAN DIEGO
MARINE PHYSICAL LABORATORY OF THE
SCRIPPS INSTITUTION OF OCEANOGRAPHY
SAN DIEGO, CALIFORNIA 92152

CHURCH ANCHOR EXPLOSIVE SOURCE (SUS) PROPAGATION MEASUREMENTS FROM R/P FLIP (U)

G. B. Morris

Sponsored by
Office of Naval Research
N00014-75-C-6049
NR 260-103

SIO REFERENCE 76-10

1 July 1976

NATIONAL SECURITY
INFORMATION
Unauthorized Disclosure Subject to
Criminal Sanctions

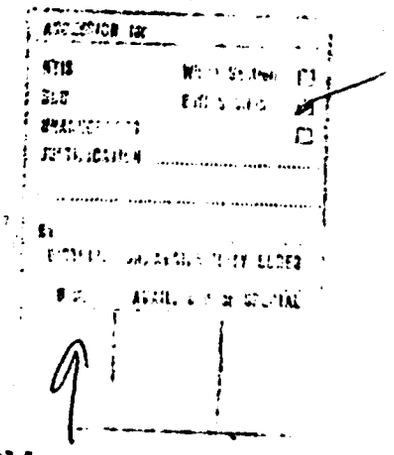

F. N. SPIESS, DIRECTOR
MARINE PHYSICAL LABORATORY

MPL-C-42/76

CHURCH ANCHOR EXPLOSIVE SOURCE (SUS) PROPAGATION MEASUREMENTS FROM R/P FLIP (U)

G. B. Morris

University of California, San Diego
Marine Physical Laboratory of the
Scripps Institution of Oceanography
San Diego, California 92152

ABSTRACT

(U) As part of the CHURCH ANCHOR Exercise conducted in the central Northeastern Pacific Ocean during August and September 1973, the received signals from underwater explosive sources (SUS) detonated at a nominal depth of 18 meters were analyzed for signal propagation measurements. The signals received at four hydrophones were detected, digitally sampled and processed on-line by a digital mini-computer system aboard the Research Platform FLIP. The four hydrophone depths, 775 meters, 2492 meters, 4250 meters, and 5180 meters, correspond to depths near the sound channel axis, a depth roughly midway between the axis and the critical depth, near the critical depth, and 142 meters above the bottom, respectively. Analyses were made at selected frequencies in the band from 10 Hz to 400 Hz. Signal propagation characteristics and signal-to-noise ratios were examined as a function of source-to-receiver range, receiver depth, and frequency. Bathymetric or changing water mass effects on the sound propagation were also noted.

I INTRODUCTION

(U) The CHURCH ANCHOR Exercise, which was conducted in the central Northeastern Pacific Ocean during August and September 1973, included concurrent measurements of underwater acoustic propagation and oceanic environmental parameters. The plans and objectives for this exercise are given in Reference 1. A discussion of the types of data acquired and some of the general results are summarized in Reference 2. An extensive analysis of the sound velocity conditions existing during this exercise are reported in Reference 3.

(U) This report deals only with those segments of acoustic propagation data resulting from measurements made at receiving station B which was the Research Platform FLIP operated by the Marine Physical Laboratory. The location of FLIP together with the location of other receivers and the main track for source deployments is shown in Figure 1. Figure 2 shows a cross section along this track giving receiver locations, bathymetry and source speed structure. The propagation results for the other receivers, mostly ACODAC's, are given in Reference 4.

(U) Three types of SUS charges were used along this north-to-south propagation run. For the southern portion of the run where SUS charges were deployed from the USNS SILAS BENT, a pattern of three different detonation depths were used. A MK-61 SUS set for 244 meters (800 feet) was detonated first, followed one minute later by a MK 82 set for 91 meters (300 feet), and which was followed one minute later by a MK 61 set for 18 meters (60 feet). This pattern of three detonation depths was repeated every five minutes. Gaps in the pattern occurred on the hour to facilitate ranging and shot identification. The nominal range interval between shots at similar depths was approximately one nautical mile. For the aircraft portion of the run, a shot was dropped every minute, alternating between the 91 meter SUS and the 18 meter SUS, and the nominal range interval for similar shot depths was eight nautical miles. Although all the data are judged to be of good quality, this report deals only with the final analysis of the 18 meter SUS deployed by either the BENT or the aircraft.

(U) Signals from these SUS as received at four sensors of the MPL hydrophone system, at

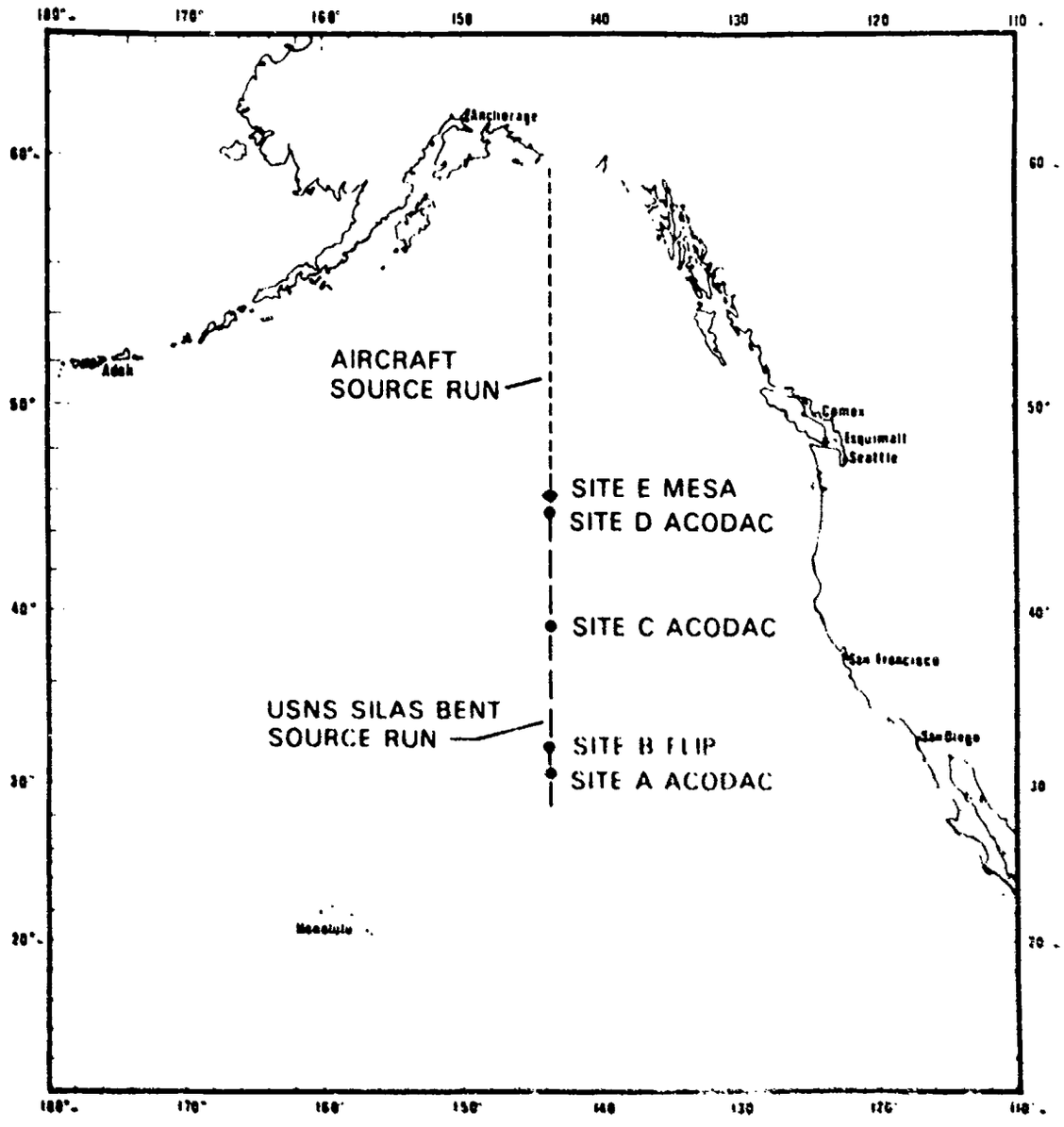

Figure 1. (U) Area Map of Source Track and Receiver Locations. (C)

depths of 775 meters, 2492 meters, 4250 meters, and 5180 meters, were detected and subjected to on-line digital sampling and spectral analysis using fast Fourier transform techniques. These digitally recorded spectral data were subjected to further post-exercise processing to yield propagation loss and signal-to-noise ratios versus range for various one-third octave and octave frequency bands covering the total band from 12.5 Hz to 400 Hz.

II SUMMARY OF RESULTS

(U) Summarized below are the observations and conclusions regarding signal propagation loss and signal-to-noise ratio characteristic and dependencies.

Propagation Loss Summary

(U) General Range Dependence. All sensor- from depths near the axis to near the bottom

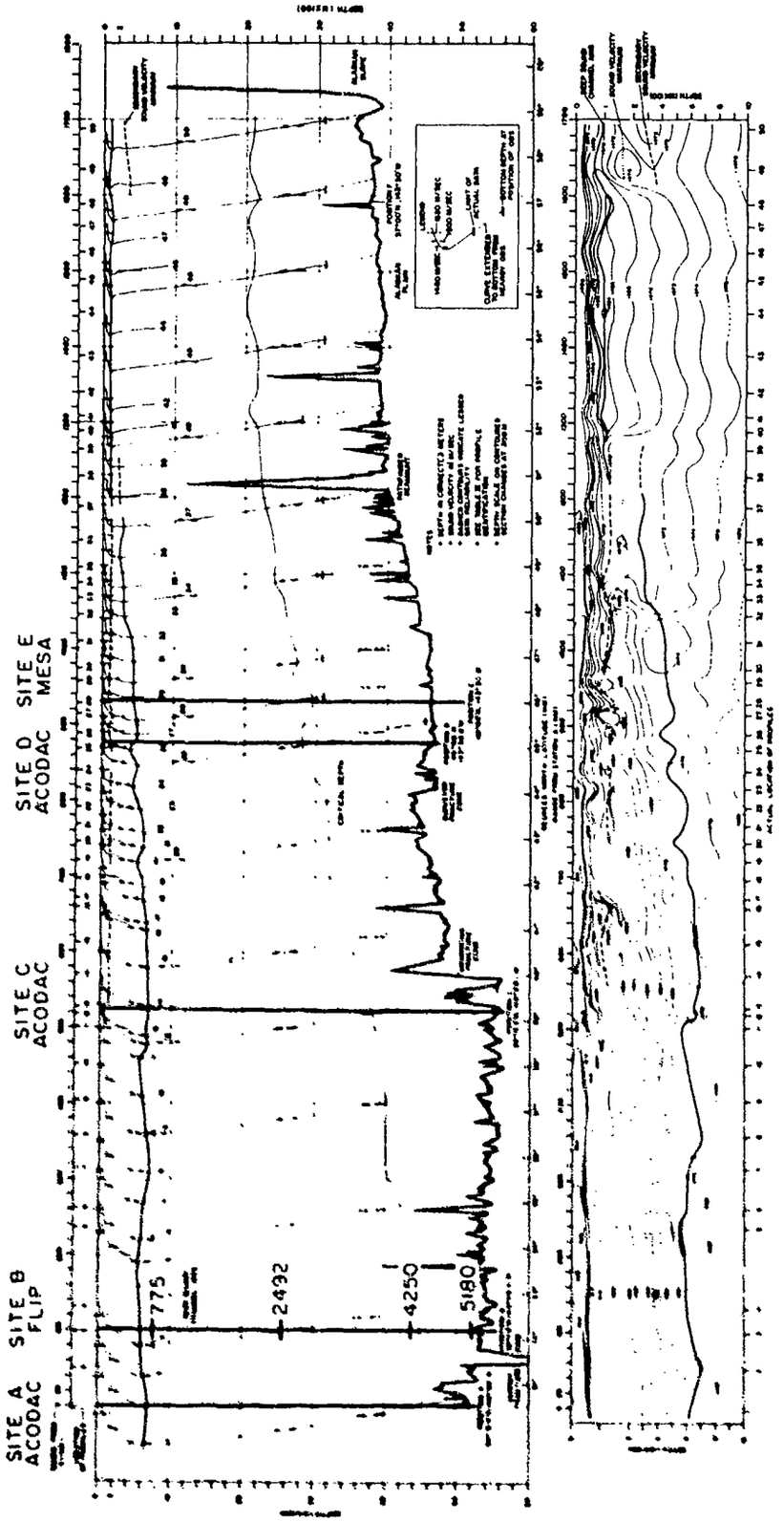

Figure 2. (U) Cross Section of Primary Source Track Showing Receiver Locations, Hydrophone Depths, Bathymetry, and Sound Speed Structure (from Ref. 3 and Ref. 4). (U)

show convergence zone propagation effects. These zonal effects are most prominent at the higher frequencies and for the hydrophone near the critical depth.

(C) Bathymetry/Water Mass Dependence. Bathymetric and/or sound speed profile changes near Pathfinder Seamount introduce as much as 7 dB additional propagation loss for SUS charges detonated north of the seamount. This increased propagation loss is most evident for frequencies of 100 Hz and greater. For frequencies of 50 Hz and less, a decrease in propagation loss (anomalously strong received signal) by as much as 10 dB is observed in the vicinity of the seamount peak.

(C) Receiver Depth Dependence. The sensors with the least propagation loss show a range dependence. At short ranges, to about 150 miles, all four sensors show about the same propagation loss. The near bottom sensor shows the greatest increase in loss with range, such that at ranges greater than about 200 miles this sensor has the highest propagation loss. At ranges from 250 miles to 500 miles, the near critical depth sensor exhibits strong convergence zone propagation, and its propagation loss in a zone is often 8 dB to 10 dB less than that measured by the two shallower sensors. At ranges beyond 500 miles, the receiver at 2492 meters shows the least loss.

(C) Frequency Dependence. The minimum propagation loss occurs at 160 Hz. Above 160 Hz the loss increases with frequency due to attenuation of sound in the sea. Below 160 Hz the loss increases with decreasing frequency due to surface image interference or Lloyd mirror effects. Attenuation coefficients were determined for frequencies above 50 Hz. The coefficients follow the relationship:

$$\alpha(f) = 0.0676f^2$$

where f in frequency in kilohertz and $\alpha(f)$ is the attenuation coefficient in dB/km. The attenuation is approximately one-half that predicted by the Thorp equation or that measured in the Atlantic Ocean or Mediterranean Sea. The image interference effect is similar to that calculated for rays departing the source at ±7.3 degrees. The maximum observed difference of this effect with frequency, from 10 Hz to 160 Hz, is 16.5 dB whereas the calculated difference is 21 dB.

Signal-to-Noise Ratio (S/N) Summary

(C) Receiver Depth Dependence. The sensor with the greatest S/N shows a strong range dependence also. At ranges out to about 150 miles to 200 miles, the near bottom receiver typically has the greatest S/N while the axis receiver has the smallest S/N. At intermediate ranges of 250 miles to 500 miles, because of the strong convergence zone propagation, the near critical depth receiver has S/N values which at times are 10 dB greater than the S/N for the other receivers. This S/N advantage of the near critical depth sensor diminishes with range so that beyond 750 miles range the 2492 meter sensor has the highest S/N ratios. Of the two shallower sensors, the one at 2492 meters has S/N ratios that are typically 3 dB to 5 dB greater than that of the sensor at 775 meters.

(C) Frequency Dependence. For the 775 meter and 2492 meter sensors, the maximum S/N values occur at 400 Hz at short ranges. With increasing range, the frequency at which the S/N is a maximum shifts downward to 160 Hz. For the 4250 meter sensor, the maximum S/N values occur at 250 Hz and shift to 160 Hz as range increases. For the 5180 meter sensor, the maximum S/N values occur at 160 Hz for all ranges. Below 160 Hz there is a decrease in S/N ratio with decreasing frequency for all hydrophones and ranges. This decrease below 160 Hz results from increased propagation loss with decreasing frequency due to the surface image interference effect.
(U) The source levels of these shallow SUS decrease with increasing frequency. Normalizing the S/N ratios to equal values of source levels at all frequencies would shift the frequency at which the maximum S/N values occur to frequencies higher than those actually observed.

Special Comments Regarding Results

(C) Many of the observations and conclusions resulting from analysis of these SUS propagation data taken with the FLIP system are in agreement with those reported in Reference 4 which were observed using the ACODAC systems. Certainly this is not surprising as the signals received by both the FLIP and ACODAC systems came from common explosive sources. However, there are some differences in observations and conclusions. Some of these apparent discrepencies can be related to different locations of the receivers, particularly differences in hydrophone depths used by the FLIP and ACODAC systems. However, many of the differences are due to system overloads experienced by the ACODACS during reception of high level signals. Much of the data at short ranges and at the strong convergence zone ranges were lost due to these overloads. As a result many of the conclusions in Reference 4 are based on propagation loss results for regions between convergence zone peaks, regions where the propagation loss is strongly influenced by the

reflection loss characteristics of the ocean bottom as opposed to the transmission characteristics of the ocean medium itself. Other differences between the conclusions of the two reports are related to the fact that only the 18 meter SUS were analyzed for the FLIP system whereas both the 18 meter and the 91 meter SUS were analyzed for the ACODAC systems.

III DATA ACQUISITION SYSTEM AND CALIBRATION

(U) The acoustic-receiver system deployed beneath FLIP, which was in a moored configuration to hold station and minimize lateral movement, consisted of twenty hydrophones distributed vertically in the water column. Four of these twenty sensors were selected for the on-line SUS data acquisition and processing. Their depths and relationship to the sound speed profile at this site are given in Figure 3. The shallowest sensor used, 775 meters, was near the sound channel axis which was at approximately 700 meters. The next shallower sensor, 2492 meters, was midway between the axis and the critical depth which was 4400 meters. The third sensor, 4250 meters was near the critical depth while the fourth sensor at 5180 meters was 142 meters above the bottom.

(U) The individual hydrophone outputs were FM multiplexed and telemetered to FLIP over double armored coaxial cables as shown in Figure 4. Aboard FLIP the signals were separated according to the FM carrier frequency assigned to each hydrophone, demodulated, and made available to the amplifier, filters, and processing unit.

(U) The details of the acoustic system calibration are discussed extensively in Reference 5. The sensitivities of the hydrophones were measured at U.S. Navy Calibration facilities, the Transducer Evaluation Center of the Naval Undersea Center and the Underwater Sound Reference Division of the Naval Research Laboratory. The frequency response and gain calibrations of the FM modulators and demodulators, amplifiers, filters, and digital processor were calibrated at MPL by inserting wide-band white noise signals in place of the hydrophone signal. The calibration factor was derived from the difference in voltage levels between the final processed values and those measured by a B & K Spectrometer Type 2112.

(U) Reference 5 which describes an extensive error analysis shows that by neglecting potential SUS source level errors, the errors associated with the acoustic receiving system can be expected to be about 1 dB or less for the 18 meter SUS propagation loss.

IV DATA ANALYSIS

(U) The data analysis consists of two basic parts, the at-sea on-line processing which produced shot and noise spectra stored in digital format on magnetic tape, and the post-exercise processing which merge these data with source-to-receiver ranges, source levels and calibrations to produce the final propagation loss and signal-to-noise ratio versus range plots.

On-Line Data Processing

(U) The on-line processing began with the shot detection. During the SUS propagation run the computer continuously sampled all four hydrophone outputs into a circular buffer. Simultaneously, the analog signals from the

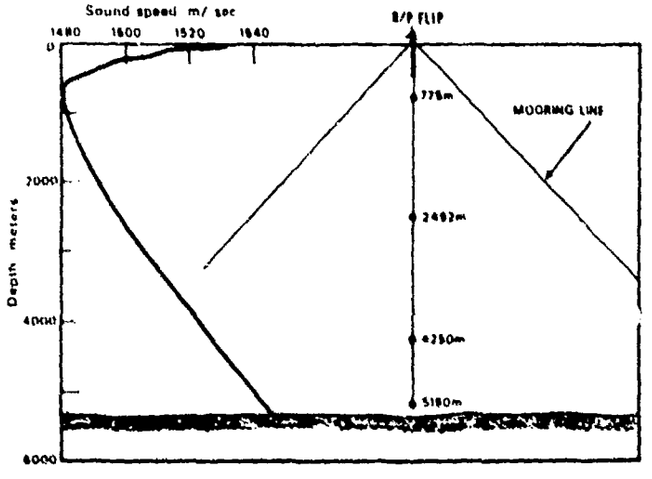

Figure 3. (U) Sound Speed Profile and Hydrophone Depths at Receiving Station. (U)

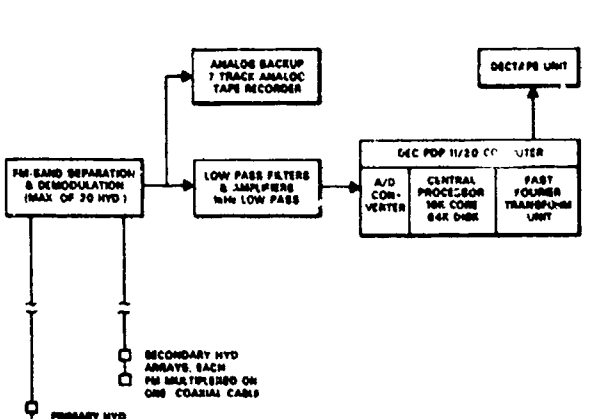

Figure 4. (U) Block Diagram of SUS Propagation Loss Data Acquisition and On-Line Processing System. (U)

four channels were low-pass filtered to remove transients and passed to a threshold detector. When the level of any of the four channels exceeded the threshold, the trigger activated, dumping the contents of the circular buffer into a sampling buffer and sampling of the shot began. The clock time to the nearest second was also read and logged as a heading for identification. In the event of a false trigger the operator could stop the sampling and re-initiate the shot detection process.

(U) The four hydrophone channels were sampled by the analog-to-digital converter. Each channel was sampled at a frequency of 900 samples per second and double buffered onto a 64,000 word, fixed-head storage disk. The total sampling time, which was limited by the disk capacity, was 13.7 seconds resulting in 49,152 data points for each shot. Once sampling was completed, the data were read from the disk in blocks of 1024 samples, fast Fourier transformed (FFT), squared and accumulated for the 12 data blocks for each channel. The resulting SUS signal plus noise spectra covering the frequency band up to 450 Hz with a frequency resolution of approximately 0.9 Hz were stored on digital magnetic tape together with heading information of data and time. These spectra were displayed for approximately 10 seconds on a video CRT device for monitoring by the operator.

(U) Between shots, noise spectra were taken utilizing the same sampling and processing techniques by manually triggering the detection system.

Post-Exercise Data Processing

(U) The first phase of the post-exercise processing consisted of identifying the recorded spectra as to whether they were for an 18 meter SUS, 91 meter SUS, 244 meter SUS, or noise. Where doubts as to identity arose, individual spectra were plotted. Identification was easily made from the different bubble-pulse frequency patterns associated with the different SUS detonation depths.

(U) The received shot spectra often contained signals other than those from the SUS. CW transmission runs were being conducted simultaneously with the SUS transmission runs. An example of a 38 Hz CW tone contained in a shot spectrum is shown in Figure 5. Also certain machinery tonal frequencies radiated from FLIP were received at the hydrophones. Prior to any further processing these tonal lines were detected and removed from both the received shot energy plus noise energy spectra and the noise energy spectra.

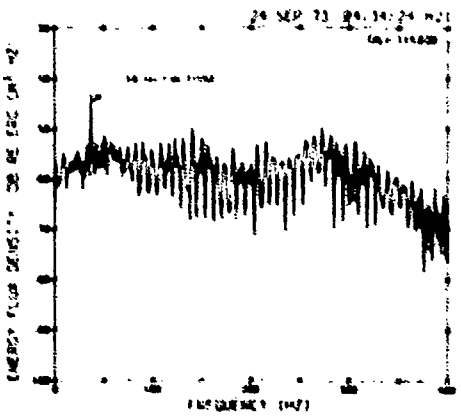

Figure 5. (U) Received SUS Spectrum Showing Presence of Other Interfering Signals. Hydrophone Receiver Depth is 775 Meters. Source-to-Receiver Range for SUS is 357.7 Miles. Source-to-Receiver Range for 38 Hz Source is 400 Miles. (U)

(U) For the 18 meter SUS, the total received shot energy plus noise energy and the total noise energy were integrated in standard 1/3-octave and octave bands. The filter bands used were ideal (not physically realizable for analog filters) in that they passed all energy between the limiting frequencies and no energy from outside these frequencies. Such idealized filters are the same, however, as those used by Gaspin and Shuler (Reference 6) for determining SUS source levels. In each of these frequency bands the received SUS energy determination was made by subtracting the noise energy from the SUS signal-plus-noise energy. Signal-to-noise ratios (S/N) were determined by dividing this SUS energy by the noise energy.

(U) The output from the spectral processing was combined with source-to- receiver range information (from a digital tape containing date, time and range information supplied by the Naval Oceanographic Office), with the hydrophone- processing system calibration, and with source level information to produce propagation loss and signal-to-noise ratio versus range values.

(U) The explosive source levels for 1.8 pound SUS charges detonated at a nominal depth of 18 meter were obtained from Gaspin and Shuler (Reference 6). Small corrections were made to the source levels because of differences in actual detonation depth from the nominal 18 meter depth. The statistics regarding the actual detonation depths and some of the source level correction factors are given in Reference 7.* The source levels used are given in Table I. Where octave source levels were not specifically listed, the levels were obtained by summing the energies in the appropriate 1/3-octave frequency bands.

(U) The propagation loss and signal-to-noise data were subject to two editing processes prior to final plotting. First editing of the data was performed on the computer on the basis of signal-to-noise ratio (S/N). If for a particular hydrophone and frequency band, the S/N ratio, using the noise measured just prior to the SUS detection, was less than 0 dB then the propagation loss and S/N values were rejected. Plotting of the data after this initial editing, however, revealed some data points which appeared to be anomalous. The individual raw 0.9 Hz spectra for these suspect points were plotted. Usually the cause of the anomaly could be identified, and the anomalous values were deleted prior to final plotting. These anomalous values were more prevalent at the lowest and highest frequency bands where the S/N values were lower than those at the intermediate frequencies.

TABLE I (U)

Source Levels for 1.8 lb 17 meter (56 ft) MK-61 SUS (dB re 1 erg/cm^2/Hz at 100 yds). (U)

Band Center Frequency Hz	1/3-Octave Source Level	Octave Source Level
10		24.4*
12.5		22.8*
16		20.5
20		19.1
25		18.7
31.5		18.1
40		16.9
50		16.0
63	15.5	15.4
80	15.1	14.6
100	13.4	13.5
125	12.0	
160	10.7	
200	9.8	
250	8.8	
315	7.7	
400	6.8	

*Estimated from spectral plots of Gaspin and Shuler.

V. DISCUSSION OF PROPAGATION LOSS

General

(U) The propagation loss results are plotted as functions of range in Appendix A for the following hydrophone depths: 775 meters, 2492 meters, 4250 meters, and 5180 meters. The losses for seven frequency bands are given; octave bands at 12.5 Hz, 25 Hz and 50 Hz and 1/3-octave bands at 100 Hz, 160 Hz, 250 Hz, and 400 Hz. Table II provides a summary of the propagation loss values in 250 mile range segments for these hydrophone depths and frequencies. These data may be examined for the effects of source-to-receiver

* Where depth corrections for particular frequency bands were not given in Reference 7, those provided by Reference 6 were used. It should be noted that these corrections were at most 1.0 dB and typically amounted to only a few tenths of a dB.

range, bathymetry, sensor depth, and frequency on the propagation loss. To some extent the effects of these parameters on propagation loss are apparent from both the figures and the table. Naturally greater details are contained in the figures as Table II represents only a subjective summary.

(U) Note in plotting the closely-spaced ship launched SUS (approximately 1 per mile) the data are shown as lines connecting the data points. Such a representation was selected to display the fine details contained in these data. The aircraft launched SUS, which were more widely spaced, are shown as individual symbols. Note also that the 110 dB propagation loss line has been included on each plot for a reference level.

(U) The effects of source-to-receiver range, bathymetry, receiver depths and frequency on propagation loss are all interrelated; however, in some instances it is possible to discuss these effects separately in general terms.

Source-to-Receiver Range Dependence

(U) Since the range dependence of each loss curve is of a complicated nature, any simple discussion or comparison such as that given in Table II will be some what subjective.

(C) The most prominent characteristic of the range dependence is the convergence zone focusing effects evident for all hydrophones and all frequencies. The presence of zones is denoted in Table II by a range of loss values. The two shallower hydrophones, 775 meters and 2492 meters, show prominent zonal effects out to ranges of about 250 to 300 miles at which point the zones begin to overlap in range. The near critical depth hydrophone, 4250 meters, shows zonal effects out to much greater ranges with some effects persisting out at ranges beyond 750 miles. For the near bottom hydrophone, the zones are more difficult to define because of the high propagation loss, but they are apparent at ranges in the 250 mile to 500 mile interval for the 160 Hz data. The amplitude of these zonal effects, defined as the difference between the propagation loss in the shadow regions or between zones and that in the convergence zones, is given in Table III for the range interval from 100 miles to 200 miles. The hydrophone at 4250 meters, the one nearest the conjugate depth for these shallow shots, shows the greatest extremes in loss due to the zonal effects. The effects are a maximum at 250 Hz and decrease with decreasing frequency for all sensor depths.

(C) At short ranges, about 150 miles and less, all sensors show about the same propagation loss values. The loss for the near bottom sensor increases more rapidly with range, and beyond about 150 miles its loss is clearly greater than that of the others. At intermidiate ranges, from 150 miles to 750 miles, the propagation loss for the 4250 meter sensor is dominated by convergence zone effects which cause oscillations of up to 30 dB with range. Beyond the distinct convergence zone regions for the shallower two sensors, ranges greater than 300 miles, there is little range dependence in loss for frequencies of 160 Hz and less. Frequencies of 50 Hz and less even show a local maximum in loss at a range near 350 miles with some slight decrease in loss with increasing range.

Bathymetry/Water Mass Effects

(C) At a source-to-receiver range of about 1100 miles the source track crossed Pathfinder seamount. At about this same range, see Figure 2, the sound speed profiles also changed abruptly indicating passage into a different water mass. Anomalous propagation loss effects were noted at this range and because of the near coincident occurrence of the bathymetric and water mass changes their effects cannot be isolated. Consequently, these anomalous propagation loss effects occurring at and beyond this range may be caused by either or both of these physical changes.

(C) These abrupt changes occurring at this range of about 1100 miles are most evident on the loss plots for the two shallower hydrophones and for frequencies of 100 Hz, 160 Hz, and 250 Hz. Beyond a range of about 1100 miles, the propagation loss values exhibit more scatter and show on the average about 6-7 dB more loss. At lower frequencies, 12.5 Hz, 25 Hz, and 50 Hz, the hydrophone at 2492 meters is the only one which contains any appreciable information at these long ranges. The most prominent anomaly displayed by this sensor at the low frequencies is an anomalously low loss value, lower by about 10 dB, occurring at 1117 miles range. This loss or strong received signal may be due, perhaps, to some sort of reflection enhancement of the signal caused by Pathfinder Seamount.

Receiver Depth Dependence

(C) The propagation loss versus range plots for the two shallowest sensors, 775 meters and 2492 meters, are quite similar in overall character. However, the measured loss at the 2492 meter sensor is almost always less than that at 775 meters by about 2 dB. The differences in propagation losses for these two sensors, as determined from the values of Table II, are given in Table IV.

(C) The two deeper hydrophones, 4250 meters and 5180 meters, show strong convergence zone effects. Of all the sensors, the near bottom phone at 5180 meters shows the greatest loss, particularly at ranges beyond 200 miles. As

TABLE II (C)

Summary of Propagation Loss in Decibels for 18 Meters SUS. (U)

Hydrophone Depth (Meters)	Range Interval (Miles)	Frequency (Hz)						
		12.5	25	50	100	160	250	400
	60-250	110-124 (WZ)	104-116 (WZ)	101-113 (WZ)	95-116 (Z)	90-121 (Z)	93-123 (Z)	92-124 (Z)
	250-500	121	114	111	103-116 (WZ)	106 (WZ)	110 (WZ)	113→119
	500-750		115	112	110	107	111→114	119→124
775	750-1000				110	109	114→116	
	1000-1250				114	110→115	114→120	
	1250-1500				116	115	121	
	1500-1750				116	116	122	
	60-250	109-126 (WZ)	102-120 (WZ)	100-119 (WZ)	94-119 (Z)	92-125 (Z)	94-122 (Z)	94-125 (Z)
	250-500	120	114	110	106	104 (WZ)	107	112→117
	500-750	119	113	109	106	105	109	117→122
2492	750-1000		113	110	107	106	111	122→
	1000-1250		116	112	110	107→112	113→117	
	1250-1500				114	114	120	
	1500-1750				115	115	122	
	60-250	108-128 (Z)	100-122 (Z)	107-119 (Z)	92-121 (Z)	85-122 (Z)	88-124 (Z)	91-125 (Z)
	250-500	114-128 (Z)	115-123 (Z)	110-119 (Z)	97-120 (Z)	90-120 (Z)	95-124 (Z)	103-126 (Z)
	500-750	120-130 (WZ)	114-124 (WZ)	105-119 (WZ)	100-121 (WZ)	100-120 (WZ)	112→122	120→128
4250	750-1000		121	110-120 (WZ)	110-121 (WZ)	114→118	>122	
	1000-1250				118	>120		
	1250-1500							
	1500-1750							

TABLE II (Continued)

Summary of Propagation Loss in Decibels for [illegible] Meters SUS. (U)

Hydrophone Depth (Meters)	Range Interval (Miles)	Frequency (Hz)						
		12.5	25	50	100	160	250	400
5180	60-250	112-130 (Z)	102-127 (Z)	97-125 (Z)	91-126 (Z)	90-127 (Z)	96-128 (Z)	101-127 (Z)
	250-500				>126	120->127 (Z)	124→128	
	500-750					126→132	128→136	
	750-1000							
	1000-1250							
	1250-1500							
	1500-1750							

(Z) Strong convergence zones.

(WZ) Weak convergence zones.

→ Denotes a change with increasing range from lower propagation loss to higher propagation loss.

> Greater than.

TABLE III (U)

Approximate Amplitude in Decibels of Convergence Zone Effects, Range Interval 100-200 Miles. (U)

Hydrophone Depth, Meters	Frequency, Hz						
	12.5	25	50	100	160	250	400
775	5	8	10	15	22	25	20
2492	6	9	12	16	20	25	20
4250	12	15	16	20	25	30	25
5180	5	10	10-15	10-15	10-15	10-15	10

TABLE IV (C)

Propagation Loss at 775 Meter Sensor Minus Propagation Loss at 2492 Meter Sensor in Decibels. (U)

Range Interval, Miles	Frequency, Hz						
	12.5	25	50	100	160	250	400
250-500	+1	0	+1		+2	+3	+1 to +2
500-750		+2	+3	+4	+2	+3	+2
750-1000				+3	+3	+4	
1000-1250				+4	+3	+1 to +3	
1250-1500				+2	+1	+1	
1500-1750				+1	+1	0	

the near critical depth sensor, 4250 meters, shows strong convergence zone propagation, its losses when measured in a zone are frequently 10 decibels less than those measured at the shallower sensors. Between convergence zones, the propagation loss for the 4250 meter sensor is greater than that for the shallower sensors.

Frequency Dependence

(U) There are two frequency dependent propagation loss effects apparent in these data. One effect is range dependent and is due to attenuation. This effect is most apparent in the 400 Hz propagation loss data for the 775 meter and 2492 meter hydrophones. The other effect is independent of range and is believed to be caused principally by the surface image interference or Lloyd mirror effect associated with these shallow sources. This effect is most apparent at the low frequencies and is the constant offset in the low frequency propagation loss curves. For example, in the range interval from 250 miles to 750 miles the 2492 meter sensor shows a propagation loss at 12.5 Hz that is 6 dB less than that at 25 Hz, which in turn is 4 dB less than that at 50 Hz.

(C) The minimum propagation losses are usually observed at a frequency of 160 Hz. At frequencies greater than this, the loss increases with increasing frequency due to attenuation. At frequencies less than 160 Hz, the loss increases with decreasing frequency due to the image interference effect.

(U) Attenuation. The total propagation loss may be considered to be the sum of a loss due to geometrical spreading of the energy and a loss due to attenuation. This is true provided the boundary effects can be neglected. As will be seen later a range interval has been selected to minimize the effects of the ocean bottom boundary. In this context, the attenuation loss will include the effects of absorption, scattering and leakage of the energy out of the sound channel. The attenuation coefficients resulting from these measurements should, therefore, be considered to be "effective attenuation coefficients" which include all of these frequency dependent losses.

(U) The approach used is to assume that if the geometrical spreading loss can be determined and subtracted from the total propagation loss, the losses that remain can be assumed to be due to this "effective attenuation." The technique used to determine the values of attenuation coefficients is basically the same as that used by Sheehy and Halley (1957). This method uses the propagation loss at a low frequency for estimating the geometrical spreading loss instead of using a theoretically calculated loss such as cylindrical spreading that is commonly used. The measured propagation loss at 50 Hz was used as the reference frequency for this analysis. This frequency is sufficiently low so that the attenuation loss is small over the range interval of interest. On an individual data point basis, the propagation loss at 50 Hz was subtracted from the measured propagation loss at other frequencies. The resulting differential propagation loss was then fit by least squares to a linear function of range of the form:

$$PL(f) - PL(50\ Hz) = \beta_0 + \beta_1 \times range + \epsilon. \quad (1)$$

The first term, β_0 which is the zero-range intercept, yields the constant offset between the propagation loss at a frequency and that at 50 Hz. This constant which yields the surface-image interference effect will be discussed later. The second constant, β_1, is a differential attenuation coefficient which expresses the difference in attenuation at the particular frequency and that at 50 Hz, or

$$\beta_1 = \alpha(f) - \alpha(50\ Hz) \quad (2)$$

where $\alpha(f)$ is the attenuation at the particular frequency and $\alpha(50)$ is that at 50 Hz. In equation (1), the error term is given by ϵ.

(U) These differential propagation loss plots and the associated least squares solutions were made for frequency bands extending from 10 Hz to 400 Hz. The differential propagation loss plots for the 1/3-octave frequency bands of 100 Hz, 160 Hz, 200 Hz, 250 Hz, 315 Hz, and 400 Hz are given in Appendix B. The results of all the least squares solutions for the hydrophones at 775 meters and 2492 meters are summarized in Table V. The deeper hydrophones were not suitable for these analyses because of their strong convergence zone propagation and also because of their more limited range coverage.

(U) As mentioned previously, the ocean bottom boundary can contribute a bottom bounce propagation path to the total transmitted energy. To eliminate the effects of the strong convergence zones and the need to make a bottom-bounce path correction, no data at ranges less than 300 miles were used in the least squares solutions. Similarly, to eliminate the bathymetric/water mass effects occurring at ranges beyond 1100 miles, no data from beyond this range were used.

(U) Table V lists the resulting differential attenuation coefficients, the standard error in the attenuation coefficient, the standard deviation about the regression equation, and the number of data points where differential propagation losses were available and used in the solution. Those coefficients that do not satisfy the 95% confidence limits (See Draper and Smith, 1966) are enclosed in parenthoses. Note that for frequencies less than 100 Hz only two coefficients are significant at the 95% confidence level.

(U) The data from the two hydrophones were assumed to provide independent estimates of the differential attenuation coefficients. To get a single best estimate at each frequency, the results for the two hydrophones were combined according to an inverse variance weighting scheme (Davies, 1958). The best solutions or the ones with the smallest variance have the greatest weight in such an averaging.

(U) The final step in this analysis was to determine the value for the attenuation coefficient at 50 Hz. This was accomplished by assuming that the attenuation of sound in the sea in this frequency range can be expressed in the form of

$$\alpha(f) = kf^n$$

where f is frequency, kilohertz (3)

k, n are constants.

The differential attenuation can be expressed in the same form minus a constant

$$\alpha(f) - \alpha(0.05) = kf^n - k'. \quad (4)$$

Figure 6 shows the least squares solutions to the weighted differential attenuation coefficients for the cases of frequency raised to the second power (n = 2) and also the three-halves power (n = 3/2). Both are good fits, but the data conform to the

TABLE V (U)

Differential Attenuation Coefficients for Two Hydrophone Depths (dB/km Above Loss at 50 Hz). (U)

Frequency Band Hz		Hydrophone Depth 2492 M				Hydrophone Depth 775 M			
		$\alpha(f) - \alpha(50)$ dB/km	Standard Error dB/km	Standard Deviation dB	Number of Points	$\alpha(f) - \alpha(50)$ dB/km	Standard Error dB/km	Standard Deviation dB	Number of Points
10	OCTAVE	(-0.00005)	0.00054	2.14	232	(0.00215)	0.00571	1.90	49
12.5	"	(0.00018)	0.00030	1.85	330	(-0.00077)	0.00166	1.78	94
16	"	(-0.00024)	0.00029	1.79	342	(-0.00164)	0.00157	1.60	79
20	"	(0.00023)	0.00027	1.72	372	(-0.00096)	0.00050	1.41	165
25	"	(0.00012)	0.00023	1.55	392	(-0.00069)	0.00038	1.51	214
31.25	"	(0.00022)	0.00018	1.25	429	(-0.00041)	0.00038	1.75	283
40	"	(0.00004)	0.00010	0.72	431	-0.00054	0.00027	1.25	295
50	"	(0.00000)	0.00000	0	440	(0.00000)	0.00000	0	362
62.5	"	(-0.00021)	0.00011	0.78	440	(0.00022)	0.00015	0.82	358
80	"	(0.00005)	0.00019	1.33	440	0.00058	0.00026	1.40	360
100	1/3 OCTAVE	(0.00032)	0.00030	2.10	440	0.00082	0.00039	2.13	360
125	"	0.00069	0.00034	2.43	440	0.00145	0.00043	2.38	362
160	"	0.00139	0.00037	2.62	440	0.00199	0.00045	2.46	362
200	"	0.00233	0.00040	2.86	440	0.00282	0.00048	2.60	362
250	"	0.00434	0.00041	2.89	440	0.00322	0.00052	2.86	362
315	"	0.00670	0.00041	2.90	440	0.00647	0.00052	2.82	362
400	"	0.00993	0.00041	2.43	440	0.00715	0.00068	2.67	267

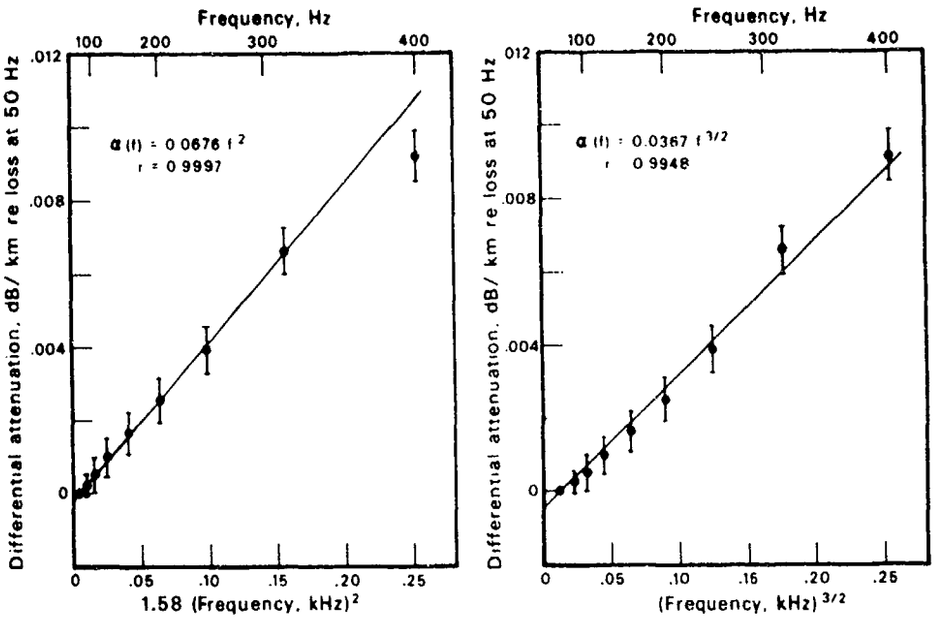

Figure 6. (U) Differential Attenuation Plotted as $\Delta\alpha = \alpha(f) - \alpha(50\ Hz) = k\alpha^n - k'$; $n = 3/2.2$ (U)

frequency-squared relationship a bit more closely.

(U) The final expression for frequency-dependent attenuation is

$$\alpha(f) = 0.0676\ f^2 \qquad (5)$$

where f is frequency in kilohertz. Equation (5) yields attenuation coefficients that are approximately one-half of those predicted by the Thorp equation (Thorp, 1965, 1967). These low attenuation coefficients are in agreement with results reported by Lovett (1975) for 750 Hz, 1500 Hz, and 3000 Hz CW sources.

(U) Surface Image Interference Effects.

The β_0 term of Equation (1) represents the constant offset between the propagation loss data at particular frequencies and that at 50 Hz. This β_0 term describes the frequency-dependent loss effects that are independent of range.

(U) Calibration errors in both the source and the receiving system could manifest themselves in this β_0 term. However, as these frequency dependent effects were examined relative to a frequency of 50 Hz, only relative calibration errors, as opposed to absolute level errors, will appear in the β_0 term. For example, the receiving system has a nearly flat spectrum response over the band of frequencies considered here. There are slight departures of 1 to 2 dB from a perfectly flat frequency response at the extreme ends of the 10 Hz to 400 Hz band. However, these effects are well known and corrections were made. While the source levels as given by Gaspin and Shuler are well documented, source level determination by several different laboratories do show disagreement. (Reference 13). The possibility that source level errors relative to 50 Hz are contained in this β_0 term cannot be discarded.

(C) The β_0 terms resulting from the least squares solutions are shown plotted versus frequency in Figure 7. The results for the two hydrophones are in excellent agreement. Those values below the 0 dB fiducial line indicate a loss that is greater than that at 50 Hz. Those values above the 0 dB line indicate a loss that is less than that at 50 Hz. From the data, the minimum loss can be seen to occur in the 160 Hz to 200 Hz region. The maxima and minima of the image interference pattern for plane waves propagating in an isovelocity ocean depend upon the source depth, frequency and the ray departure angle from the source (see Urick, 1967, p. 110-112). For a 55 foot deep source, a minimum loss at 175 Hz occurs for rays with departure angles from the source of ±7.3 degrees (measured from the horizontal). The calculated image interference pattern for these rays is given by the solid line in Figure 7. The calculated and measured effects are in

reasonable agreement although the total magnitude of the effect is greater for the calculated values than for the measured values. The total magnitude of the calculated effect is 21 dB whereas the measured effect is only 16.5 dB.

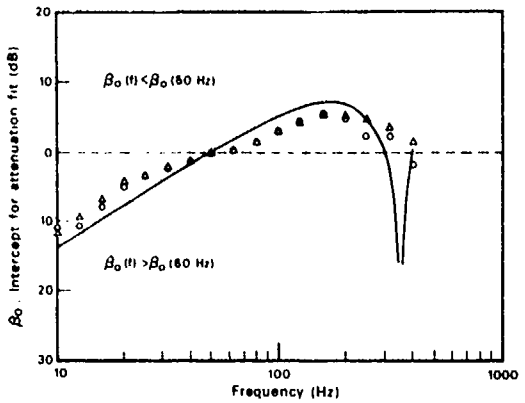

Fig. 7. (U) Comparison between observed Range Independent Frequency Effects on Propagation Loss and Calculated Surface Image Interference Effect. Observed Values at Hydrophone Depths 0 -775 Meters, Δ-2492 Meters. ——Calculated Surface Image Interference Loss for 7.3 Degree Ray and 55 Foot Source Depth. (U)

VI DISCUSSION OF SIGNAL-TO-NOISE RATIOS

General

(U) In calculating the signal-to-noise ratios (S/N) there are two effects which must be considered. First, during this signal transmission study, ships passed close to the receiving station raising the noise level by as much as 20 dB above the ambient level at certain frequencies. Second, there were times when amplifier gains were set low to avoid overloading by strong, received shot signals and the limiting noise was not ambient but instead was electronic system noise. This system noise limit was more prevalent at short ranges where strong convergence zone effects produced received signal levels as much as 40 dB over ambient noise levels. This system-noise limitation, which is a dynamic range limitation, was further compounded by the fact that the deeper SUS, 91 meters and 244 meters, were interspersed with these 18 meter SUS. At times, these deeper SUS produced received signals which were 20 dB greater than those produced by the shallower SUS.

(U) These effects of nearby passing ships and system noise were identified and edited from the ambient noise data. The remaining ambient noise information was averaged for each particular hydrophone-frequency combination and used in calculating the S/N ratios. In effect, the data presented are signal-to-average ambient noise levels. The average ambient noise levels are given in Table VI.

TABLE VI (C)

Average Ambient Noise Levels for Signal-to-Noise Ratios Determinations During SUS Propagation Run. (U)

Frequency Band Hz	Average Ambient Noise Levels, Re 1μPa			
	Depth in Meters			
	775	2492	4250	5180
Octave				
12.5	79.7	77.8	76.0	69.0
25	82.3	80.1	77.9	69.4
50	83.1	81.2	79.4	70.4
1/3 Octave				
100	77.9	75.8	73.6	63.5
160	69.0	67.9	66.8	58.5
250	63.0	62.7	62.5	56.0
400	58.0	58.6	59.2	54.2

(U) The S/N ratio versus range plots are given in Appendix C. As was the case for the propagation loss versus range plots, a summary of the S/N data is given in tabular form, Table VII.

(U) In addition to the S/N ratio plots for individual hydrophones, differences between the hydrophones were also computed and plotted versus range in Appendix D. These plots give the S/N ratio for a hydrophone minus that for the near axis hydrophone, 775 meters. Positive values occur where the S/N ratio for a particular phone is greater than that for the near axis phone.

Source-to-Receiver Range Dependence

(U) As averaged ambient noise levels were used for calculating the signal-to-noise ratios, the range dependence for these ratios will be the same as for propagation loss. As was the case for propagation loss, the S/N versus range plots are of a complicated nature, particularly at short ranges where strong convergence zone effects are prominent.

TABLE VII (C)

Summary of Signal-to-Average Noise Ratios in Decibels for 18 Meter SUS. (U)

Hydrophone Depth (Meters)	Range Interval (Miles)	Frequency (Hz)						
		12.5	25	50	100	160	250	400
775	60-250	12-2 (Z)	12-0 (Z)	12-0 (Z)	[illegible] (Z)	32-2 (Z)	33-3 (Z)	38-7 (Z)
	250-500	3	3	3	13-0 (WZ)	16 (WZ)	17 (WZ)	16→12
	500-750		2	2	6	14	16→12	12→7
	750-1000				6	13	12→10	
	1000-1250				5→1	12→8	12→7	
	1250-1500				1	7	5	
	1500-1750				1	6	5	
2492	60-250	14-4 (Z)	17-0 (Z)	15-0 (Z)	24-0 (Z)	31-0 (Z)	33-6 (Z)	37-5 (Z)
	250-500	6	5	6	11	19	20	18→12
	500-750	7	7	6	11	18	18	12→8
	750-1000	5	6	5	12	17	16	8→6
	1000-1250	4	3	3	10	16→10	14→8	
	1250-1500				3	8	6	
	1500-1750				2	7	5	
4250	60-250	20-0 (Z)	20-0 (Z)	20-0 (Z)	28-0 (Z)	40-2 (Z)	40-4 (Z)	38-4 (Z)
	250-500	10-0 (Z)	16-0 (Z)	17-0 (Z)	24-0 (Z)	35-5 (Z)	32-4 (Z)	24-4 (Z)
	500-750	2	10-0 (Z)	12-0 (Z)	18-0 (Z)	24-5 (Z)	14→4	8→0
	750-1000		4	3→0	10-0 (WZ)	12→4		
	1000-1250		1		3			
	1250-1500							
	1500-1750							
5180	60-250	22-0 (Z)	28-2 (Z)	29-1 (Z)	40-0 (Z)	40-6 (Z)	37-5 (Z)	33-7 (Z)
	250-500				5*	16-6*	6*	
	500-750					5*	3*	
	750-1000							
	1000-1250							
	1250-1500							
	1500-1750							

(Z) Distinct convergence zones.

(WZ) Weak convergence zones.

→ Denotes a decrease with range from highest to lowest value.

* Sparse scattered data for only strong signals; lower S/N ratios unavailable.

Receiver Depth Dependence

(U) The dependence of S/N ratio on receiver depth is summarized in Table VII.

(C) At short ranges, particularly out to about 150 miles to 200 miles, the S/N ratio exhibits a clear depth dependence. At most frequencies, the deepest hydrophone has the highest S/N with the shallowest hydrophone (775 meters) having the lowest S/N. This depth advantage of the deepest sensor is at a maximum at a frequency of 100 Hz, and the advantage diminishes at frequencies higher than this. At 400 Hz, the deepest sensor has the lowest S/N values while the other three sensors are roughly equivalent.

(C) At intermediate ranges of 250 miles to 750 miles, the near bottom sensor clearly has the lowest S/N values. The two shallower hydrophones, 775 meters and 2492 meters, do not show strong convergence zone effects, and the S/N values are relatively constant with range showing only a modest scatter. This is in contrast to the large oscillations in S/N values with range exhibited by the near critical depth sensor, 4250 meters. Because of the strong convergence zone effects, at some ranges the critical depth sensor has higher S/N values than the shallower phones, often by as much as 10 dB. At other ranges the S/N ratios for the shallower phones exceed those of the critical depth phone. This S/N advantage of the near critical depth sensor diminishes with range so that beyond 500 miles most, if not all, of this advantage is lost to the shallow sensors.

(C) At long ranges, 750 miles to 1750 miles, and where information is available, the shallower sensors clearly exhibit S/N ratios greater than that of the deeper sensors. Of the two shallow sensors, the one at 2492 meters shows higher S/N values than that of the sensor of 775 meters, typically by 3 dB to 5 dB, (see Table VIII). This 3 dB to 5 dB S/N advantage of the 2492 meter sensor over that of the near axis sensor, 775 meters, is true for practically all ranges and frequencies.

Frequency Dependence

(C) The frequency dependence for the S/N ratios occurring for these 18 meter SUS is summarized in Table VII. For the two shallowest sensors, 775 meters and 2492 meters, and for the shortest range interval, 60 miles to 250 miles the maximum S/N ratios occur for the 400 Hz data. At the next range interval, 250 miles to 500 miles, the peak S/N ratio occurs at 250 Hz. For ranges beyond 500 miles the maximum S/N values usually occurs at 160 Hz. For the two deeper hydrophones, 4250 meters and 5180 meters, the maximum S/N ratio is almost always observed at 160 Hz.

TABLE III (C)

Differences in Decibels between S/N for Hydrophone at 2492 Meters and S/N for Hydrophone at 775 Meters (S/N at 2492 m Minus S/N at 775 m. (U)

Range Interval Miles	Frequency, Hz						
	12.5	25	50	100	160	250	400
250-500	3	3	4	5	4	4	2
500-750		5	5	7	5	5	2
750-1000				5	5	4	
1000-1250				5	4	3	
1250-1500				3	3	1	
1500-1750				2	1	0	

(U) In any discussion of the frequency dependence of the S/N ratio, one should keep in mind the fact that the signal levels themselves contain a strong frequency dependence. For example, referring to Table I shows that the source level for the 12.5 Hz octave band is 16 dB greater than the source level for the 400 Hz octave band. If the source levels were the same for all the frequency bands there would be two effects. First, the frequency at which the S/N ratio shows a maximum would be shifted towards a higher frequency. For some cases, where the maximum occurs at 160 Hz, normalizing to equal source levels would shift the maximum to 250 Hz. Second, the difference in S/N ratios between high frequencies and that at low frequencies would be greater than that given by Table VII. For example, for the 2492 meter hydrophone at the range interval from 500 miles to 750 miles, the difference in S/N values at 12.5 Hz and 100 Hz is only 4 dB. However, from Table I the source level at 12.5 Hz is 9.4 dB higher than that at 100 Hz. Normalizing to the same source level across the frequency band would yield a S/N difference of 13.4 dB instead of 4 dB between 12.5 Hz and 100 Hz.

VII ACKNOWLEDGMENTS

(C) This report represents only one of many resulting from a large cooperative exercise, CHURCH ANCHOR, designed to provide environmental acoustic data in the Northeastern Pacific. This exercise was sponsored by the Long Range Acoustic Propagation Project under the direction of R.D. Gaul.

(U) This specific report was generated by a cooperative effort at the Marine Physical

Laboratory and included the individual efforts of W.B. Fincke, R.E. Gorman, and D.E. Gleason. These persons assisted in all aspects of the data acquisition, data processing and analysis. This work was sponsored by the Office of Naval Research, Code 102-06, the Long Range Acoustic Propagation Project, through contract N00014-75-C-0749.

VIII REFERENCES

1. CHURCH ANCHOR Exercise Plan (U), Long Range Propagation Project Ocean Science Program, Maury Center for Ocean Science, Department of the Navy, Washington, D.C., June 1973. (CONFIDENTIAL)
2. CHURCH ANCHOR Environmental Acoustics Summary (U), Long Range Propagation Project, Ocean Science Program, Maury Center for Ocean Science, Department of the Navy, Washington, D.C., September 1974. (SECRET)
3. Bucca, P.J., "Sound Velocity Conditions During the CHURCH ANCHOR Exercise," (U), NOO TR 230, U.S. Naval Oceanographic Office, Washington, D.C., 1975.
4. CHURCH ANCHOR Explosive Source (SUS) Propagation Measurements (U), Applied Research Laboratories, The University of Texas at Austin, ARL-TR-74-53, December 1974. (CONFIDENTIAL)
5. "Estimated Accuracy for Acoustic Data from R/P FLIP-CHURCH ANCHOR," Underwater Systems Inc., Silver Springs, Maryland, March 1974.
6. Gaspin, J.B., and V.J. Shuler, "Source Levels of Shallow Underwater Explosions," Naval Ordnance Laboratory, NOLTR-71-160, 13 October 1971.
7. Weinstein, M.S. and R.J. Hecht, "SUS Quality Assessment, "Underwater Systems, Inc., Silver Spring, Maryland, June 1974.
8. Sheehy, M.J. and R. Hailey, "Measurements of the Attenuation of Low Frequency Sound," J. Acoust. Soc. Am., 29, pp. 464-469, 1957.
9. Draper, N.R. and H. Smith, Applied Regression Analysis, John Wiley & Sons, New York, 1966.
10. Davies, O.L., Statistical Methods in Research and Production, Hafner Publishing Co., New York, 1958.
11. Thorp, W.H., "Deep-Ocean Sound Attenuation in the Sub-and-Low-Kilocycle-per Second Region," J. Acoust. Soc. Am., 38, pp. 648-654, 1965.
12. Thorp, W.H., "Analytic Expression of the Low-Frequency Attenuation Coefficient," J. Acoust. Soc. Am., 42, p. 270, 1967.
13. Lovett, J.R., "Northeastern Pacific Sound Attenuation Using Low-Frequency CW Sources," J. Acoust. Soc. Am., 58, pp. 620-625, 1975.
14. "SUS Source Level Committee Report," Long Range Acoustic Propagation Project, Maury Center for Ocean Science, Department of the Navy, Washington, D.C. November 1975.
15. Urick, R.J., Principles of Underwater Sound for Engineers, McGraw-Hill Book Co., New York, 1967.

APPENDIX A

PROPAGATION LOSS VERSUS RANGE PLOTS

(U) The propagation loss values versus range in nautical miles discussed in Section V are given in Figures A-1 through A-7. Each figure consists of four plots, one for each hydrophone. The a-plots are for the shallowest sensor at 775 meters, b-plots are for the 2492 meter sensor, c-plots for the 4250 meter sensor, and d-plots for 5180 meter sensor.

(U) For the portion of the transmission run where the SUS were deployed from a ship with a nominal spacing of one nautical miles, the propagation loss values are plotted by connecting the values. Discontinuities in the line indicate that values were edited-out. The portion of the run where the SUS were deployed from aircraft, and the spacing is about eight miles, the propagation loss values are plotted as unconnected discrete symbols.

(U) Each plot is identified by the caption in the upper right corner. The "BN2060" refers to the USN SILAS BENT, run number 2, which was north of FLIP, and the 60 foot source depth. The "H 1," "H 12," "H 15," and "H 21" are the hydrophone number designations and are followed by the hydrophone depth in meters. The final entry gives the geometric mean frequency of the filter band and whether it is one-octave or one-third of an octave wide.

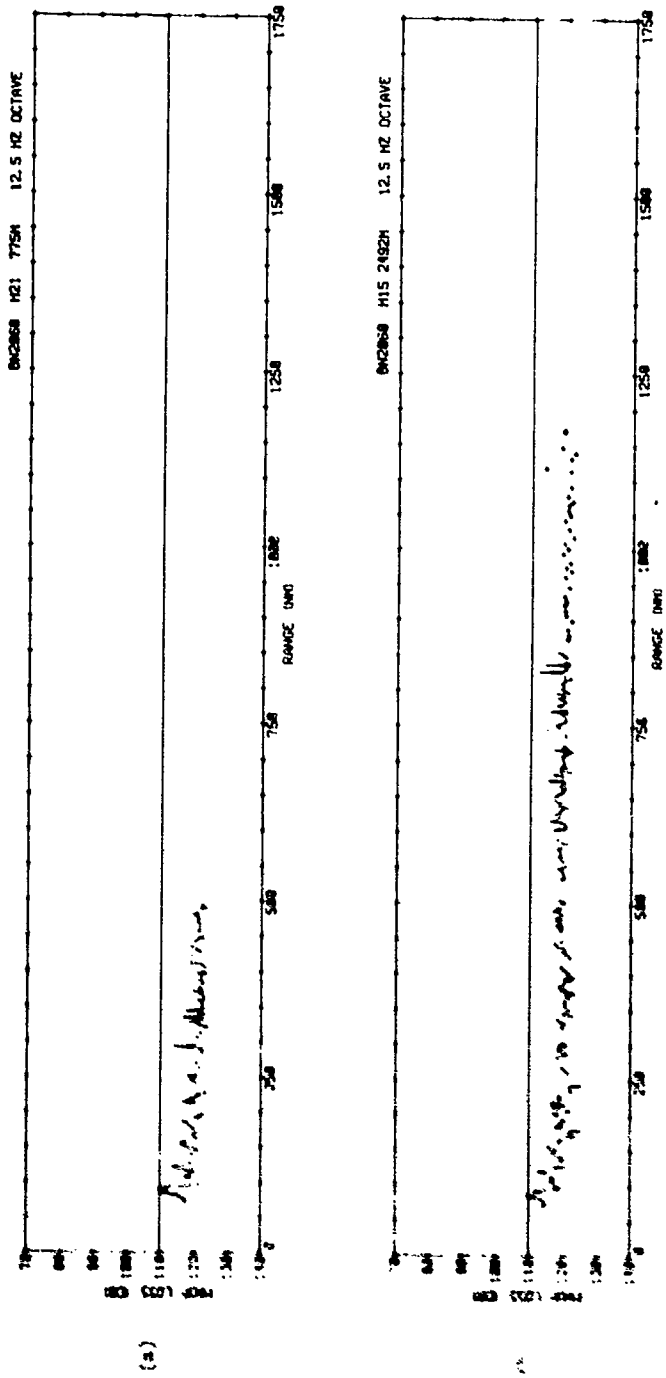

(a)

Figure A-1

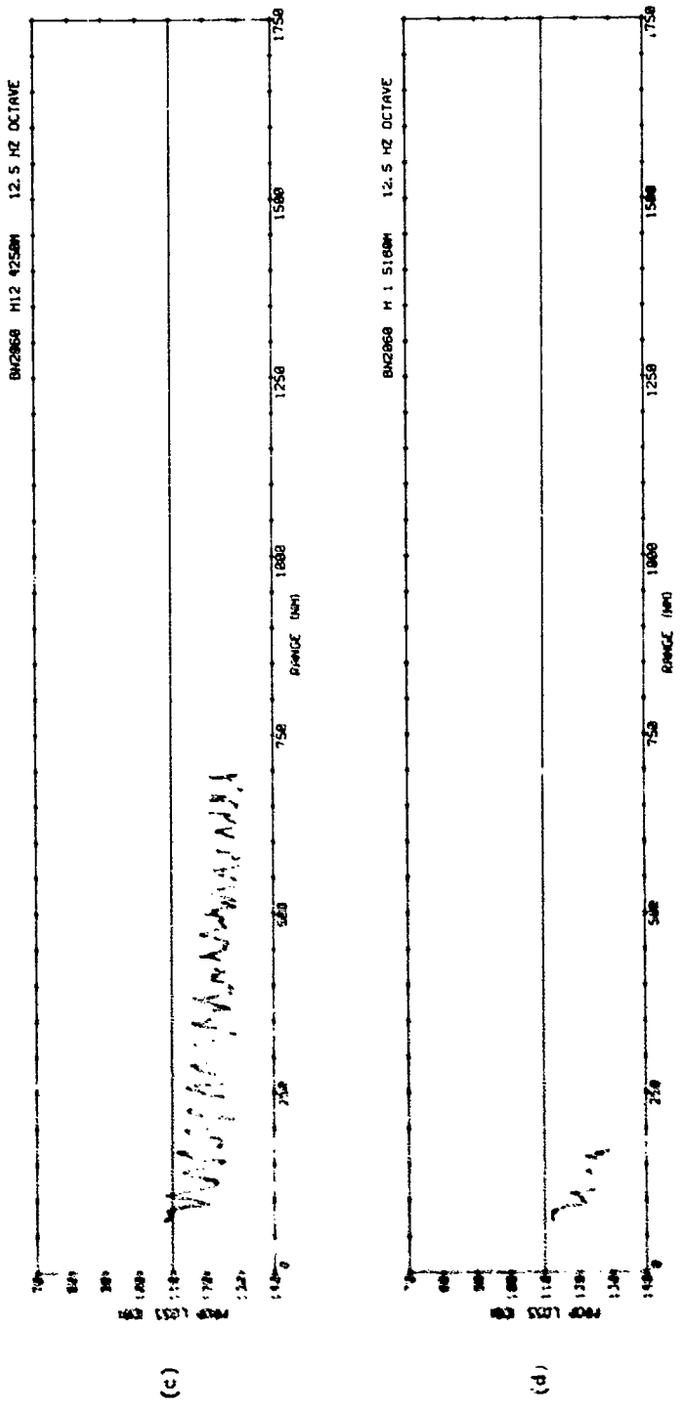
BW2050 M12 4250M 12.5 HZ OCTAVE
BW2050 M 1 5160M 12.5 HZ OCTAVE
RANGE (NM)
RANGE (NM)
(c)
(d)

Figure A-1

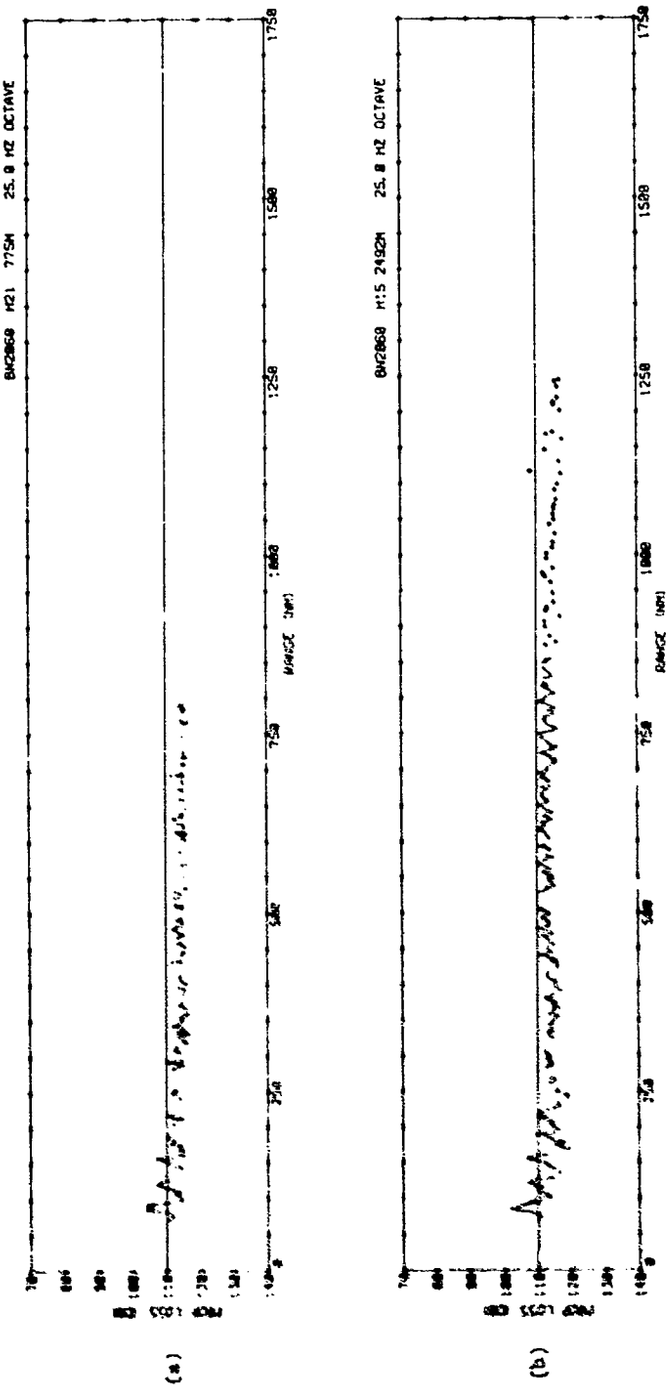
BW2868 M21 775M 25.0 HZ OCTAVE
BW2868 M:5 2492M 25.0 HZ OCTAVE
RANGE (NM)
(a)
(b)

Figure A-2

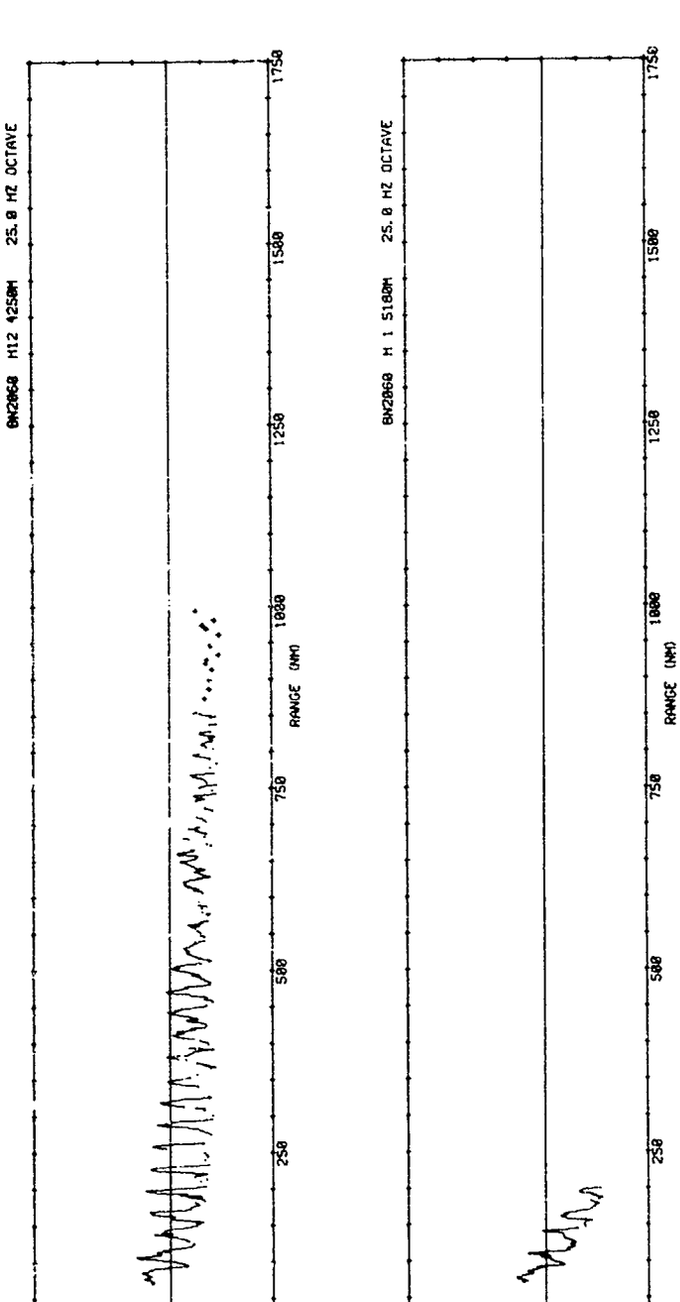
BW2060 H12 4250M 25.0 HZ OCTAVE
BW2060 H 1 5180M 25.0 HZ OCTAVE
PROP LOSS (DB)
RANGE (NM)
0
250
500
750
1000
1250
1500
1750
70
80
90
100
110
120
130
140

(c) (d)

Figure A-2

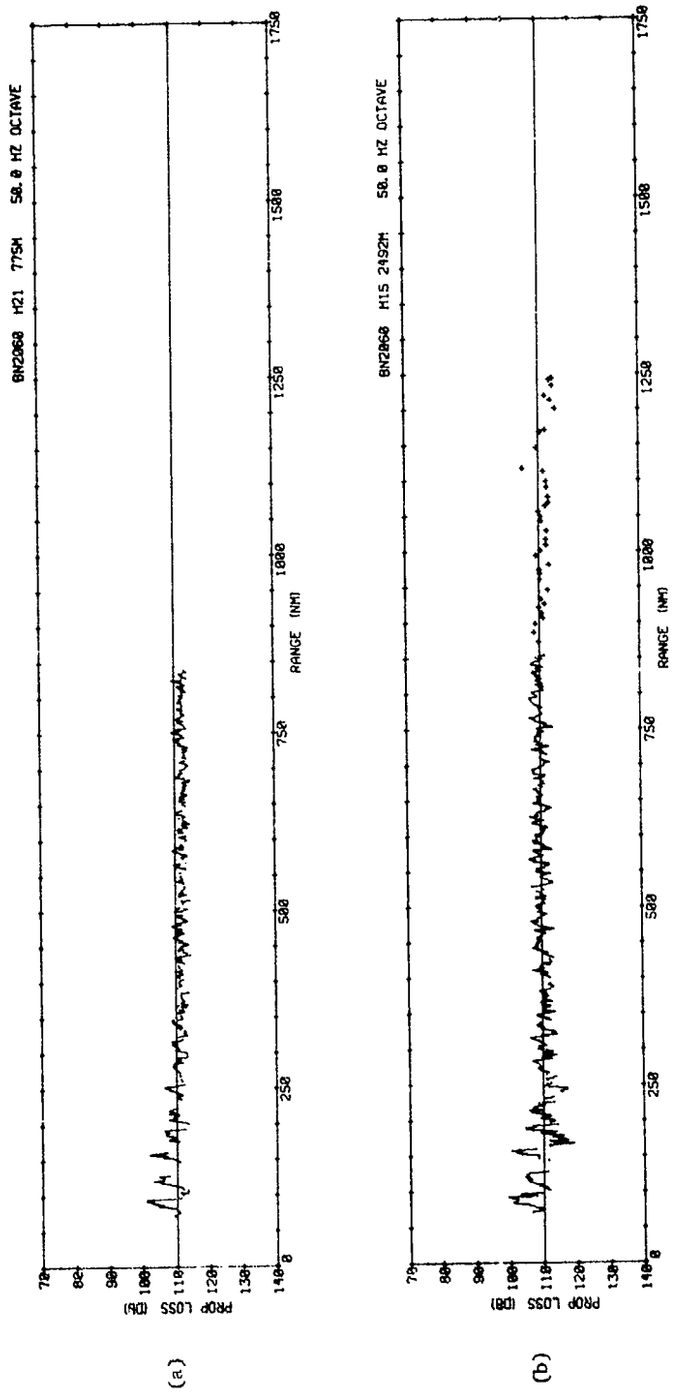
BN2060 M21 775M 50.0 HZ OCTAVE
PROP LOSS (DB)
RANGE (NM)
0
250
500
750
1000
1250
1500
1750
70
80
90
100
110
120
130
140
(a)
BN2060 M15 2492M 50.0 HZ OCTAVE
PROP LOSS (DB)
RANGE (NM)
(b)

Figure A-3

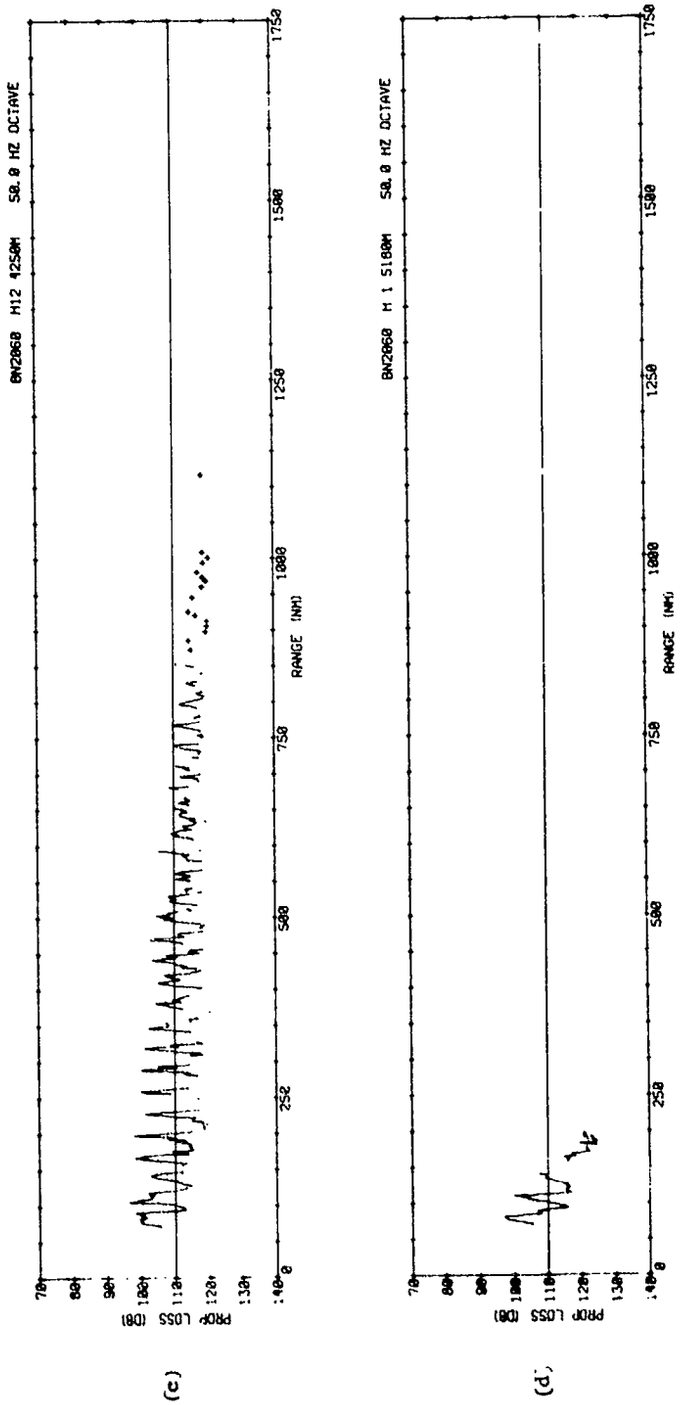
BW2060 M12 4250M 50.0 HZ OCTAVE
PROP LOSS (DB)
RANGE (NM)
(c)
BW2060 M 1 5180M 50.0 HZ OCTAVE
PROP LOSS (DB)
RANGE (NM)
(d)

Figure A-3

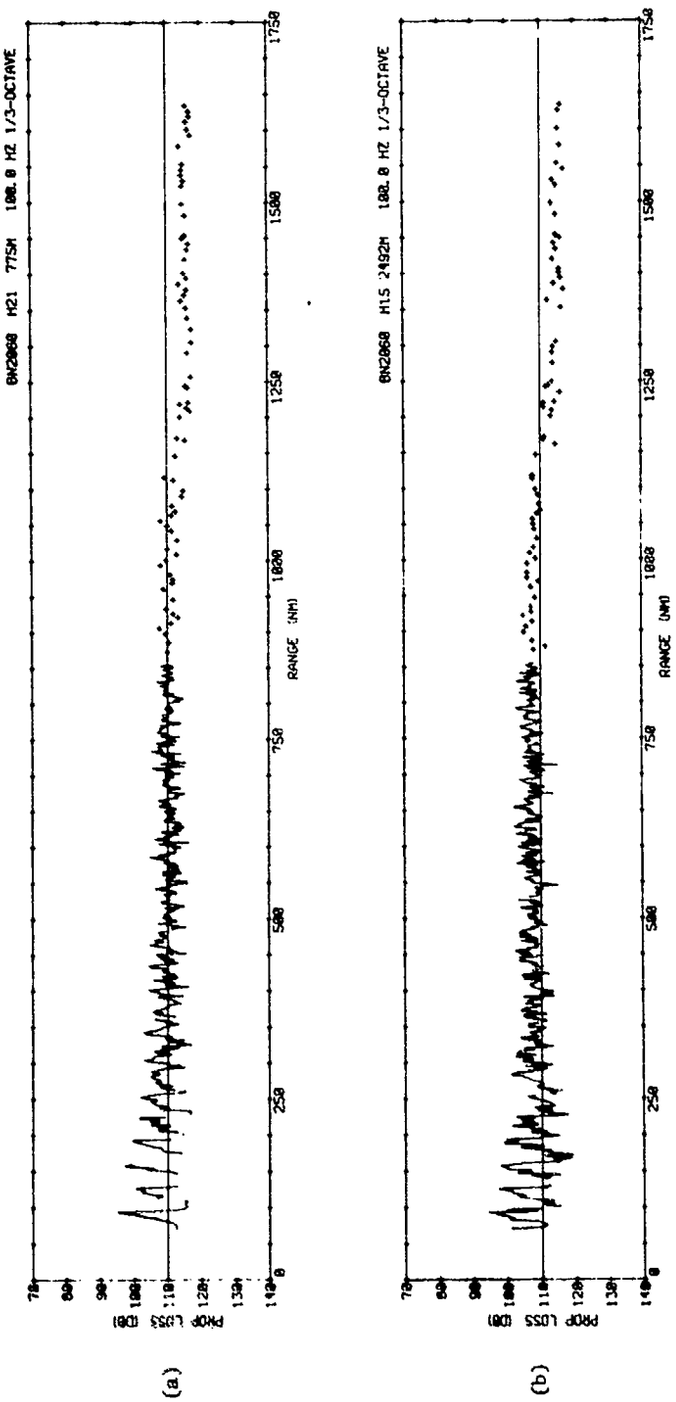
BN2868 M21 775M 100.0 HZ 1/3-OCTAVE
BN2868 M15 2492M 100.0 HZ 1/3-OCTAVE
PROP LOSS (DB)
RANGE (NM)
(a)
(b)

Figure A-4

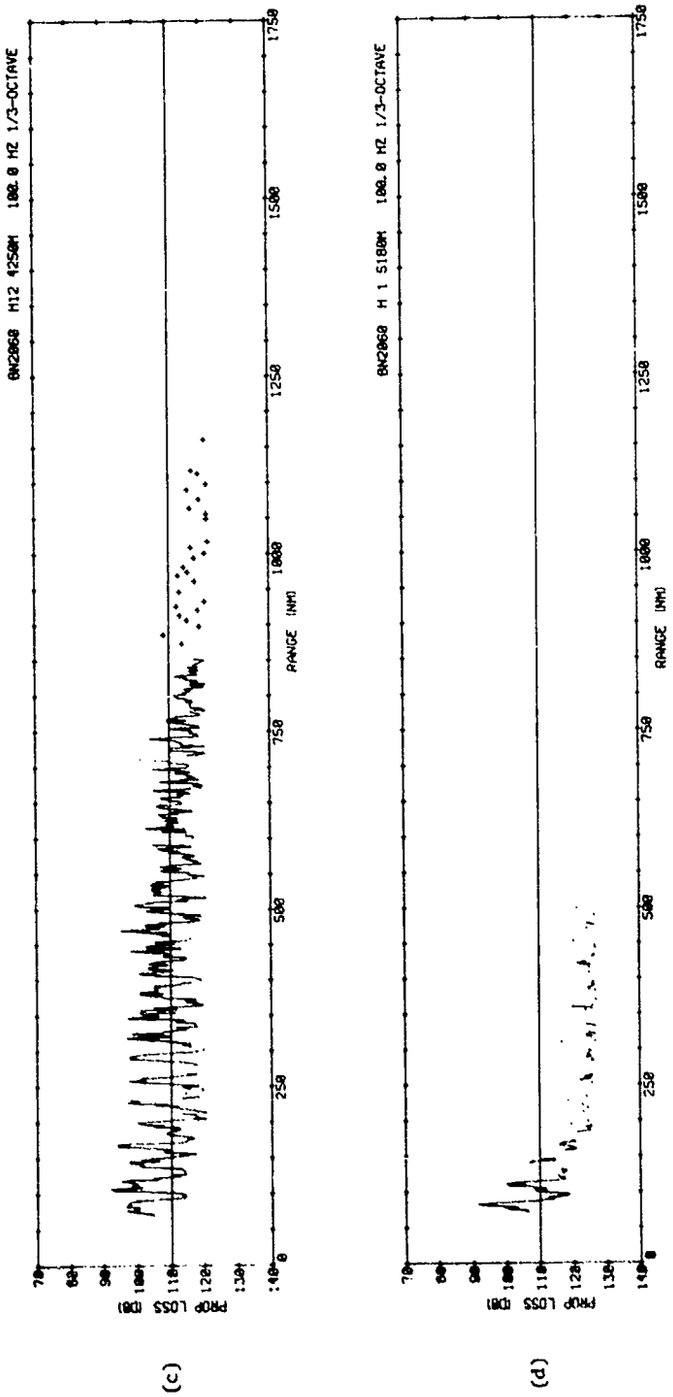
BN2868 M12 425BM 100.0 HZ 1/3-OCTAVE
PROP LOSS (DB)
RANGE (NM)
(c)
BN2868 M 1 518BM 100.0 HZ 1/3-OCTAVE
PROP LOSS (DB)
RANGE (NM)
(d)

Figure A-4

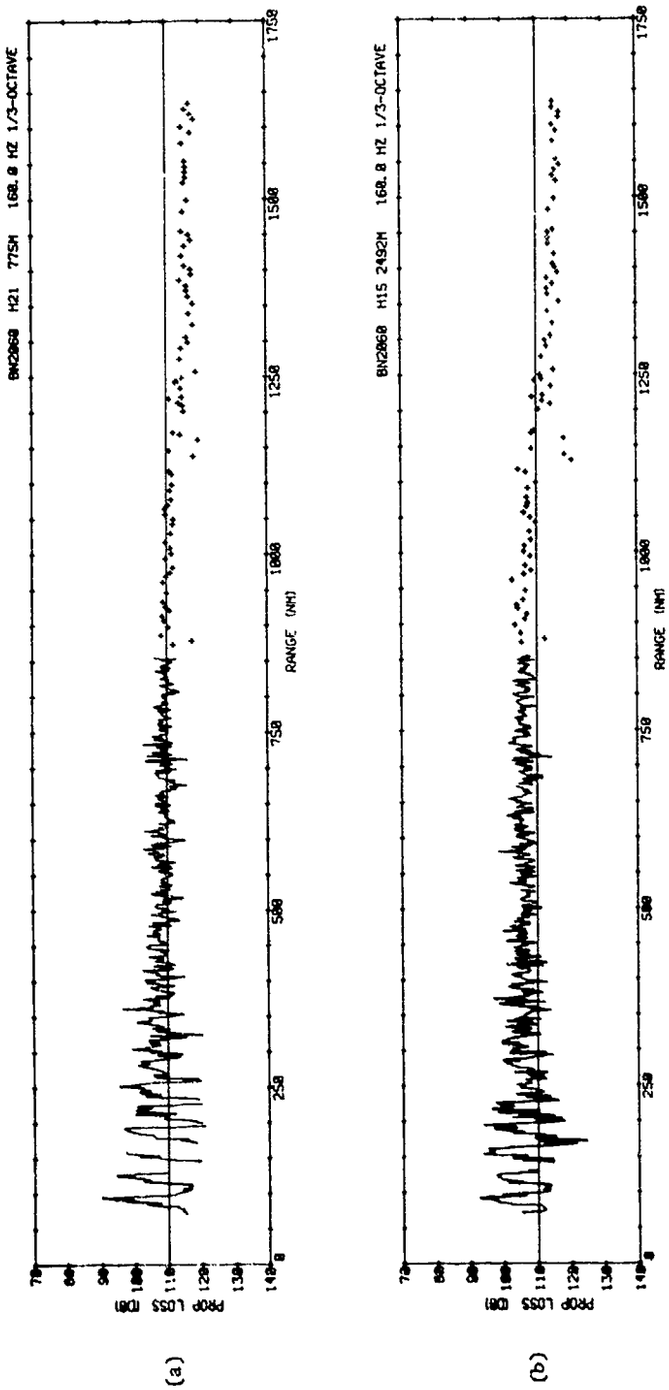
BN2060 H21 775M 160.0 HZ 1/3-OCTAVE
PROP LOSS (DB)
RANGE (NM)
(a)
BN2060 H15 2492M 160.0 HZ 1/3-OCTAVE
PROP LOSS (DB)
RANGE (NM)
(b)

Figure A-5

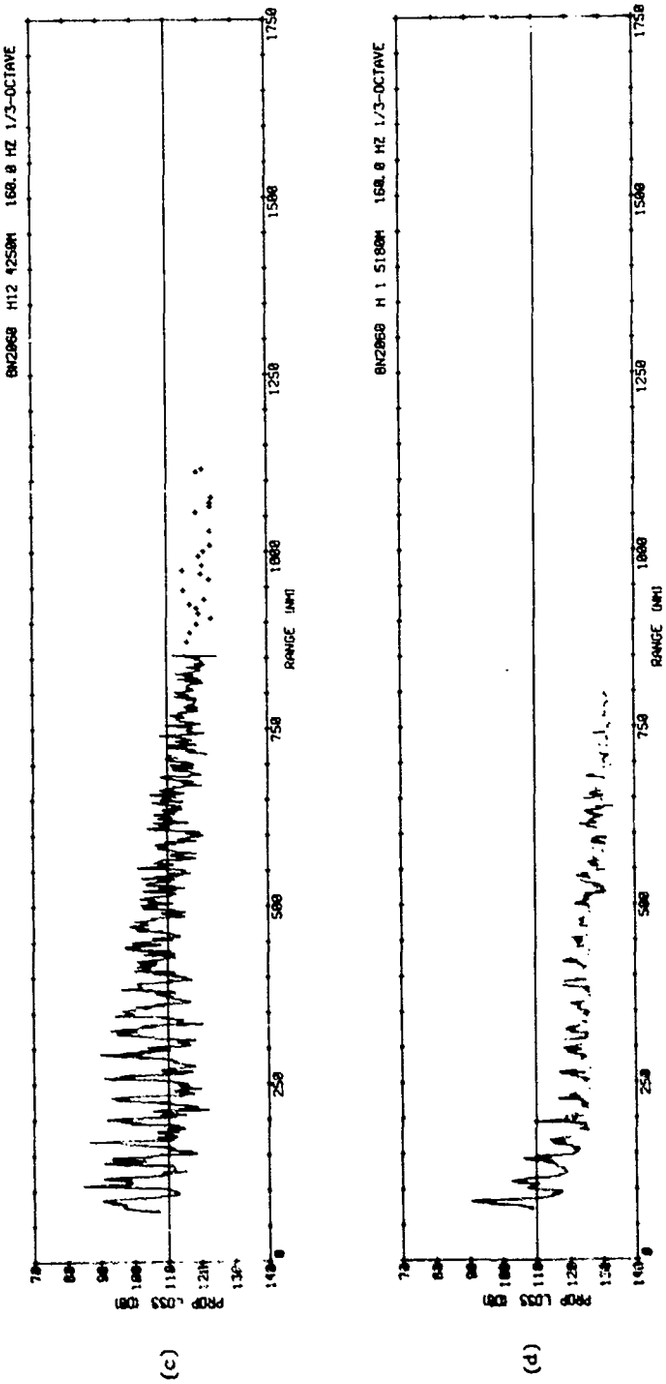
BW2060 H12 4250M 160.0 HZ 1/3-OCTAVE
RANGE (NMI)
PROP LOSS (DB)
(c)
BW2060 H 1 5100M 160.0 HZ 1/3-OCTAVE
RANGE (NMI)
PROP LOSS (DB)
(d)

Figure A-5

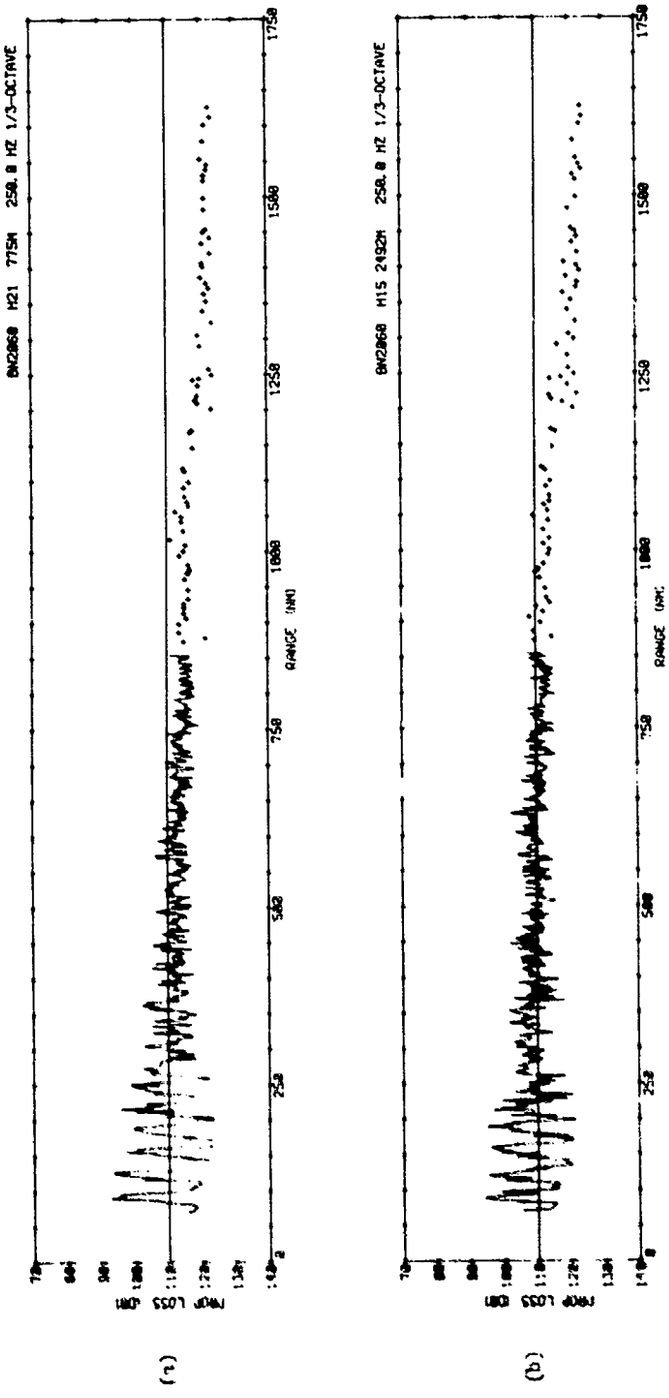
BW2868 H21 775M 250.0 HZ 1/3-OCTAVE
BW2868 H15 2492M 250.0 HZ 1/3-OCTAVE
RANGE (NM)
(a)
(b)

Figure A-6

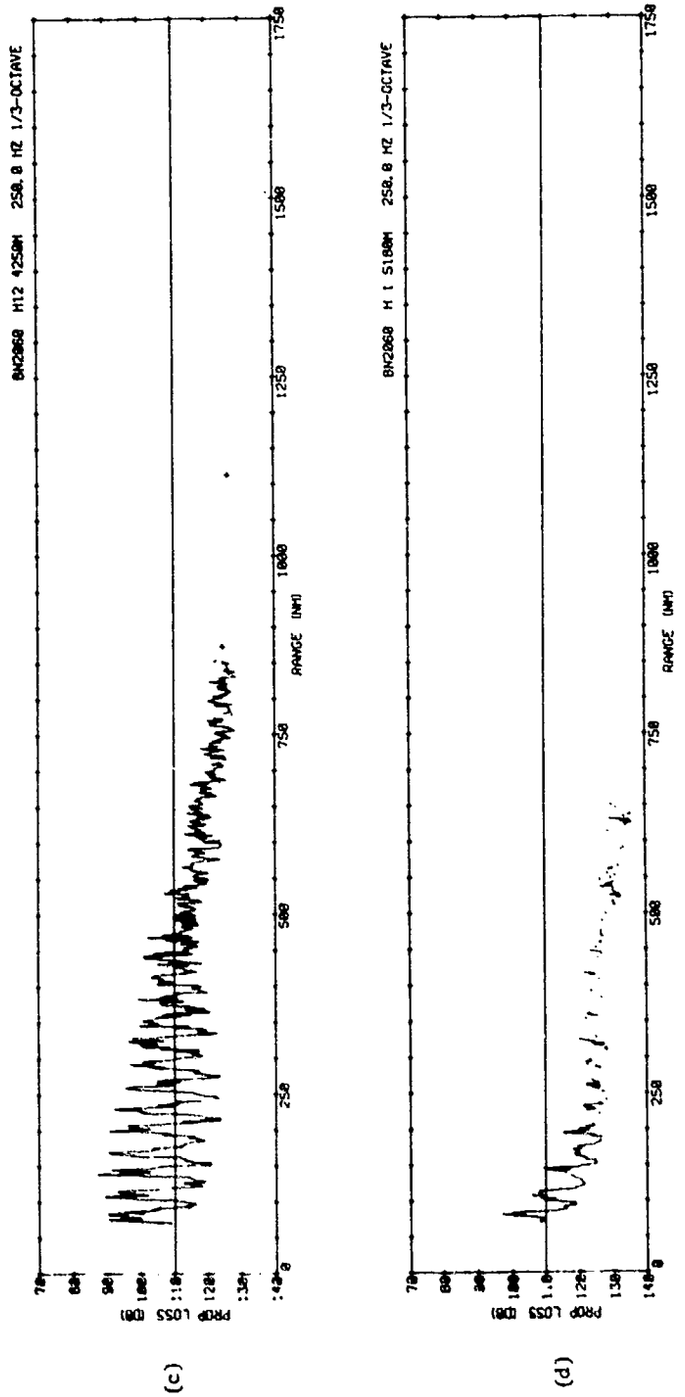
BN2060 H12 4250M 250.0 HZ 1/3-OCTAVE
RANGE (NM)
PROP LOSS (DB)
(c)
BN2060 H 1 5100M 250.0 HZ 1/3-OCTAVE
RANGE (NM)
PROP LOSS (DB)
(d)

Figure A-6

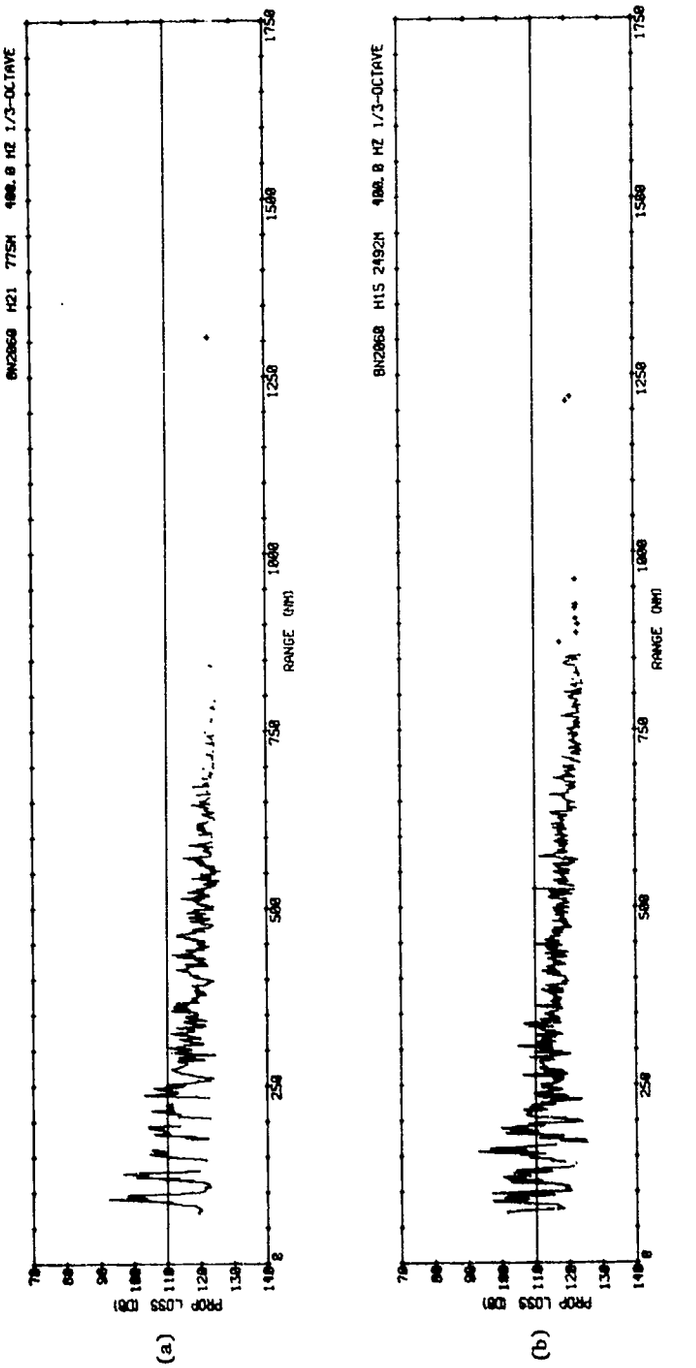
BN2060 H21 775M 400.0 HZ 1/3-OCTAVE
BN2060 H15 2492M 400.0 HZ 1/3-OCTAVE
RANGE (NM)
PROP LOSS (DB)
(a)
(b)

Figure A-7

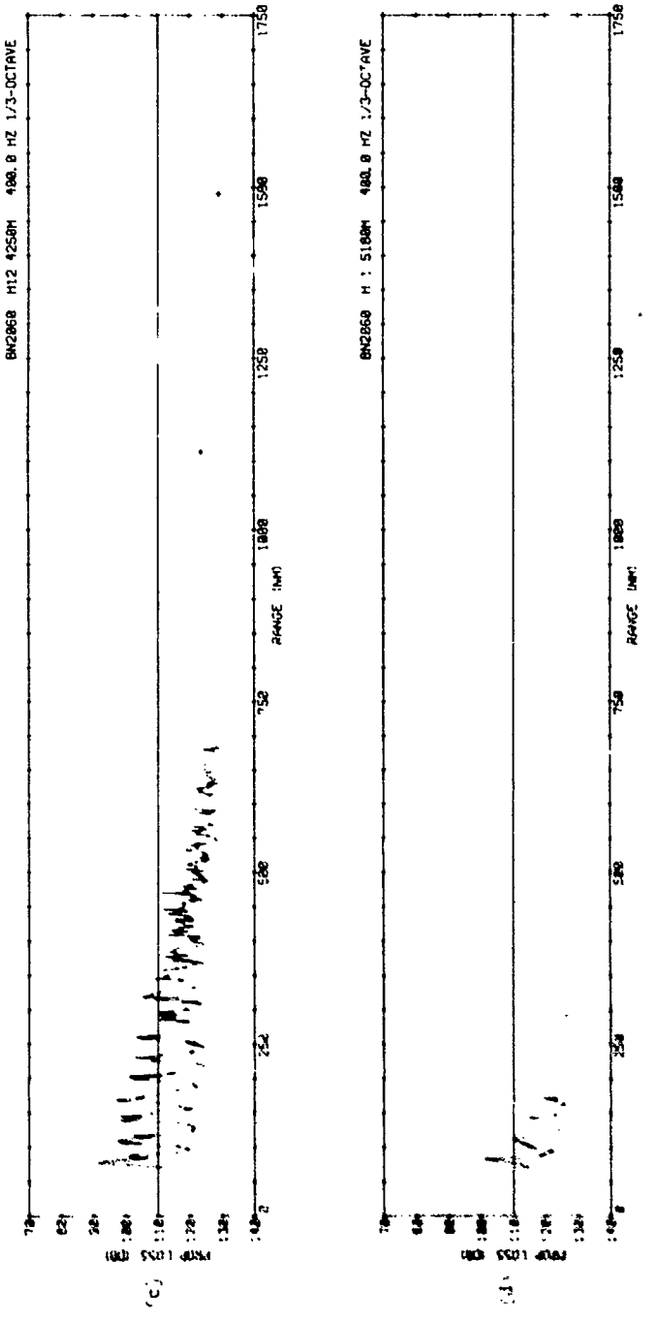
BW2868 M12 4250M 400.0 HZ 1/3-OCTAVE
BW2868 M : 5100M 400.0 HZ 1/3-OCTAVE
RANGE (NM)
1750
1500
1250
1000
750
500
250
0

Figure A-7

APPENDIX B

DIFFERENTIAL PROPAGATION LOSS VERSUS RANGE PLOTS

(U) The differential propagation loss values versus range plots discussed in Section V are given in Figures B-1 through B-7. Each figure consists of two plots, the a-plots are for the hydrophone at 775 meters and the b-plots are for the hydrophone at 2492 meters. The differential propagation loss values are differences between the prop loss at the frequency band given in the upper right corner and the prop loss for the 50 Hz octave band. The straight line passing through the data is the least squares fit to the values occurring between the minimum range of 300 miles and the maximum range of 1100 miles.

(U) As was the case for the propagation loss plots in Appendix A, the ship deployed portion of the run are plotted by connecting points while the aircraft portion of the run are plotted as discrete symbols.

(U) As in Appendix A each plot is identified by the caption in the upper right corner.

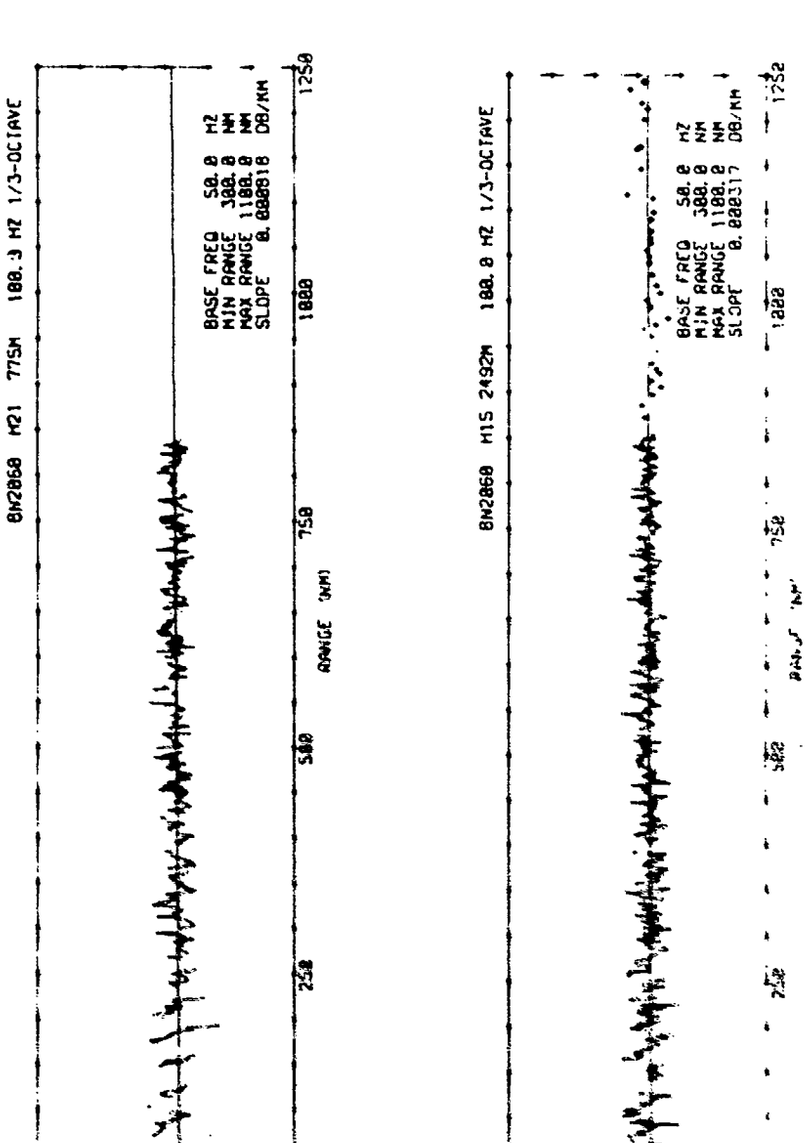
8N2868 M21 77SM 180.3 HZ 1/3-OCTAVE
BASE FREQ 50.0 HZ
MIN RANGE 300.0 NM
MAX RANGE 1100.0 NM
SLOPE 0.000018 DB/KM
RANGE (NM)
8N2868 M1S 2492M 180.0 HZ 1/3-OCTAVE
BASE FREQ 50.0 HZ
MIN RANGE 300.0 NM
MAX RANGE 1100.0 NM
SLOPE 0.000317 DB/KM

Figure 5-1

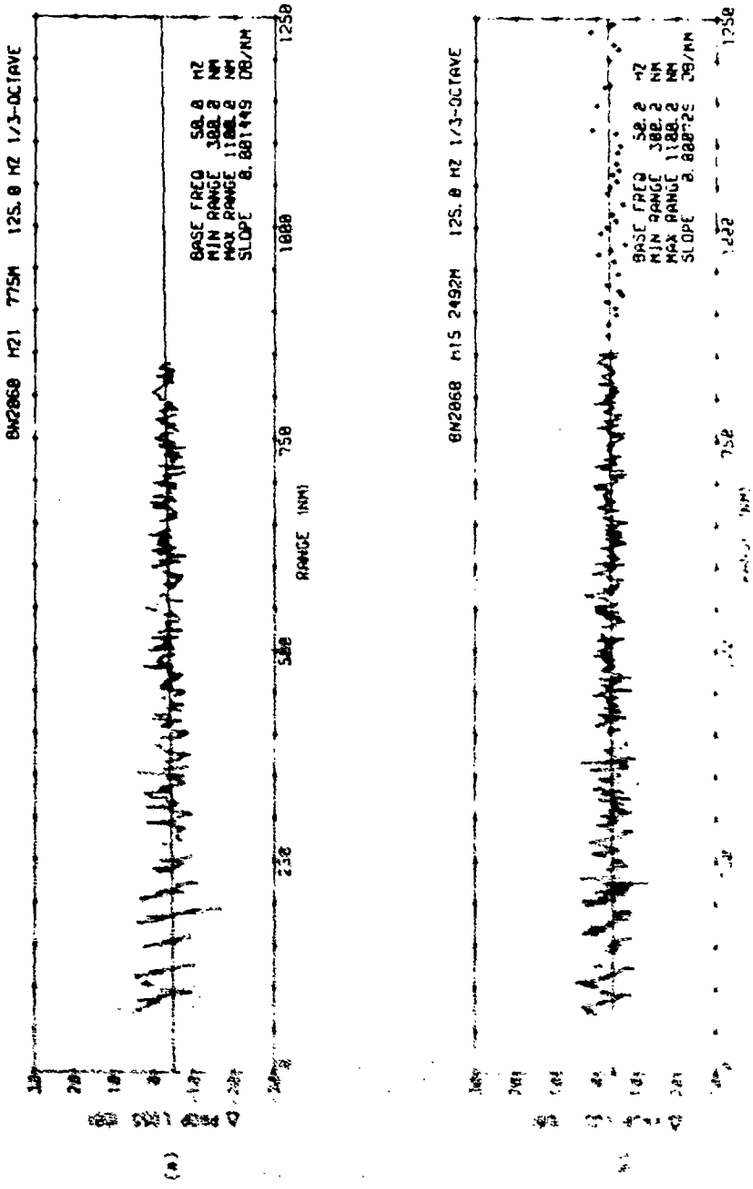

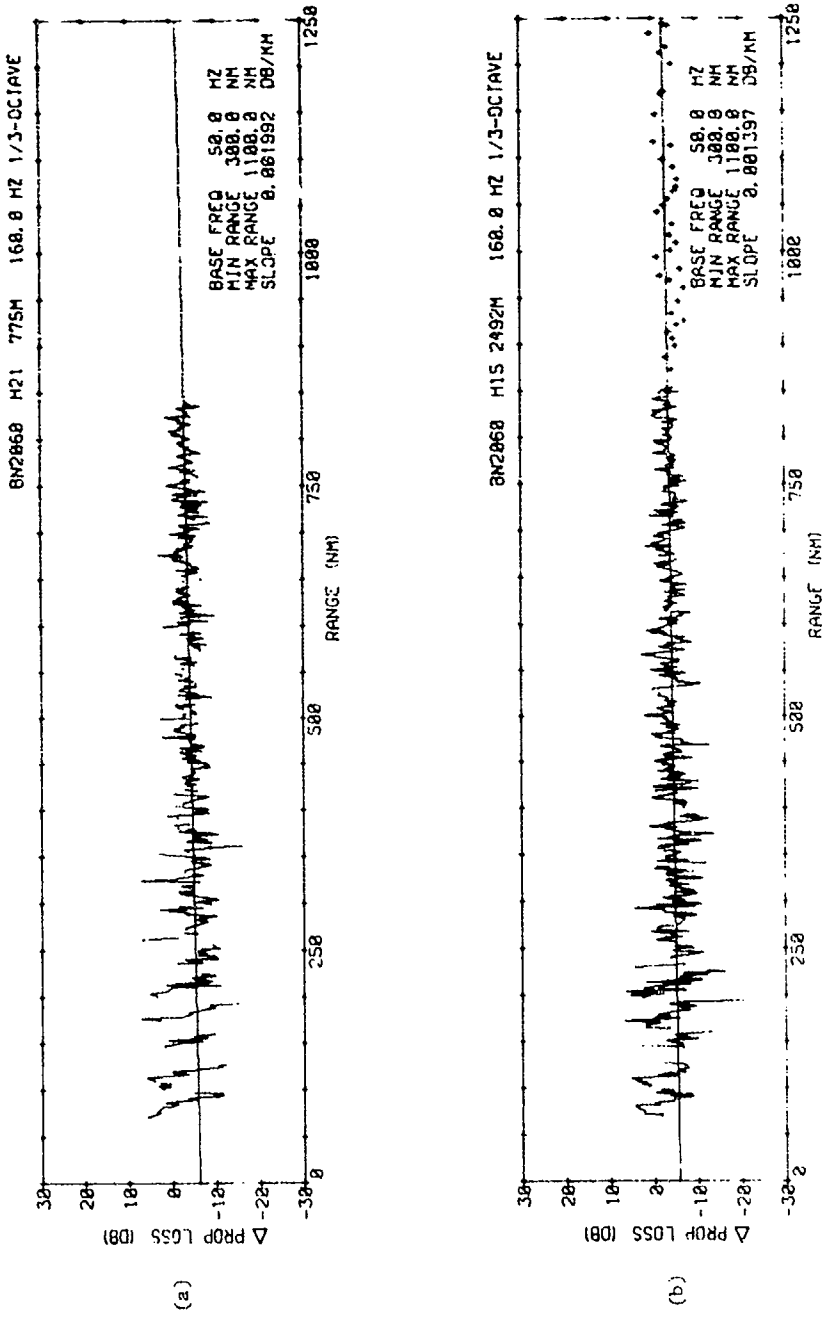
BW2868 H21 775M 160.0 HZ 1/3-OCTAVE
BASE FREQ 50.0 HZ
MIN RANGE 300.0 NM
MAX RANGE 1100.0 NM
SLOPE 0.001992 DB/KM
Δ PROP LOSS (DB)
RANGE (NM)
(a)
BW2868 H1S 2492M 160.0 HZ 1/3-OCTAVE
BASE FREQ 50.0 HZ
MIN RANGE 300.0 NM
MAX RANGE 1100.0 NM
SLOPE 0.001397 DB/KM
Δ PROP LOSS (DB)
RANGE (NM)
(b)

Figure B-3

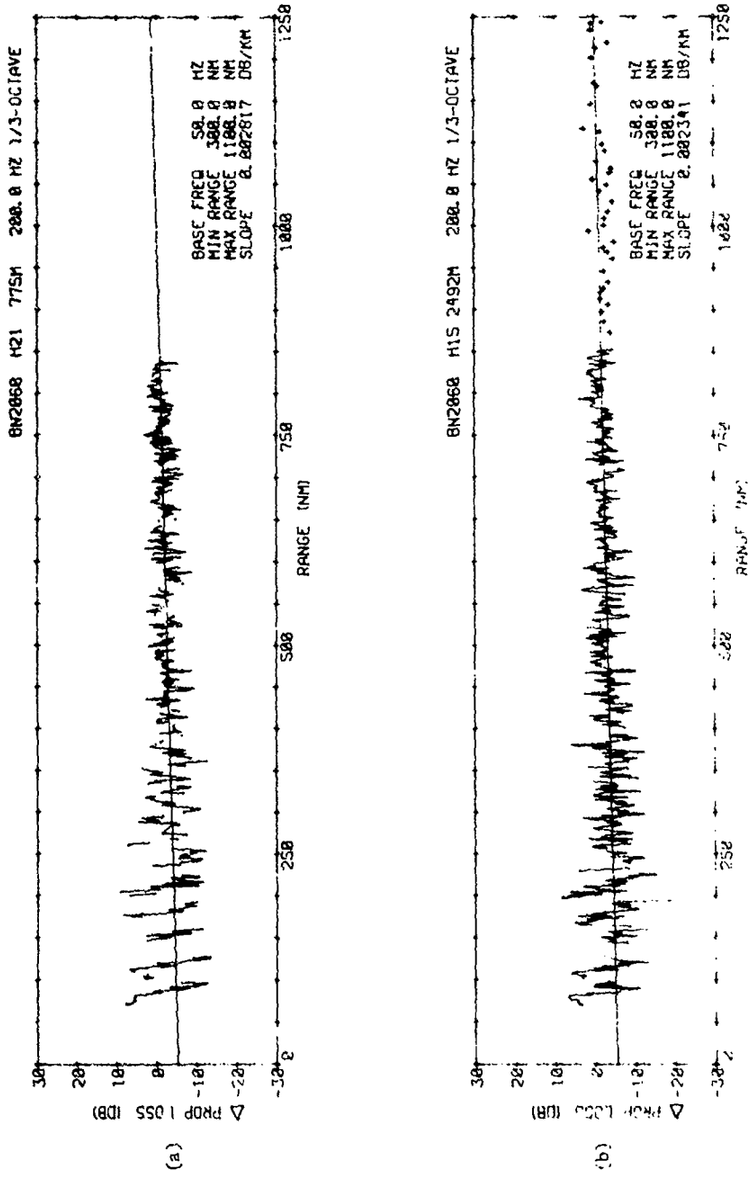

Figure B-4

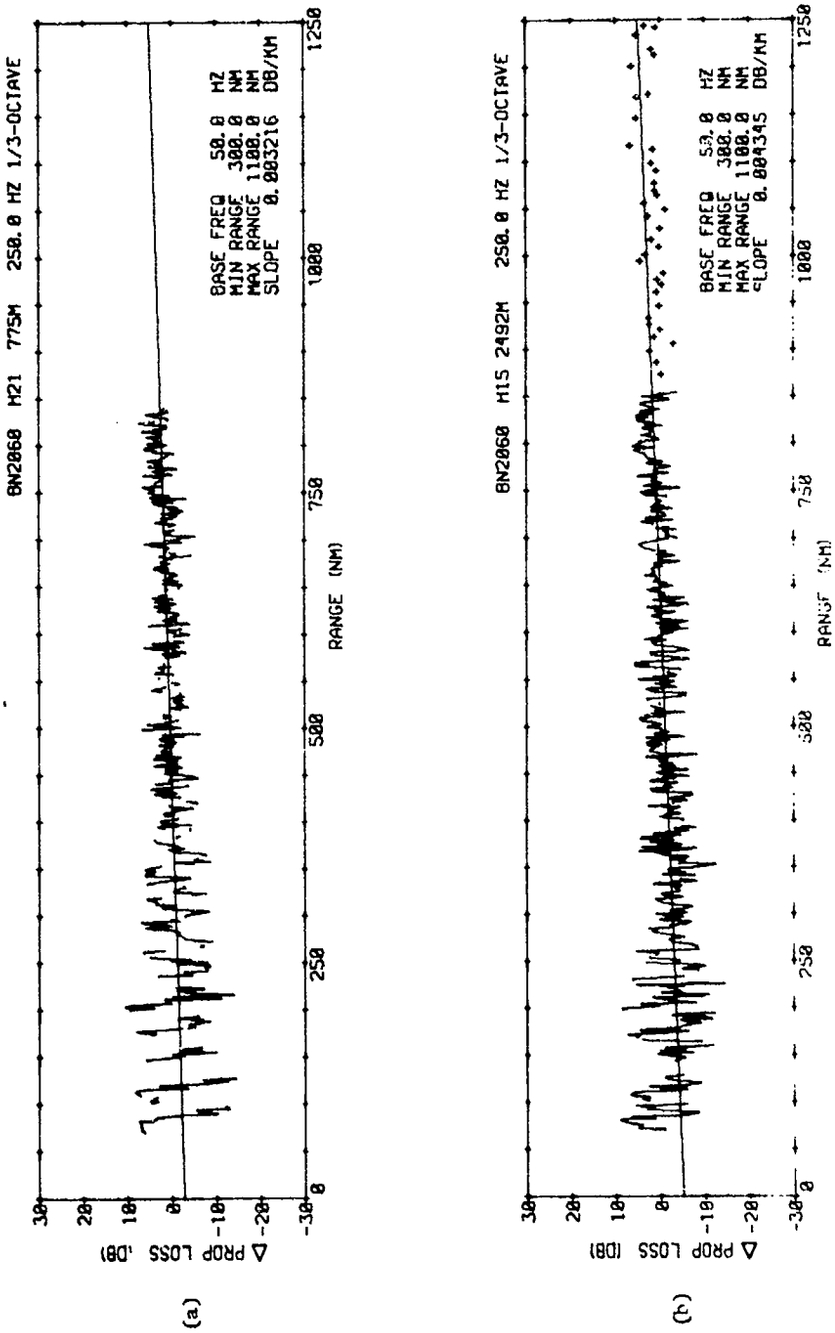
BN2060 M21 775M 250.0 HZ 1/3-OCTAVE
BASE FREQ 50.0 HZ
MIN RANGE 300.0 NM
MAX RANGE 1100.0 NM
SLOPE 0.003216 DB/KM
Δ PROP LOSS (DB)
RANGE (NM)
(a)
BN2060 M15 2492M 250.0 HZ 1/3-OCTAVE
BASE FREQ 50.0 HZ
MIN RANGE 300.0 NM
MAX RANGE 1100.0 NM
SLOPE 0.004345 DB/KM
Δ PROP LOSS (DB)
RANGE (NM)
(b)

Figure B-5

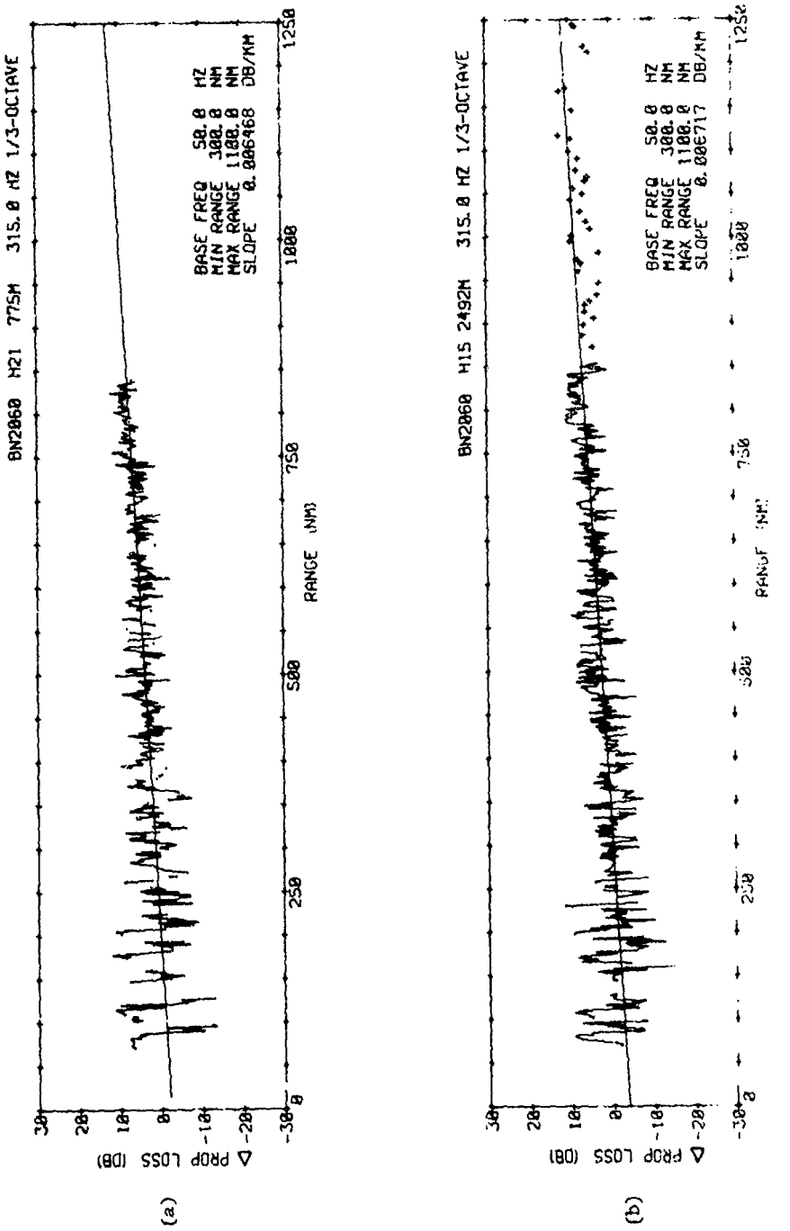

Figure B-6

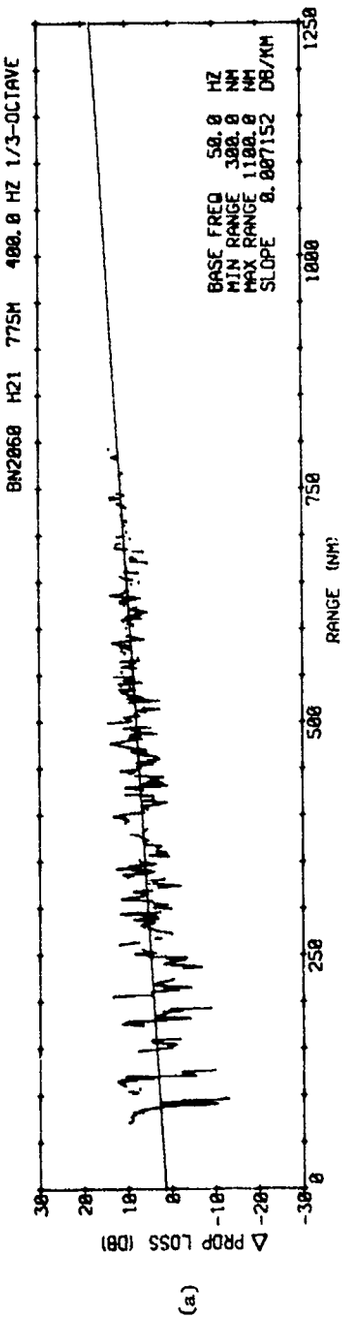
BN2060 H21 775M 400.0 HZ 1/3-OCTAVE
BASE FREQ 50.0 HZ
MIN RANGE 300.0 NM
MAX RANGE 1100.0 NM
SLOPE 0.007152 DB/KM
Δ PROP LOSS (DB)
RANGE (NM)
30
20
10
0
-10
-20
-30
0
250
500
750
1000
1250

(a)

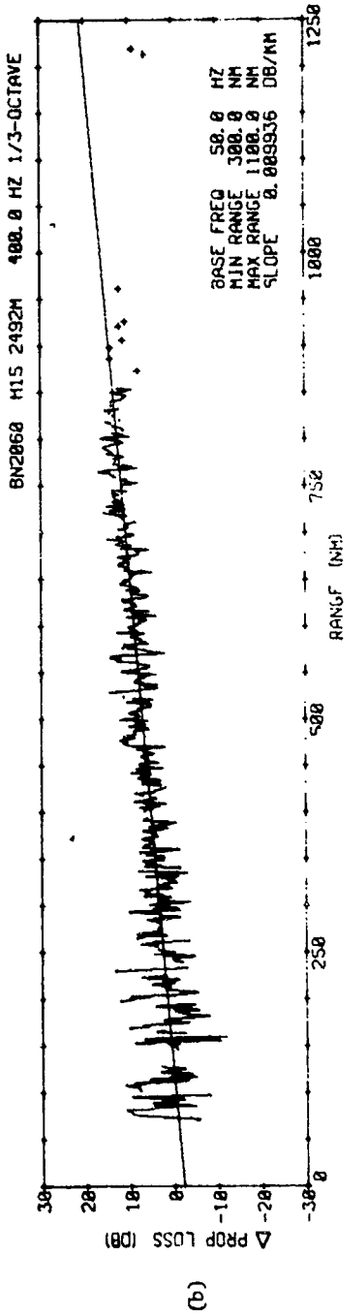
BN2060 H15 2492M 400.0 HZ 1/3-OCTAVE
BASE FREQ 50.0 HZ
MIN RANGE 300.0 NM
MAX RANGE 1100.0 NM
SLOPE 0.009936 DB/KM
Δ PROP LOSS (DB)
RANGE (NM)
30
20
10
0
-10
-20
-30
0
250
500
750
1000
1250

(b)

B-7

APPENDIX C

SIGNAL-TO-NOISE RATIO VERSUS RANGE PLOTS

(U) The signal-to-average ambient noise ratio values versus range plots discussed in Section VI are given in Figures C-1 through C-7. As in Appendix A each figure consists of four plots, one for each hydrophone.

(U) The ship portion of the run is again depicted by lines connecting the values whereas the aircraft portion of the run is given by discrete symbols.

(U) The captions in the upper right corner identify each plot as to the hydrophone depth and frequency band.

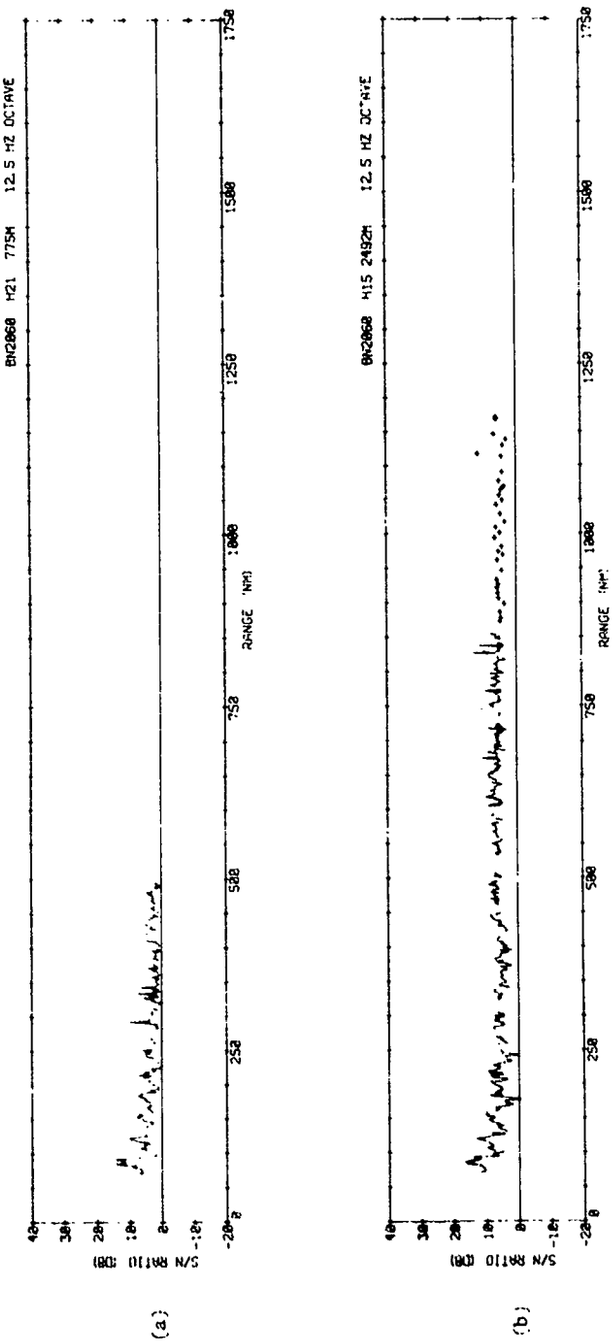
BN2868 H21 775M 12.5 HZ OCTAVE
BN2868 H15 2492M 12.5 HZ OCTAVE
S/N RATIO (DB)
RANGE (NM)
40
30
20
10
0
-10
-20
0
250
500
750
1000
1250
1500
1750
(a)
(b)

Figure C-1

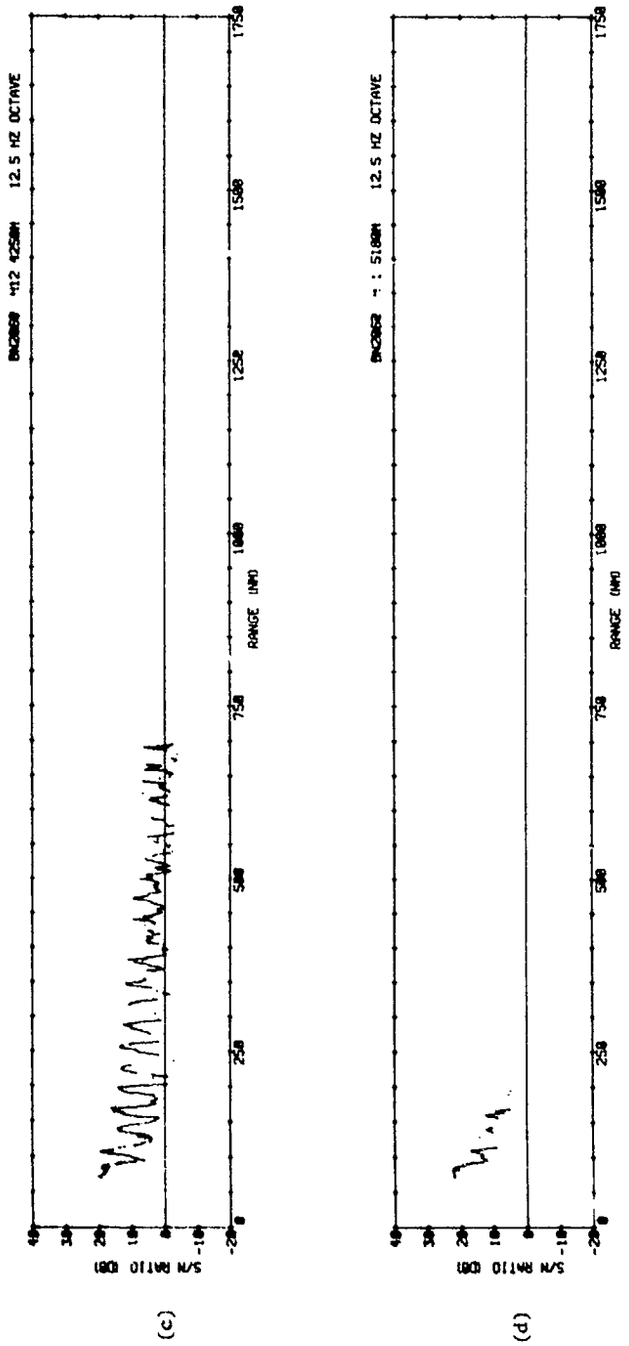
12.5 HZ OCTAVE
S/N RATIO (DB)
RANGE (NMI)
(c)
12.5 HZ OCTAVE
S/N RATIO (DB)
RANGE (NMI)
(d)

Figure C-1

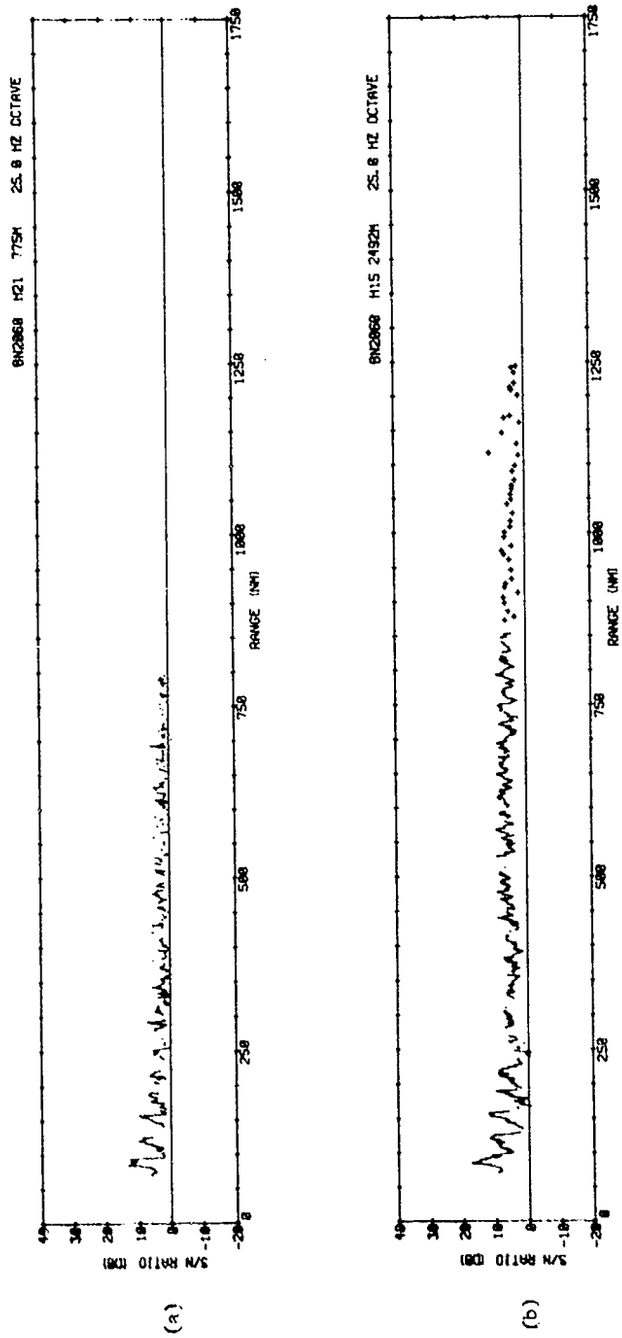
BN2868 H21 775M 25.8 HZ OCTAVE
BN2868 H15 2492M 25.8 HZ OCTAVE
S/N RATIO (DB)
RANGE (NM)
0
250
500
750
1000
1250
1500
1750
40
30
20
10
0
-10
-20
(a)
(b)

Figure C-2

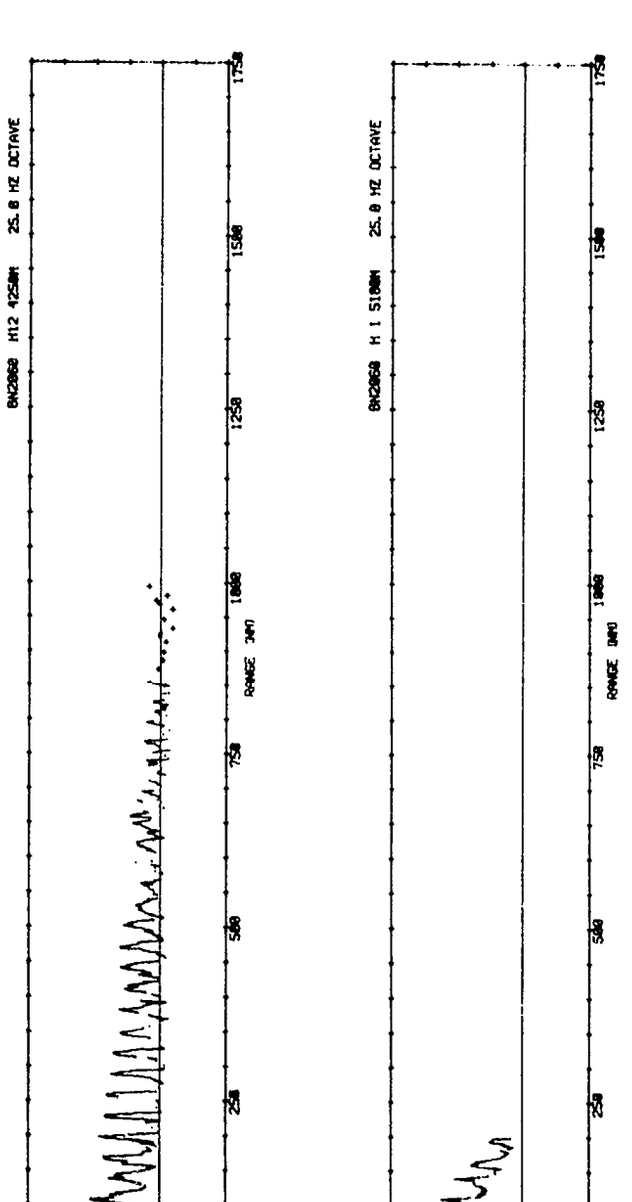
BH2868 H12 425BH 25.0 HZ OCTAVE
BH2868 H 1 S108H 25.0 HZ OCTAVE
RANGE 2NM
S/N RATIO (DB)
(c)
(d)

Figure C-2

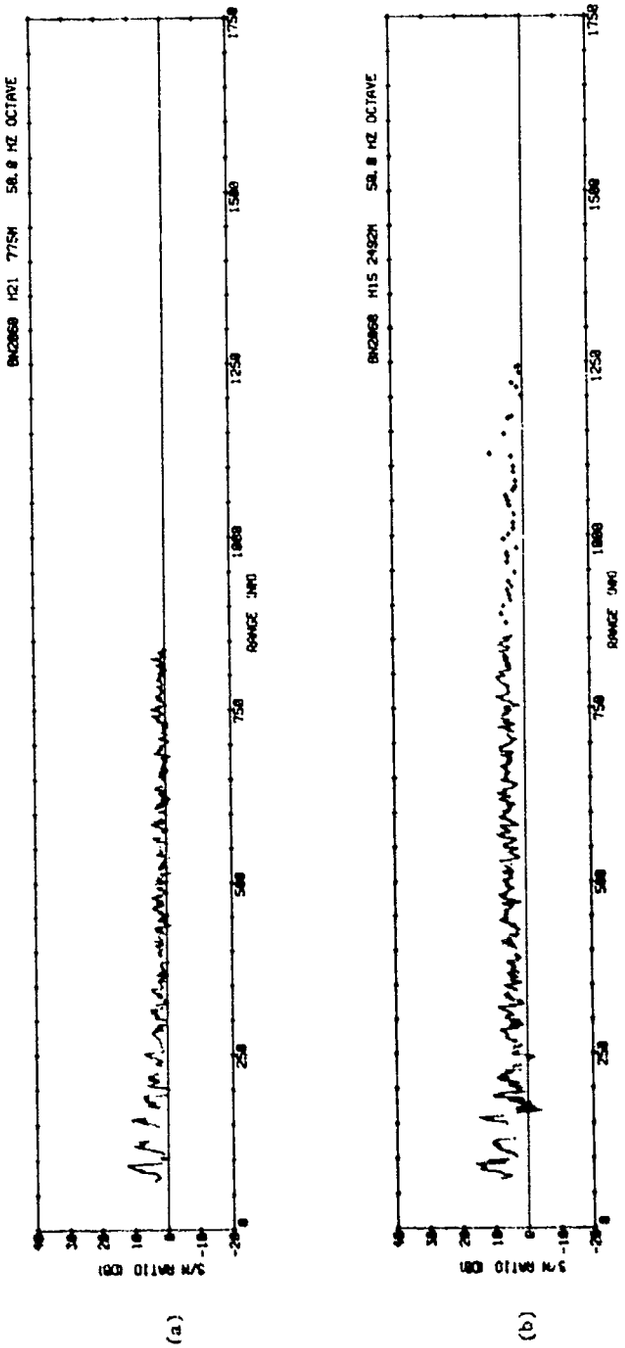
BNDBSB H21 775M 50.8 HZ OCTAVE
BNDBSB H15 2492M 50.8 HZ OCTAVE
S/N RATIO (DB)
RANGE (NM)
(a)
(b)

Figure C-3

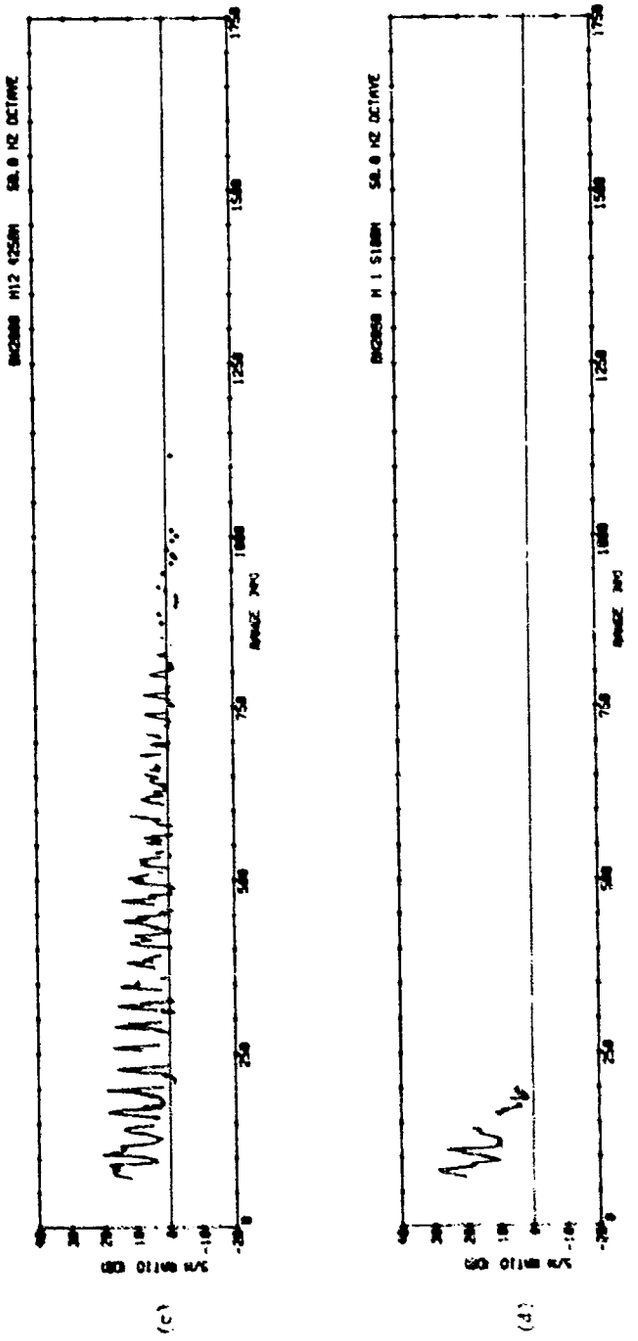

Figure C-3

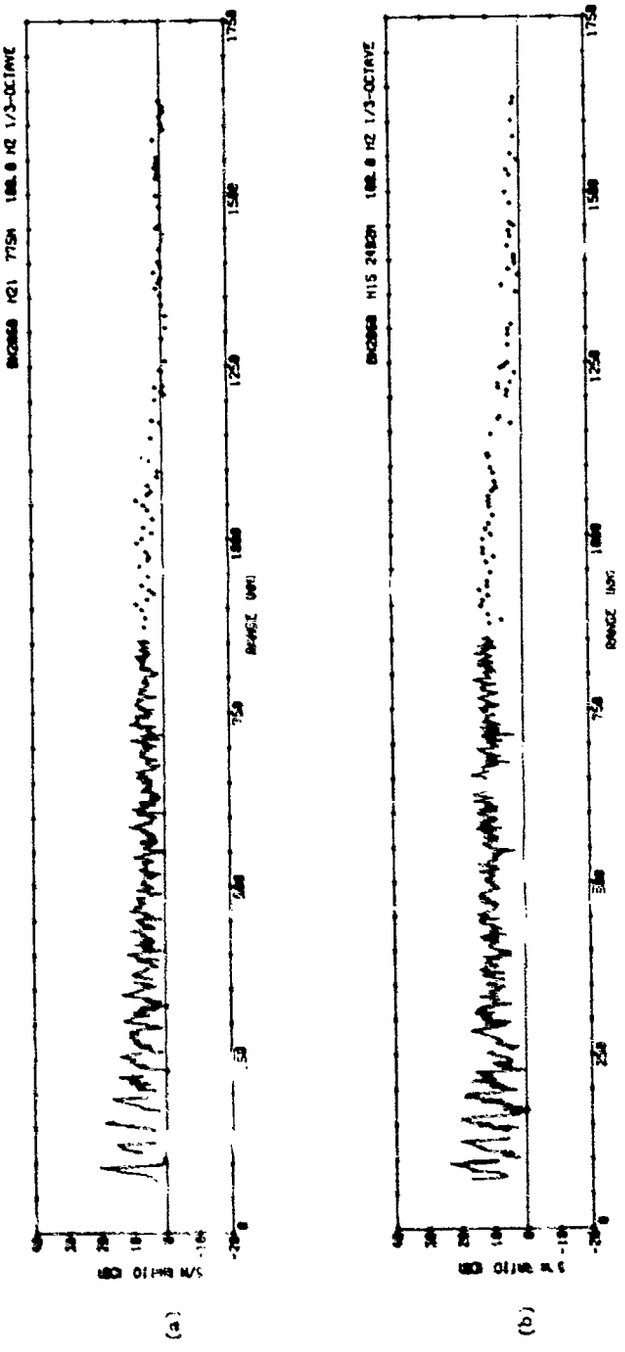

Figure C-4

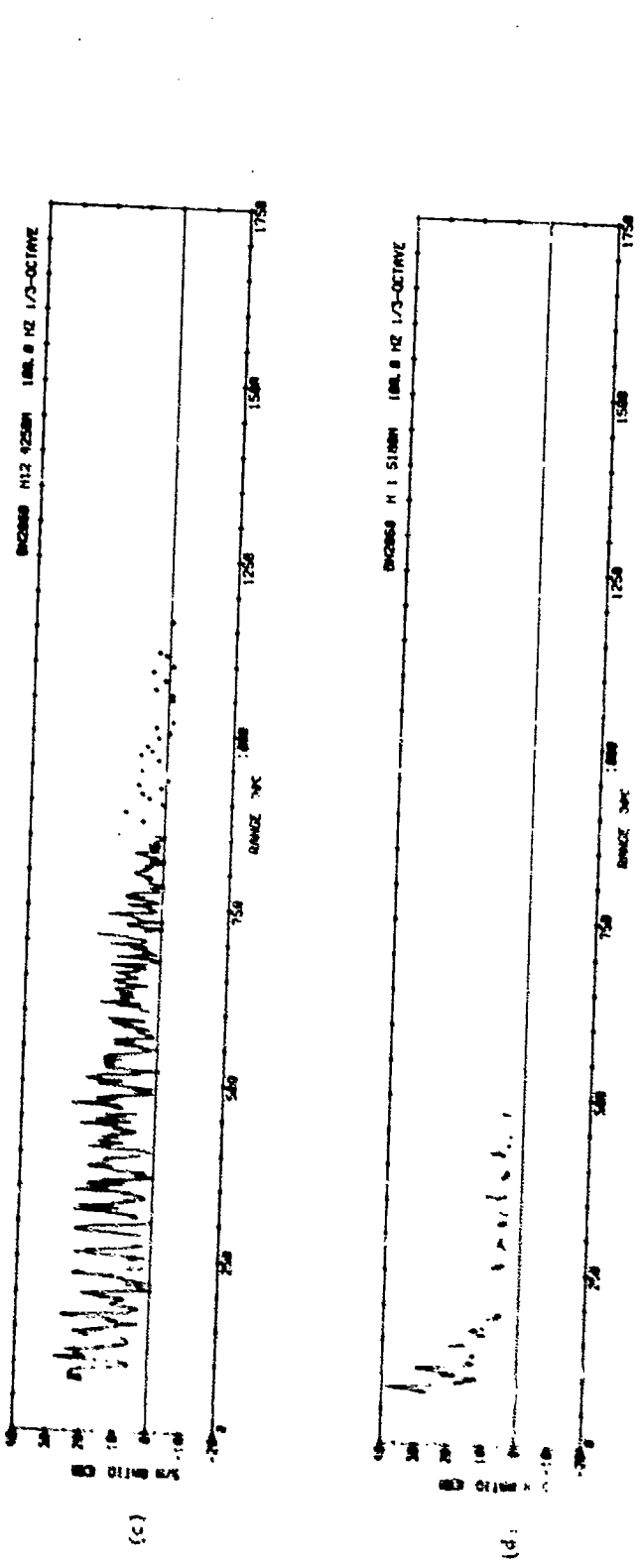

Figure 3-4

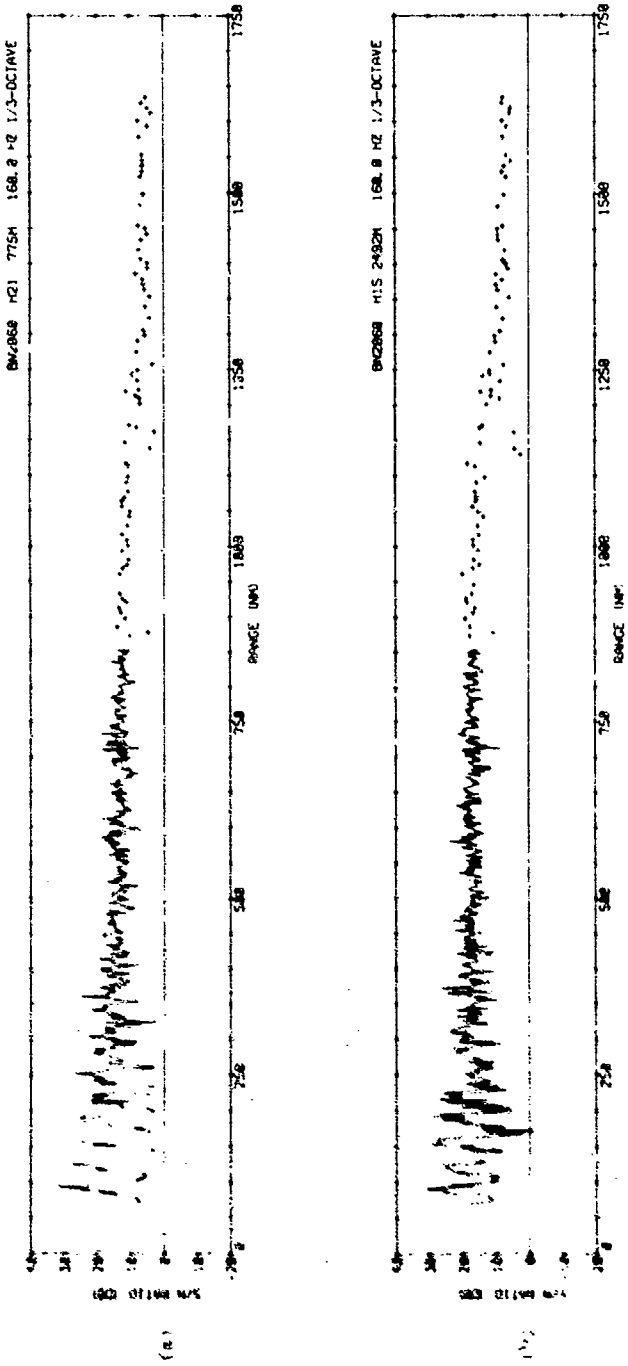
BW2868 H21 775M 160.0 HZ 1/3-OCTAVE
1750
1500
1250
1000
750
500
250
0
RANGE (NM)
(a)
BW2868 H15 2482M 160.0 HZ 1/3-OCTAVE
1750
1500
1250
1000
750
500
250
0
RANGE (NM)

Figure C-5

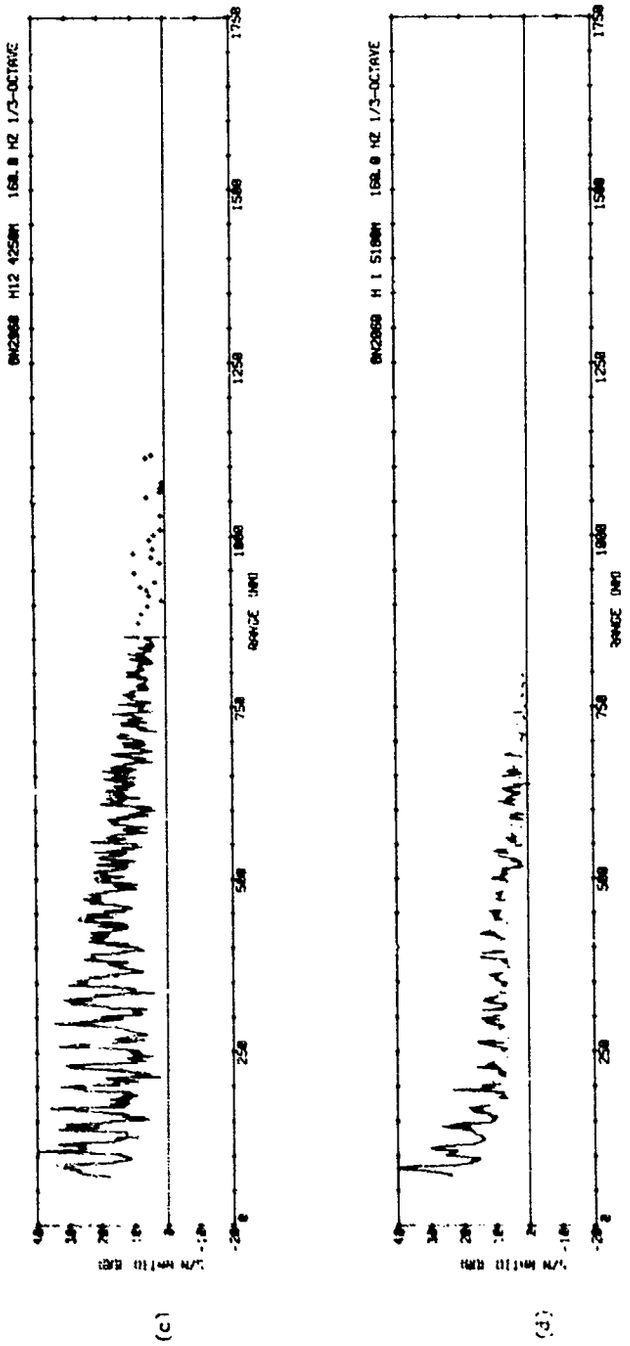

Figure C-5

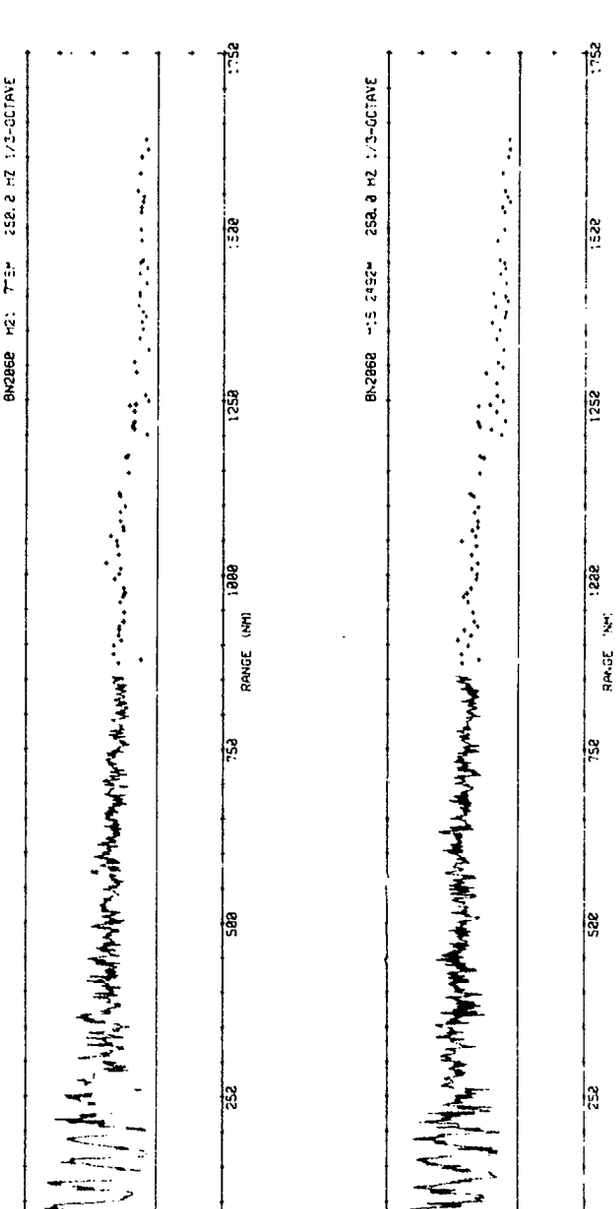
BW2868 M2: 7:3M 258.2 HZ 1/3-OCTAVE
S/N RATIO (DB)
RANGE (NM)
(a)
BW2868 -:S 2932M 258.0 HZ 1/3-OCTAVE
S/N RATIO (DB)
(b)

Figure C-6

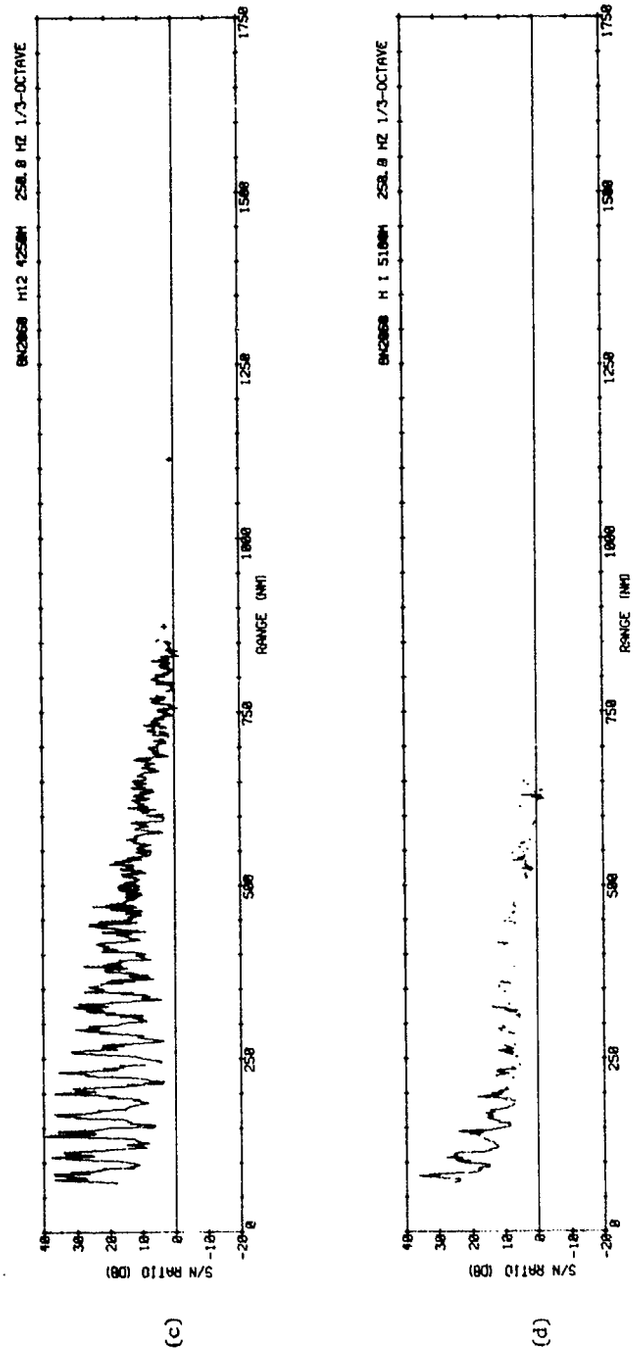
BH2868 H12 425HH 258.8 HZ 1/3-OCTAVE
RANGE (NM)
S/N RATIO (DB)
(c)
BH2868 H 1 518HH 258.8 HZ 1/3-OCTAVE
RANGE (NM)
S/N RATIO (DB)
(d)

Figure C-6

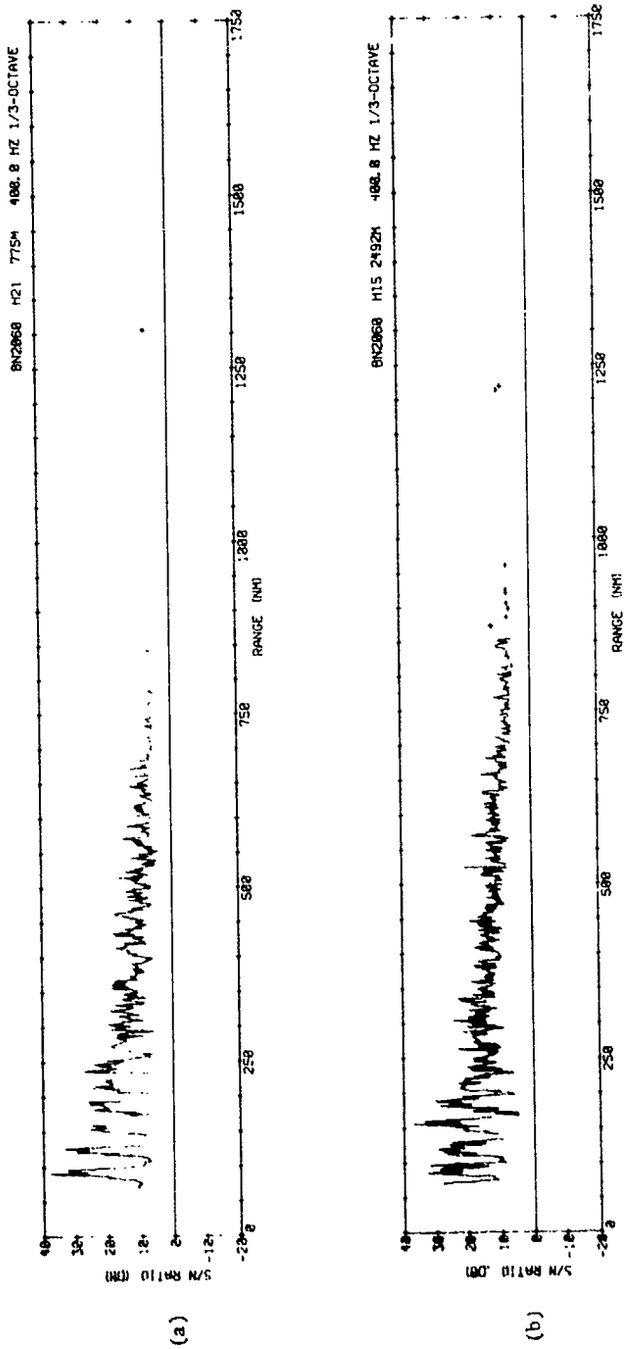
BN2060 M21 775M 400.0 HZ 1/3-OCTAVE
BN2060 M15 2492M 400.0 HZ 1/3-OCTAVE
S/N RATIO (DB)
RANGE (NM)
0
250
500
750
1000
1250
1500
1750
40
30
20
10
0
-10
-20
(a)
(b)

Figure C-7

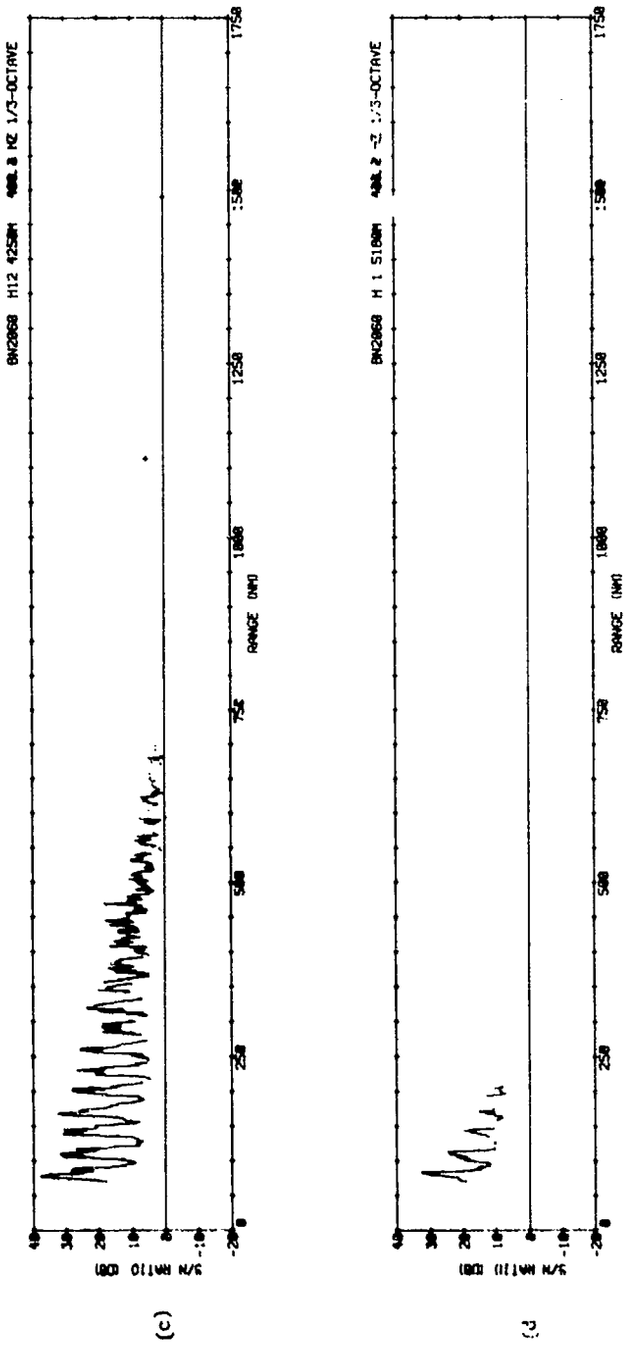
BW2868 H12 425BM
1/3-OCTAVE
RANGE (NM)
S/N RMT10 (DB)
BW2868 H 1 S18BM
1/3-OCTAVE
RANGE (NM)
S/N RMT10 (DB)

(c) (d)

Figure C-7

APPENDIX D

DIFFERENTIAL SIGNAL-TO-NOISE RATIO VERSUS RANGE PLOTS

(U) The differences in S/N for the three deeper hydrophone and that for the axis hydrophone, 775 meters, are plotted versus range in Figs. D-1 through D-7. These plots were discussed in Section VI. Positive values in the S/N difference occur where the S/N ratio for a particular hydrophone is greater than that for the near axis hydrophone. Each figure consists of three plots, a-plots are S/N at 2492 meters minus S/N at 775 meters, b-plots are S/N at 4250 meters minus S/N at 775 meters and c-plots are S/N at 5180 meters minus S/N at 775 Meters.

(U) The designation of the ship portions and aircraft portions of the run together with the identity captions in the upper right corner are identical to that given in the previous appendices.

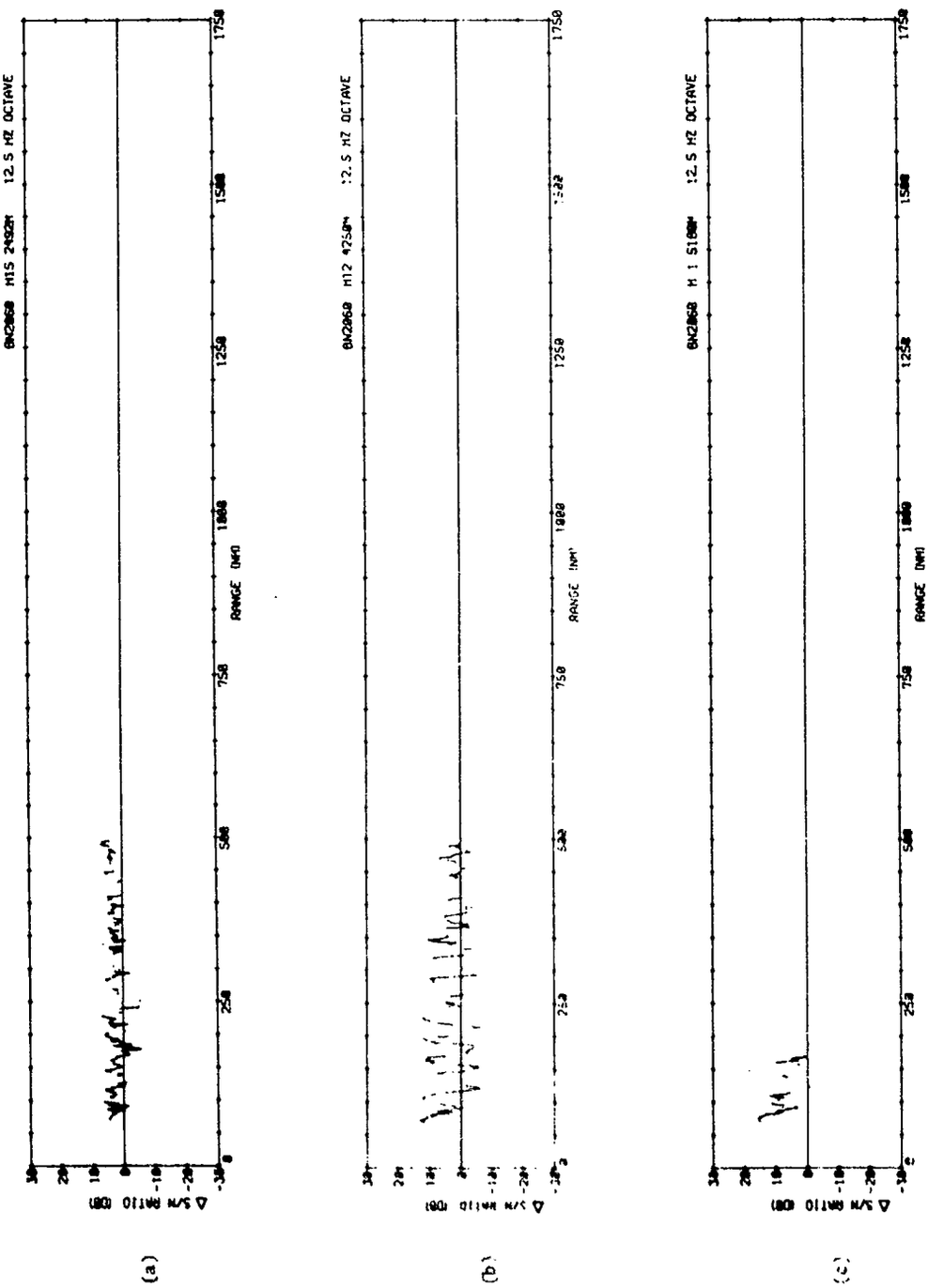

Figure D-1

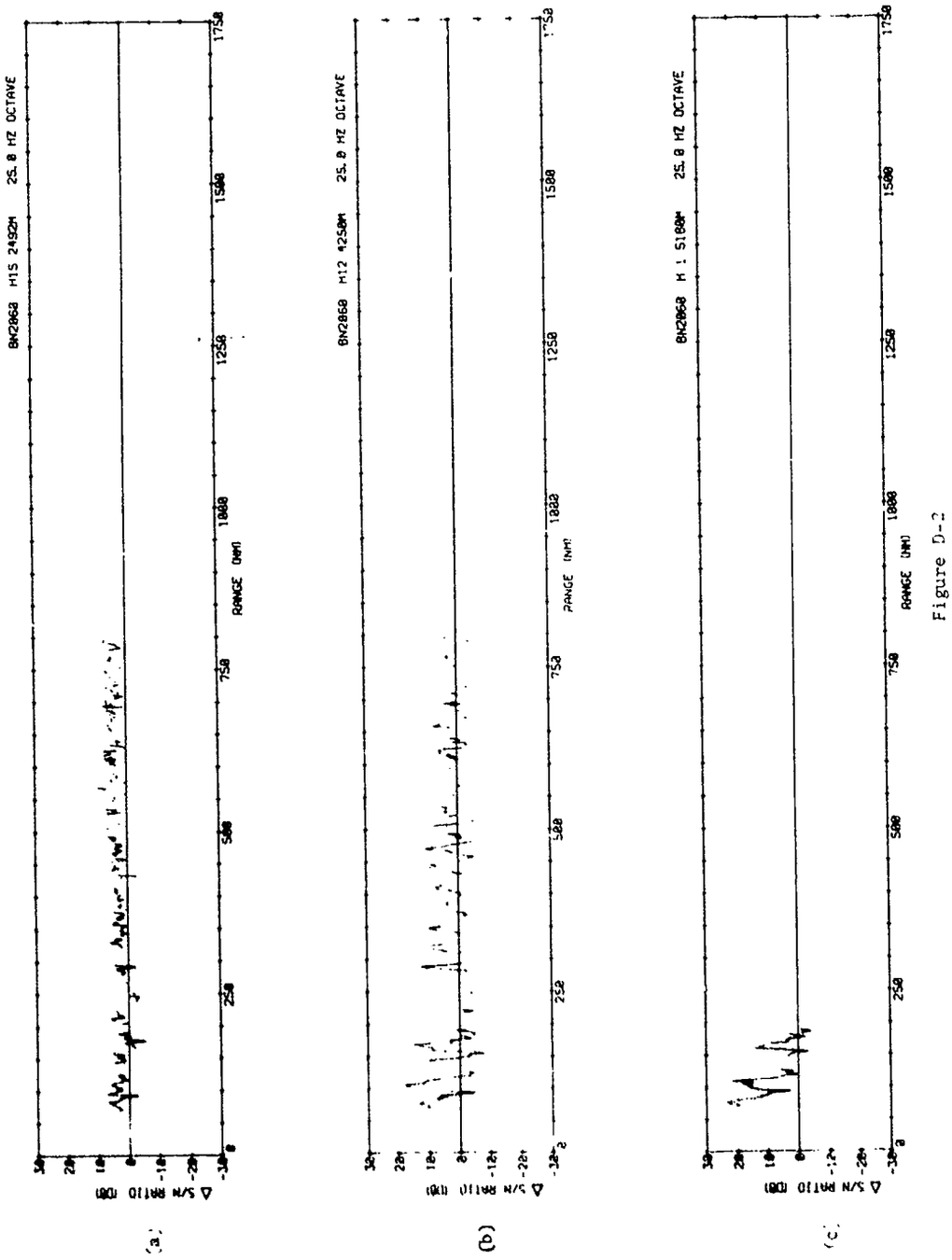
BW2868 M15 2492M 25.0 HZ OCTAVE
BW2868 M12 4258M 25.0 HZ OCTAVE
BW2868 M 1 5180M 25.0 HZ OCTAVE
RANGE (NM)
Δ S/N RATIO (DB)
(a)
(b)
(c)

Figure D-2

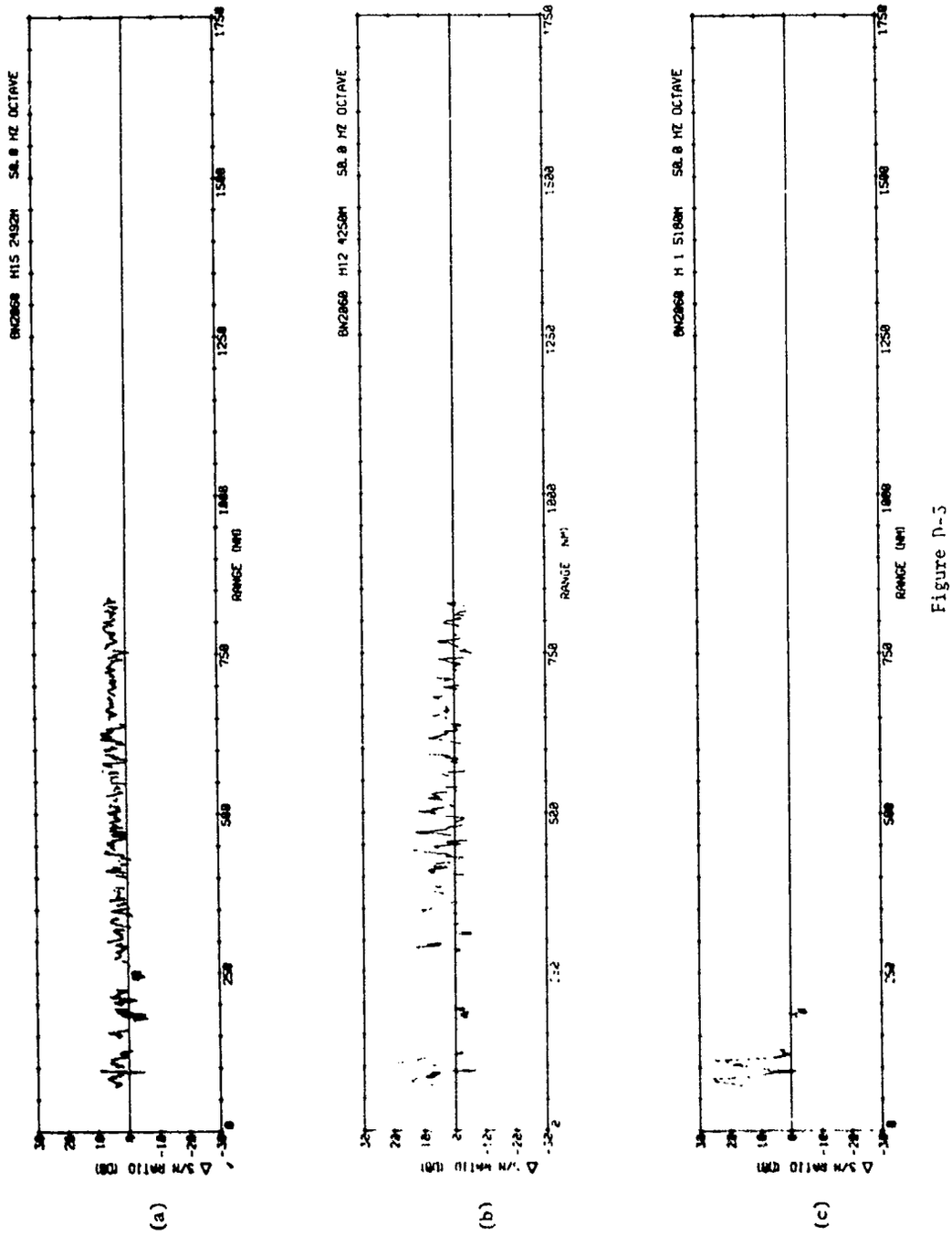
BW2060 M15 2492M 50.0 HZ OCTAVE
BW2060 M12 4250M 50.0 HZ OCTAVE
BW2060 M 1 5180M 50.0 HZ OCTAVE
RANGE (NM)
Δ S/N RATIO (DB)
(a)
(b)
(c)

Figure D-5

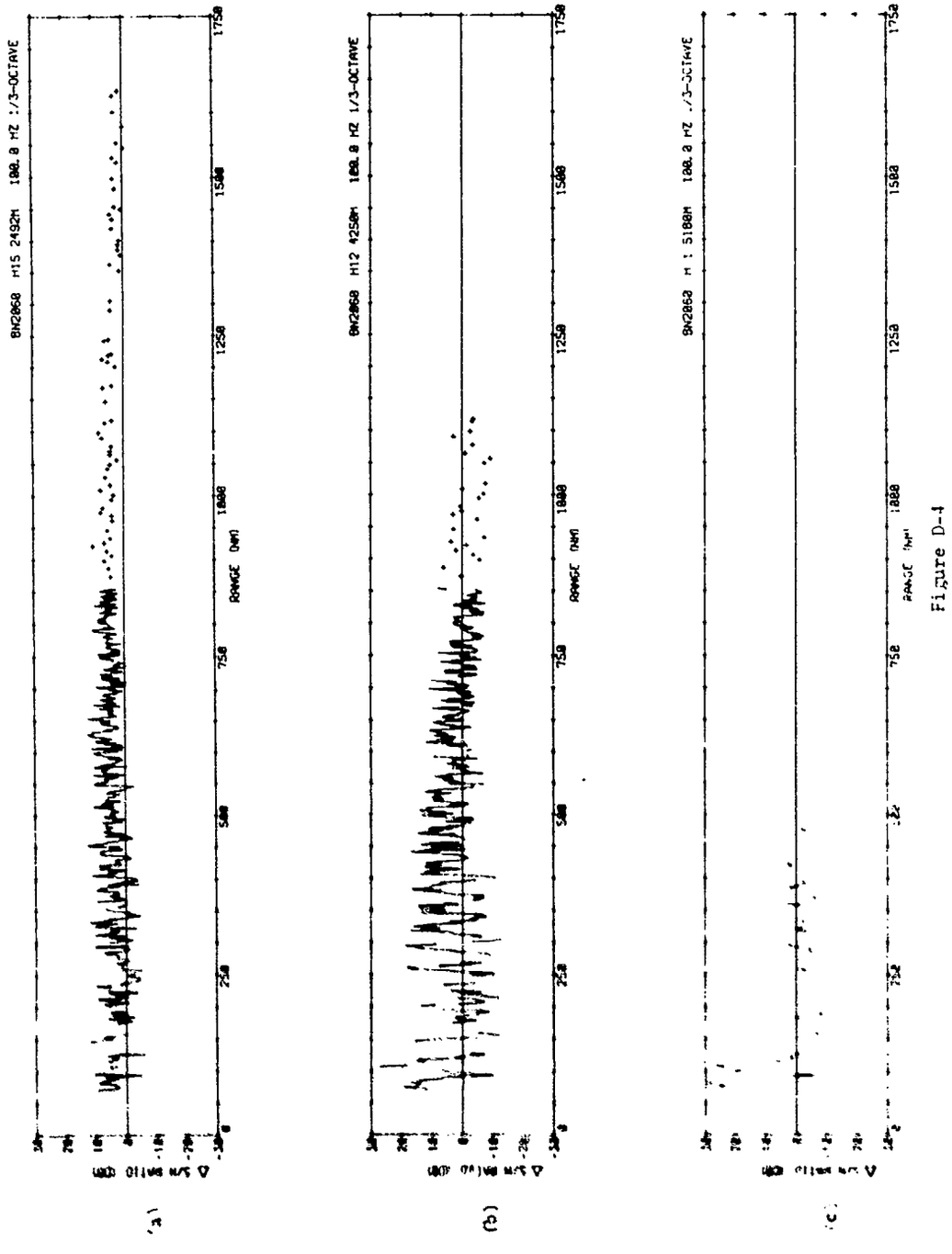
BW2060 H15 2492M 100.0 HZ 1/3-OCTAVE
BW2060 H12 4250M 100.0 HZ 1/3-OCTAVE
BW2060 H 1 5180M 100.0 HZ 1/3-OCTAVE
RANGE (NM)
(a)
(b)
(c)

Figure D-4

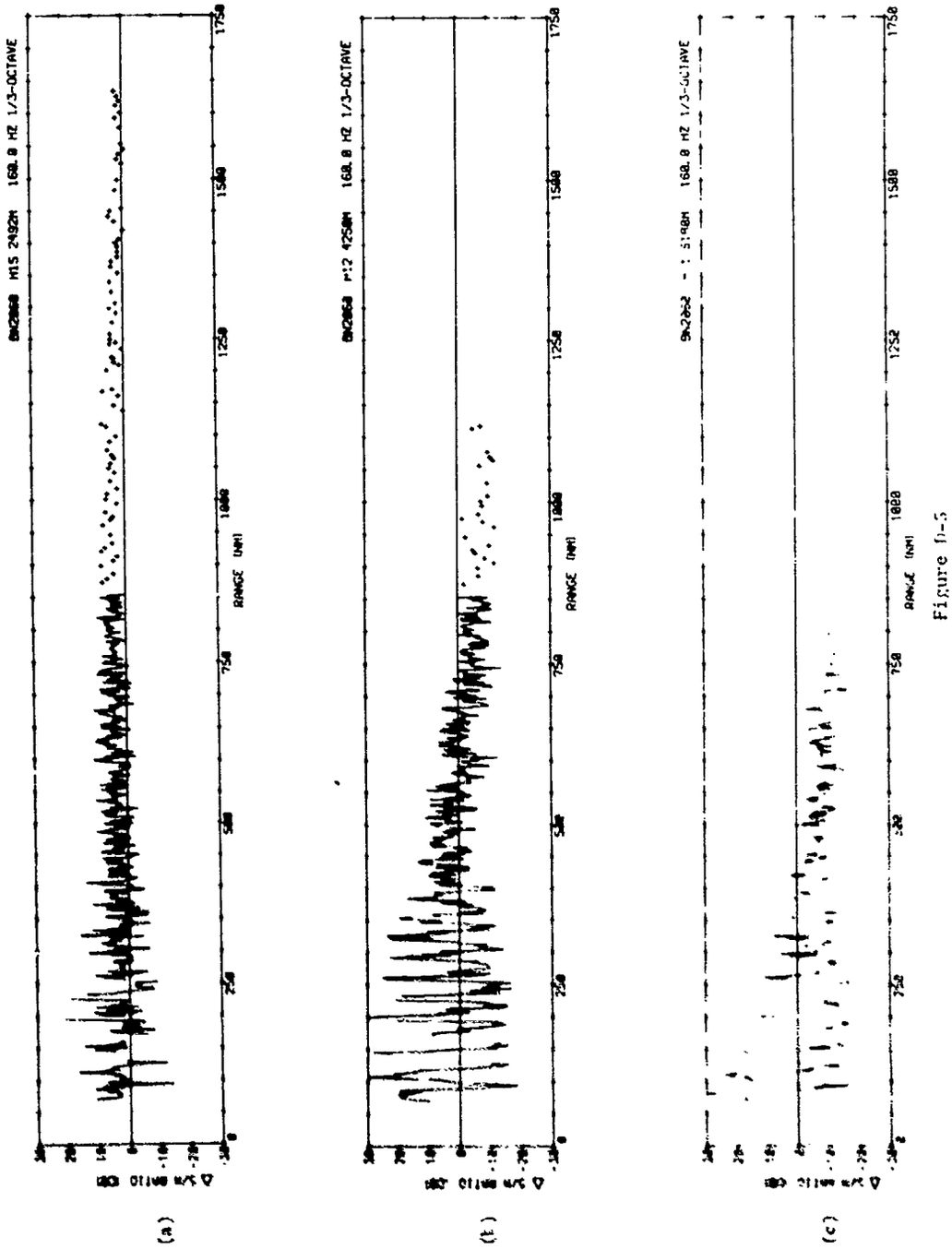
160.0 HZ 1/3-OCTAVE
RANGE (NMI)
(a)
160.0 HZ 1/3-OCTAVE
RANGE (NMI)
(b)
160.0 HZ 1/3-OCTAVE
RANGE (NMI)
(c)

Figure II-5

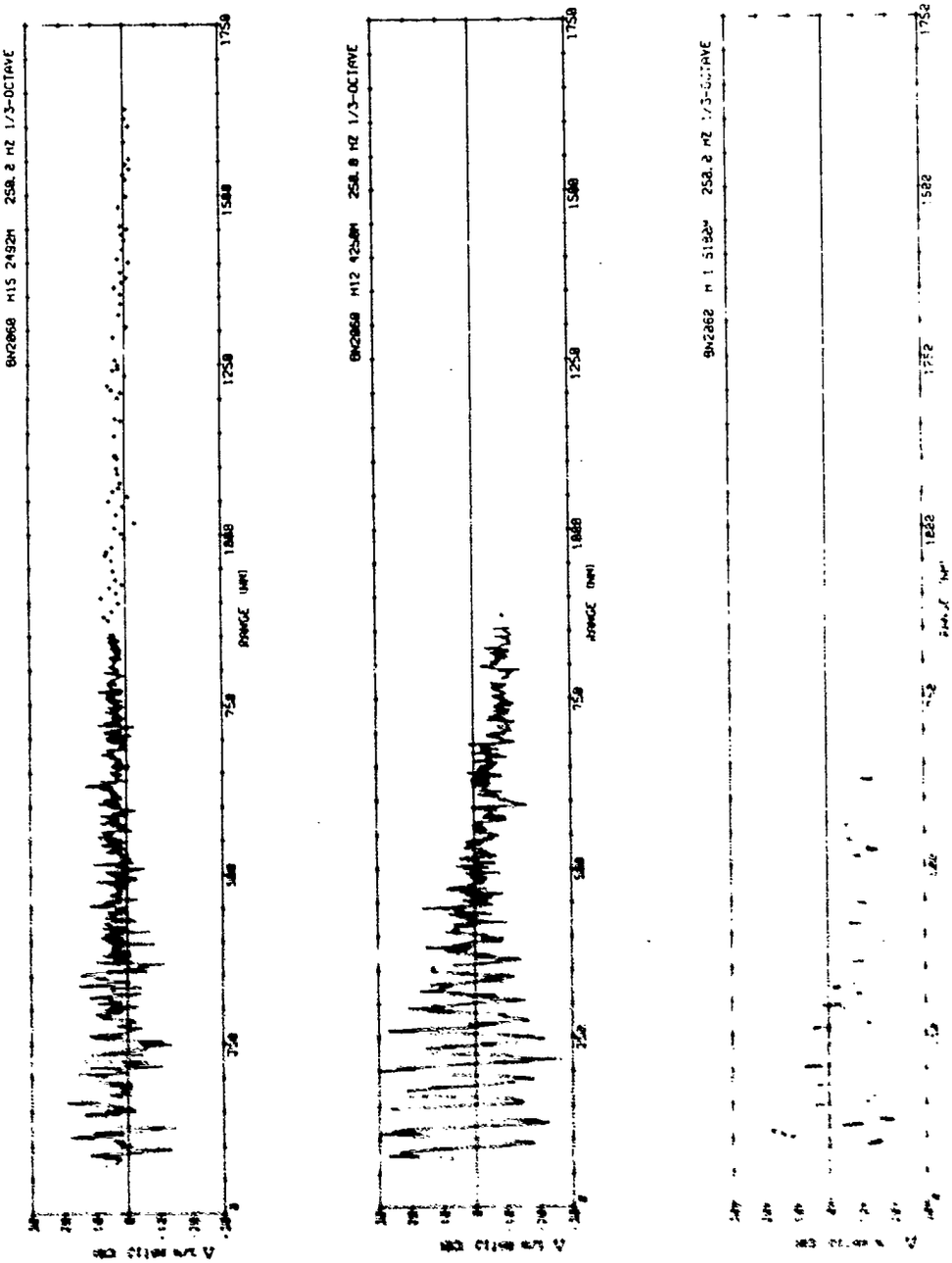
BW2868 H15 2492M 258.2 HZ 1/3-OCTAVE
BW2868 H12 2438M 258.8 HZ 1/3-OCTAVE
BW2868 H 1 2183M 258.2 HZ 1/3-OCTAVE

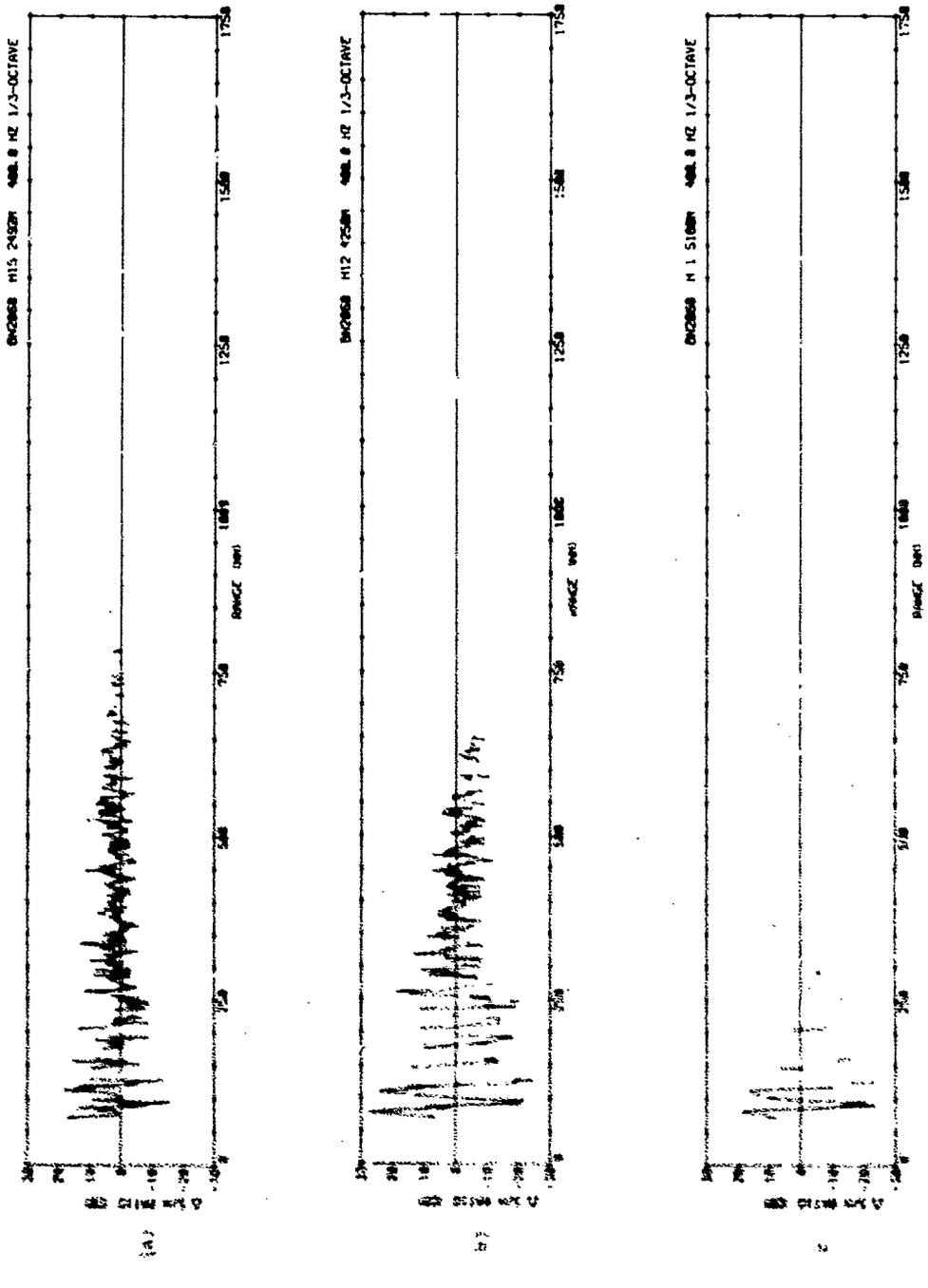

Figure D-7

DISTRIBUTION LIST

Chief of Naval Research
Department of the Navy
Arlington, Virginia 22217
- Code 200 (1)
- Code 222 (2)
- Code 102IP (1)
- Code 1020SC (1)
- Code 460 (1)
- Code 480 (1)
- Code 481 (1)
- Code 486 (1)

Director
Office of Naval Research
Branch Office
1030 East Green Street
Pasadena, California 91101 (1)

Commander
Naval Sea Systems Command
Washington, D.C. 20362
- Code 03E (1)
- Code 034 (1)
- Code 0342 (1)
- Code 036 (1)
- Code 06H1 (1)
- Code 06H2 (1)
- Code 09G3 (1)
- Code 92 (1)
- Code 662C14 (1)
- PMS 395-4 (1)
- PMS 402 B (1)

Commander
Naval Air Systems Command
Washington, D.C. 20361
- Code 370 (1)
- Code 264 (1)

Commander
Naval Electronics
Systems Command
Washington, D.C. 20360
- Code PME-124 (1)

Chief of Naval Material
Department of the Navy
Washington, D.C. 20360
- Code PM-4 (1)
- Code 034 (1)
- Code ASW121 (1)

Chief of Naval Operations
Department of the Navy
Washington, D.C. 20350
- Code Op 05 (1)
- Code Op 32 (1)
- Code Op 098 (1)
- Code Op 02 (1)
- Code Op 095 (1)
- Code Op [illegible] (1)
- Code Op 967 (1)

Commanding Officer
Naval Ocean Research &
Development Activity (NORDA)
Bay St. Louis, Mississippi 39529
- Code 100 (1)
- Code 460 (1)
- Code 500 (1)
- Code 600 (2)

Oceanographer of the Navy
The Hoffman Building
200 Stoval Street
Alexandria, Virginia 22332 (1)

Director Strategic Systems
Projects Office (PM-1)
Department of the Navy
Washington, D.C. 20360
- Code NSP-20 (1)

Director
Defense Research & Engineering
The Pentagon
Washington, D.C. 20301
- Assistant Director (Sea
Warfare Systems) (1)

Assistant Secretary of the Navy
(Research & Development)
Department of the Navy
Washington, D.C. 20350 (1)

U.S. Naval Oceanographic Office
Washington, D.C. 20373
- Code 1640 (1)
- Code 3440 (1)

Commander Operational Test &
Evaluation Force
U.S. Naval Base
Norfolk, Virginia 23511 (1)

Commander, Submarine Force
U.S. Pacific Fleet
Fleet Post Office
San Francisco, California 96601 (1)

Commander
Submarine Group FIVE
Fleet Station Post Office
San Diego, California 92132 (1)

Commander
Third Fleet
U.S. Pacific Fleet, FPO
San Francisco, California 96610 (1)

Commander
Submarine Development Group ONE
Fleet Post Office
San Diego, California 92132 (1)

Commander
Submarine Development Group TWO
Naval Submarine Base-New London
Groton, Connecticut 06340 (1)

DISTRIBUTION LIST (Continued)

Commander, Surface Force
U.S. Atlantic Fleet
Norfolk, Virginia 23511 (1)

Commander, Surface Force
U.S. Pacific Fleet
San Diego, California 92155 (1)

Reprint Custodian
Department of Nautical Science
U.S. Merchant Marine Academy
Kings Poi New York 11024 (1)

Deputy Commander
Operational Test &
Evaluation Force, Pacific
U.S. Naval Air Station
San Diego, California 92135 (1)

Commander
Naval Ship Reserach &
Development Center
Bethesda, Maryland 20084 (1)

Naval Civil Engineering Laboratory
Port Hueneme, California 93041
Code L40 (1)
Code L42

Naval Facilities
Engineering Command
Washington, D.C. 20390
Code 03 (1)
Code 032C (1)

Commanding Officer
U.S. Naval Air
Development Center
Warminster, Pennsylvania 18974 (1)

Commander
Naval Ocean Systems Center
San Diego, California 92152
Code 6700 (2)

Officer In Charge
Naval Ship Research &
Development Center
Annapolis, Maryland 21402 (1)

Commanding Officer, Naval
Coastal Systems Laboratory
Panama City, Florida 32401 (1)

Commander
Naval Surface
Combat Systems Center
White Oak
Silver Spring, Maryland 20910 (1)

Director
U.S. Naval Research Laboratory
Washington, D.C. 20375
Code 2620 (1)
Code 2627 (1)
Code 8000 (1)
Code 8100 (1)

Commanding Officer
Naval Underwater Systems Center
Newport, Rhode Island 20844 (1)

Commanding Officer
Naval Underwater Systems Center
New London, Connecticut 06320
Code 900 (1)
Code 905 (1)
Code 910 (1)
Code 930 (1)
Code 960 (1)

Commanding Officer
Naval Training Equipment Center
Orlando, Florida 32813
Tech Library (1)

Chief Scientist
Navy Underwater
Sound Reference Division
U.S. Naval Research Laboratory
P.O. Box 8337
Orlando, Florida 32806

Superintendent
U.S. Naval Postgraduate School
Monterey, California 93940 (1)

Director
Defense Documentation Center
(TIMA), Cameron Station
5010 Duke Street
Alexandria, Virginia 22314 (12)

Executive Secretary
National Academy of Sciences
2101 Constitution Avenue, N.W.
Washington, D.C. 20418 (1)

Supreme Allied Commander
U.S. Atlantic Fleet
ASW Research Center
APO
New York, New York 09019
Via: ONR 210
CNO OP092D1
Secretariat of Military
Information Control
Committee (1)

DISTRIBUTION LIST (Continued)

National Oceanic & Atmospheric
Administration
6001 Executive Boulevard
Rockville, Maryland 20852 (1)

Director of Naval Warfare Analysis
Institute of Naval Studies
1401 Wilson Boulevard
Arlington, Virginia 22209 (1)

Institute for Defense Analyses
400 Army-Navy Drive
Arlington, Virginia 22202 (1)

Director
Woods Hole
Oceanographic Institution
Woods Hole, Massachusetts 02543 (1)

Meterological &
Astrophysical Abstracts
310 E. Capitol Street
Washington, D.C. 20003 (1)

Director
Applied Physics Laboratory
University of Washington
1013 East 40th Street
Seattle, Washington 98105 (1)

National Science Foundation
Washington, D.C. 20550 (1)

Director
Lamont-Doherty
Geological Observatory
Torrey Cliff
Palisades, New York 10964 (1)

Director
College of Engineering
Department of Ocean Engineering
Florida Atlantic University
Boca Raton, Florida 33431 (1)

Director
Applied Research Laboratory
Pennsylvania State University
P.O. Box 30
State College, Pennsylvania 16802 (1)

Director
University of Texas
Applied Research Laboratory
P.O. Box 8029
Austin, Texas 78712 (1)

TACTEC
Battelle Columbus Laboratories
505 King Avenue
Columbus, Ohio 43201 (1)

Director
Institute of
Ocean Science & Engineering
Catholic University of America
Washington, D.C. 20017 (1)

Director
Marine Research Laboratories
c/o Marine Studies Center
University of Wisconsin
Madison, Wisconsin 53706 (1)

Office of Naval Research
Resident Representative
c/o University of California,
San Diego
La Jolla, California 92093 (1)

University of California,
San Diego
La Jolla, California 92093
MPL Branch Office (5)

Commander
Oceanographic Systems Pacific
Box 1390
FPO, San Francisco, California 96610 (1)

Project Manager
Antisubmarine Warfare Systems Project
Department of the Navy
Washington, D.C. 20360
Code ASW-11 (1)
ASW-111 (1)
ASW-13 (1)

Commander
Naval Electronics System Command
Department of the Navy
Washington, D.C. 20362
PME-124/TA (1)
PME-124/20 (1)
PME-124/30 (1)
PME-124/40 (1)
PME-124/60 (1)

Director
Center for Naval Analysis
Arlington, Virginia 22217

Commanding Officer
Fleet Numerical Weather Central
Monterey, California 93940 (1)

Arthur D. Little, Inc.
Acorn Park
Cambridge, Massachusetts 02140
Attn: Dr. G Raisbeck (1)

B-K Dynamic
15825 Shady Grove Road
Rockville, Maryland 20850
Attn: A. E. Fadness (1)

DISTRIBUTION LIST (Continued)

Bell Telephone Laboratories
1 Whippany Road
Whippany, New Jersey 07981
Attn: G. Fox (1)
T. Phillips (1)

Hawaii Institute of Geophysics
2525 Correa Road
Honolulu, Hawaii 96722
Attn: Director (1)
Dr. M. Odegard (1)

Planning Systems, Inc.
7900 Westpark Drive, Suite 507
The Honeywell Center
McLean, Virginia 22101
Attn: Dr. L. P. Solomon (1)

TRW Systems Group
7600 Coleshire Drive
McLean, Virginia 22101
Attn: Mr. C. C. Carter (1)
R. T. Brown (1)

Tetra Tech, Incorporated
Suite 601
1911 N. Ft. Myer Drive
Arlington, Virginia 22209
Attn: Mr. C. Dabney (1)

Texas Instruments, Inc.
13500 North Central Expressway
Dallas, Texas 75222
Attn: Mr. A. Kirst (1)

Tracor, Inc. (Rockville Laboratory)
1601 Research Blvd.
Rockville, Maryland 20850
Attn: Mr. J. Gottwald (1)
Mr. R. J. Urick (1)

Underwater Systems, Inc.
World Building
8121 Georgia Avenue
Silver Spring, Maryland 20910
Attn: Dr. M. Weinstein (1)

Xonics
6849 Hayvenhurst Avenue
Van Nuys, California 91406
Attn: Dr. N. Moise

Director
Advanced Research Projects Agency
1400 Wilson Blvd.
Arlington, Virginia 22209
Attn: Program Management (1)

STOIAC
Battelle
505 King Avenue
Columbus, Ohio 43201 (1)

Naval Ocean Systems Center
Code 4007
San Diego, California 92152
Attn: Robert R. Gardner (1)

Marine Physical Laboratory
MPL-C-42/76

CHURCH ANCHOR EXPLOSIVE SOURCE (SUS) PROPAGATION MEASUREMENTS FROM R/P FLIP (U) by G. B. Morris, University of California, San Diego, Marine Physical Laboratory of the Scripps Institution of Oceanography, San Diego, California 92152. SIO Reference 76-10, 1 July 1976.

(U) As part of the CHURCH ANCHOR Exercise conducted in the central Northeastern Pacific Ocean during August and September 1973, the received signals from underwater explosive sources (SUS) detonated at a nominal depth of 18 meters were analyzed for signal propagation measurements. The signals received at four hydrophones were detected, digitally sampled and processed on-line by a digital minicomputer system aboard the Research Platform FLIP. The four hydrophone depths 775 meters, 2492 meters, 4250 meters, and 5180 meters, correspond to depths near the sound channel axis, a depth roughly midway between the axis and the critical depth, near the critical depth, and 142 meters above the bottom, respectively. Analyses were

(Continued)

IIb. Signal Processing Techniques

G. B. Morris

Sponsored by
Office of Naval Research
N00014-75-C-6049
NR 260-103

This card is UNCLASSIFIED
Report is CONFIDENTIAL

Marine Physical Laboratory
MPL-C-42/76

CHURCH ANCHOR EXPLOSIVE SOURCE (SUS) PROPAGATION MEASUREMENTS FROM R/P FLIP (U) by G. B. Morris, University of California, San Diego, Marine Physical Laboratory of the Scripps Institution of Oceanography, San Diego, California 92152. SIO Reference 76-10, 1 July 1976.

(U) As part of the CHURCH ANCHOR Exercise conducted in the central Northeastern Pacific Ocean during August and September 1973, the received signals from underwater explosive sources (SUS) detonated at a nominal depth of 18 meters were analyzed for signal propagation measurements. The signals received at four hydrophones were detected, digitally sampled and processed on-line by a digital minicomputer system aboard the Research Platform FLIP. The four hydrophone depths 775 meters, 2492 meters, 4250 meters, and 5180 meters, correspond to depths near the sound channel axis, a depth roughly midway between the axis and the critical depth, near the critical depth, and 142 meters above the bottom, respectively. Analyses were

(Continued)

IIb. Signal Processing Techniques

G. B. Morris

Sponsored by
Office of Naval Research
N00014-75-C-6049
NR 260-103

This card is UNCLASSIFIED
Report is CONFIDENTIAL

Marine Physical Laboratory
MPL-C-42/76

CHURCH ANCHOR EXPLOSIVE SOURCE (SUS) PROPAGATION MEASUREMENTS FROM R/P FLIP (U) by G. B. Morris, University of California, San Diego, Marine Physical Laboratory of the Scripps Institution of Oceanography, San Diego, California 92152. SIO Reference 76-10, 1 July 1976.

(U) As part of the CHURCH ANCHOR Exercise conducted in the central Northeastern Pacific Ocean during August and September 1973, the received signals from underwater explosive sources (SUS) detonated at a nominal depth of 18 meters were analyzed for signal propagation measurements. The signals received at four hydrophones were detected, digitally sampled and processed on-line by a digital minicomputer system aboard the Research Platform FLIP. The four hydrophone depths 775 meters, 2492 meters, 4250 meters, and 5180 meters, correspond to depths near the sound channel axis, a depth roughly midway between the axis and the critical depth, near the critical depth, and 142 meters above the bottom, respectively. Analyses were

(Continued)

IIb. Signal Processing Techniques

G. B. Morris

Sponsored by
Office of Naval Research
N00014-75-C-6049
NR 260-103

This card is UNCLASSIFIED
Report is CONFIDENTIAL

Marine Physical Laboratory
MPL-C-42/76

CONFIDENTIAL

CHURCH ANCHOR EXPLOSIVE SOURCE (SUS) PROPAGATION MEASUREMENTS FROM R/P FLIP (U) by G. B. Morris, University of California, San Diego, Marine Physical Laboratory of the Scripps Institution of Oceanography, San Diego, California 92152. SIO Reference 76-10, 1 July 1976.

(U) As part of the CHURCH ANCHOR Exercise conducted in the central Northeastern Pacific Ocean during August and September 1973, the received signals from underwater explosive sources (SUS) detonated at a nominal depth of 18 meters were analyzed for signal propagation measurements. The signals received at four hydrophones were detected, digitally sampled and processed on-line by a digital minicomputer system aboard the Research Platform FLIP. The four hydrophone depths 775 meters, 2492 meters, 4250 meters, and 5180 meters, correspond to depths near the sound channel axis, a depth roughly midway between the axis and the critical depth, near the critical depth, and 142 meters above the bottom, respectively. Analyses were

(Continued)

IIb. Signal Processing Techniques

G. B. Morris

Sponsored by
Office of Naval Research
N00014-75-C-6049
NR 260-103

This card is UNCLASSIFIED
Report is CONFIDENTIAL

MPL-C-42/76

made at selected frequencies in the band from 10 Hz to 400 Hz. Signal propagation characteristics and signal-to-noise ratios were examined as a function of source-to-receiver range, receiver depth, and frequency. Bathymetric or changing water mass effects on the sound propagation were also noted.

MPL-C-42/76

made at selected frequencies in the band from 10 Hz to 400 Hz. Signal propagation characteristics and signal-to-noise ratios were examined as a function of source-to-receiver range, receiver depth, and frequency. Bathymetric or changing water mass effects on the sound propagation were also noted.

MPL-C-42/76

made at selected frequencies in the band from 10 Hz to 400 Hz. Signal propagation characteristics and signal-to-noise ratios were examined as a function of source-to-receiver range, receiver depth, and frequency. Bathymetric or changing water mass effects on the round propagation were also noted.

MPL-C-42/76

made at selected frequencies in the band from 10 Hz to 400 Hz. Signal propagation characteristics and signal-to-noise ratios were examined as a function of source-to-receiver range, receiver depth, and frequency. Bathymetric or changing water mass effects on the sound propagation were also noted.

DEPARTMENT OF THE NAVY
OFFICE OF NAVAL RESEARCH
875 NORTH RANDOLPH STREET
SUITE 1425
ARLINGTON VA 22203-1995

IN REPLY REFER TO:

5510/1
Ser 321OA/011/06
31 Jan 06

MEMORANDUM FOR DISTRIBUTION LIST

Subj: DECLASSIFICATION OF LONG RANGE ACOUSTIC PROPAGATION PROJECT (LRAPP) DOCUMENTS

Ref: (a) SECNAVINST 5510.36

Encl: (1) List of DECLASSIFIED LRAPP Documents

1. In accordance with reference (a), a declassification review has been conducted on a number of classified LRAPP documents.

2. The LRAPP documents listed in enclosure (1) have been downgraded to UNCLASSIFIED and have been approved for public release. These documents should be remarked as follows:

   Classification changed to UNCLASSIFIED by authority of the Chief of Naval Operations (N772) letter N772A/6U875630, 20 January 2006.

   DISTRIBUTION STATEMENT A: Approved for Public Release; Distribution is unlimited.

3. Questions may be directed to the undersigned on (703) 696-4619, DSN 426-4619.

BRIAN LINK
By direction

Subj: DECLASSIFICATION OF LONG RANGE ACOUSTIC PROPAGATION PROJECT (LRAPP) DOCUMENTS

DISTRIBUTION LIST:

NAVOCEANO (Code N121LC – Jaime Ratliff)
NRL Washington (Code 5596.3 – Mary Templeman)
PEO LMW Det San Diego (PMS 181)
DTIC-OCQ (Larry Downing)
ARL, U of Texas
Blue Sea Corporation (Dr.Roy Gaul)
ONR 32B (CAPT Paul Stewart)
ONR 321OA (Dr. Ellen Livingston)
APL, U of Washington
APL, Johns Hopkins University
ARL, Penn State University
MPL of Scripps Institution of Oceanography
WHOI
NAVSEA
NAVAIR
NUWC
SAIC

Declassified LRAPP Documents

Report Number	Personal Author	Title	Publication Source (Originator)	Pub. Date	Current Availability	Class.
ARLTR7952	Focke, K. C., et al.	CHURCH STROKE 2 CRUISE 5 PAR/ACODAC ENVIRONMENTAL ACOUSTIC MEASUREMENTS AND ANALYSIS (U)	University of Texas, Applied Research Laboratories	791029	ADC025102; NS; AU; ND	C
Unavailable	Van Wyckhouse, R. J.	SYNBAPS. VOLUME I. DATA BASE SOURCES AND DATA PREPARATION	Naval Ocean R&D Activity	791201	ADC025193	C
NORDATN63	Brunson, B. A., et al.	ENVIRONMENTAL EFFECTS ON LOW FREQUENCY TRANSMISSION LOSS IN THE GULF OF MEXICO (U)	Naval Ocean R&D Activity	800901	ADC029543; ND	C
NORDATN80C	Gereben, I. B.	ACOUSTIC SIGNAL CHARACTERISTICS MEASURED WITH THE LAMBDA III DURING CHURCH STROKE III (U)	Naval Ocean R&D Activity	800915	ADC023527; NS; AU; ND	C
NOSCTR664	Gordon, D. F.	ARRAY SIMULATION AT THE BEARING STAKE SITES	Naval Ocean Systems Center	810401	ADC025992; NS; AU; ND	C
NOSCTR703	Gordon, D. F.	NORMAL MODE ANALYSIS OF PROPAGATION LOSS AT THE BEARING STAKE SITES (U)	Naval Ocean Systems Center	810801	ADC026872; NS; AU; ND	C
NOSCTR680	Neubert, J. A.	COHERENCE VARIABILITY OF ARRAYS DURING BEARING STAKE (U)	Naval Ocean Systems Center	810801	ADC028075; NS; ND	C
HSECO735	Luehrmann, W. H.	SQUARE DEAL R/V SEISMIC EXPLORER FIELD OPERATIONS REPORT (U)	Seismic Engineering Co.	731121	AD0530744; NS; ND	C; U
MPL-C-42/76	Morris, G. B.	CHURCH ANCHOR EXPLOSIVE SOURCE (SUS) PROPAGATION MEASUREMENTS FROM R/P FLIP (U)	Marine Physical Laboratory	760701	ADC010072; AU; ND	C; U
ARLTR7637	Mitchell, S. K., et al.	SQUARE DEAL EXPLOSIVE SOURCE (SUS) PROPAGATION MEASUREMENTS. (U)	University of Texas, Applied Research Laboratories	760719	ADC014196; NS; AU; ND	C; U
NORDAR23	Fenner, D. F.	SOUND SPEED STRUCTURE OF THE NORTHEAST ATLANTIC OCEAN IN SUMMER 1973 DURING THE	Naval Ocean R&D Activity	800301	ADC029546; NS; ND	C; U
NOOTR230	Bucca, P. J.	SOUND VELOCITY CONDITIONS DURING THE CHURCH ANCHOR EXERCISE (U)	Naval Oceanographic Office	751201	NS; AU; ND	C;U
ONR SP 2-69; MC PLAN-01	Unavailable	PARKA II EXPERIMENT UTILIZING SEA SPIDER, ONR SCIENTIFIC PLAN 2-69 (U)	Maury Center for Ocean Science	690626	ADB020846; ND	U
Unavailable	Unavailable	PARKA I EXPERIMENT	Maury Center for Ocean Science	691101	AD0506209	U
USRD CR 3105	Unavailable	SEA SPIDER TRANSPONDER TRANSDUCER	Naval Research Laboratory	700505	ND	U
MC PLAN 05; ONR Scientific Plan 1-71	Unavailable	ATLANTIC TEST BED MEASUREMENT PROGRAM (U)	Maury Center for Ocean Science	701020	ND	U
ACR-170 VOL.1	Hurdle, B. G.	PROJECT NEAT- A COLLABORATIVE LONG RANGE PROPAGATION EXPERIMENT IN THE NORTHEAST ATLANTIC, PART I (U)	Naval Research Laboratory	701118	ND	U
MC-003-VOL-2	Unavailable	THE PARKA I EXPERIMENT. APPENDICES- PACIFIC ACOUSTIC RESEARCH KANEOHE-ALASKA (U)	Maury Center for Ocean Science	710101	ND	U

ENCL (1)